

Hydrothermal ageing of fire protective fabrics and fabrication of an end-of-life sensor

by

Ankit Saha

A thesis submitted in partial fulfillment of the requirements for the degree of

Master of Science

In

Materials Engineering

Department of Chemical and Materials Engineering

University of Alberta

© Ankit Saha, 2021

Abstract

The outer shell of firefighter protective clothing is prepared from high performance polymer fibers such as Kevlar®, Nomex®, PBI, PBO and LCP. They are designed to withstand extreme temperatures and provide protection against service hazards to firefighters. However, these fabrics show continuous deterioration of mechanical properties when exposed to heat, UV, and moisture. This thesis work focusses on studying eight different outer shell fabrics with varying fiber contents and fabric structures in the unaged condition and after immersion of the fabric specimens in water at varying temperatures between 60°C and 90°C for up to 1200 hours. The effect of hydrothermal ageing was studied by analysing the residual tensile strength of these fabric specimens. This study also gives us quantitative information about the effect of fiber content and the influence of fabric structure on the fabric resistance to hydrothermal ageing and creates a foundation for the development of end-of-life sensors for fire protective clothing.

A second part of the work relates to the development of a fabrication process for the production of robust end-of-life sensors for the outer shell fabrics that can sustain the normal conditions experienced by the firefighter protective clothing. The overarching theme of the work is to develop an end-of-life sensor for firefighter garment, whereas the scope of my thesis study was to develop sensors that are free from premature failure. Specifically, I worked on reinforcing encapsulation by careful selection of electrode materials, developing processing methods, and establishing the testing protocols to monitor the deterioration of the sensor properties. The sensor development work was still in progress at the time of my thesis defense.

This ageing study provides a basis for understanding the behaviour of these outer shell fabrics when exposed to water to help in estimating the service life of these fabrics and protect firefighters from safety hazards. The sensor study can impact the fields of wearable sensor and e-textiles by providing insights in developing effective encapsulation technologies and in testing the reliability of these devices.

Preface

Chapter 1 is the introduction

Chapter 2 is the literature/background review of the current work

Chapter 3 is the materials and methods section for the experimental work performed.

In Chapter 4 of this thesis, the experimental work has been done by Ankit Saha and Md Saiful Hoque (a PhD student in Dr Dolez's group) with instructions from Dr Patricia Dolez and Dr Hyun-Joong Chung. The data interpretation has been done by Ankit Saha with instructions from Dr Patricia Dolez.

In Chapter 5 of this thesis, the experimental work and data interpretation has been done by both Ankit Saha and Reza Khalkhali (a Research assistant in Dr Chung's group) with instructions from Dr Hyun-Joong Chung and Dr Patricia Dolez.

Chapter 6 summarises the conclusion and the future work related to the projects

Acknowledgement

First of all, I would like to thank Dr. Hyun-Joong Chung and Dr Patricia Dolez for giving me the opportunity to join and work in their group. They have been always supported me to broaden the scope of my work and project. They inspired me with their enthusiasm and dedication for research. They tried to understand student's problem and tried to help me in the best way possible. I am grateful for them to have put together the project and provide me with this grateful opportunity.

I also would like to thank everyone in Dr. Chung and Dr. Dolez's group, Dr. Wendy Tran (former student), Dr Chungyeon Cho (former student), Lelin Zheng (former students and RA), Dr Christina Braun, Rosmi Abraham, Pradipika Natamai Vasudevan, Nathan Jen, Jiayao Cui, Marwa Khemir, Reza Khalkhali, Diana Yehia (former student), and Md Saiful Hoque. I also like to thank the Department of Human Ecology, University of Alberta and especially Dr Jane Batcheller for her continued efforts and support for all my projects.

As an international student coming to Canada, I am highly grateful for the opportunity being provided to me by the University of Alberta. I would like to thanks my friends, Yogashree Bharath, Roshni Sajiv Kumar, Karthik Srinivasan and Bhubesh Balasubramaniam for providing me the constant support and motivation during my studies and research here at University of Alberta. Lastly, I do thank my parents and my sister for their unconditional support they provided me throughout my life and believing in my potential.

TABLE OF CONTENTS

ABSTRACT.....	ii
PREFACE.....	iii
ACKNOWLEDGEMENT.....	iv
LIST OF FIGURES.....	vii
LIST OF TABLES.....	xii
CHAPTER 1 INTRODUCTION.....	1
1.1 INTRODUCTION.....	1
CHAPTER 2 LITERATURE REVIEW.....	4
2.1 HIGH PERFORMANCE TEXTILES FOR PROTECTIVE CLOTHING.....	4
2.2 FIRE PROTECTIVE CLOTHING.....	4
2.3 HIGH PERFORMANCE POLYMER FIBERS.....	6
2.4 FABRIC CHARACTERISTICS RELEVANT TO OUTER SHELL FABRICS FOR FIRE PROTECTIVE CLOTHING.....	15
2.5 LOSS IN PERFORMANCE OF FIREFIGHTER GARMENTS.....	27
2.6 DEGRADATION OF POLYMERS.....	28
2.7 HYDROTHERMAL AGEING OF HIGH-PERFORMANCE POLYMER FIBERS.....	35
2.8 MECHANICAL TESTING.....	38
CHAPTER 3 MATERIALS AND METHODS.....	42
3.1 MATERIALS TESTED.....	42
3.2 SPECIMEN PREPARATION.....	43
3.3 HYDROTHERMAL AGEING.....	44
3.4 YARN CRIMP AND LINEAR DENSITY MEASUREMENT.....	47
3.5 RESIDUAL STRENGTH MEASUREMENTS.....	48
3.6 OPTICAL MICROSCOPY.....	50
3.7 SENSOR FABRICATION AND TESTING.....	51
3.8 STATISTICAL ANALYSIS.....	55
CHAPTER 4 RESULTS AND DISCUSSION.....	56
4.1 FABRIC CHARACTERISATION.....	56
4.2 MECHANICAL BEHAVIOUR OF THE UNAGED FABRICS.....	58
4.2.1 FABRIC SCALE.....	58
4.2.2 YARN SCALE.....	69

4.2.3 DISCUSSION.....	80
4.3 AGEING BEHAVIOUR.....	91
4.3.1 FABRIC AND YARN BEHAVIOUR.....	91
4.3.2 DISCUSSION.....	127
CHAPTER 5 FABRICATION OF END OF LIFE SENSORS AND THEIR CHARACTERISATION.....	134
5.1 INTRODUCTION.....	134
5.2 LASER INDUCED GRAPHENE (LIG) LAYER ON PEI FILM.....	139
5.3 FABRICATION OF PEI-LIG SENSOR.....	141
5.4 ACCELERATED WATER AGEING OF THE PEI-LIG SENSOR.....	143
5.5 STABILITY OF THE PEI-LIG SENSOR AGAINST BENDING TEST.....	145
5.6 FATIGUE TESTS.....	148
CHAPTER 6 CONCLUSION AND FUTURE WORK.....	150
6.1 MECHANICAL BEHAVIOUR OF OUTER SHELL FABRICS.....	150
6.2 HYDROTHERMAL AGEING OF OUTER SHELL FABRICS AND ITS EFFECT ON MECHANICAL BEHAVIOUR.....	151
6.3 FABRICATION OF END OF LIFE SENSORS AND THEIR CHARACTERISATION.....	152
6.4 FUTURE WORK.....	152
REFERENCES.....	154

LIST OF FIGURES

Figure 1.1 Textile performance as a function of time used	2
Figure 2.1 Layers of a fire protective clothing	5
Figure 2.2 Chemical structure of p-aramids	6
Figure 2.3 Chemical structure of m-aramid	8
Figure 2.4 Chemical structure of PBI	10
Figure 2.5 Flowchart depicting the procedure of formation of PBI fibers	10
Figure 2.6 Chemical structure of PBO	11
Figure 2.7 Schematic representation of the chain orientation in (a) conventional polyester (b) LCP fibers	14
Figure 2.8 Fiber to Fabric manufacturing process	16
Figure 2.9 (a) Schematic representation of the warp and weft yarn orientation; Schematic representation of (a) plain weave (b) 2/1 twill weave	17
Figure 2.10 Microscopy image (a) a spun yarn, (b) a filament yarn	19
Figure 2.11 Example of the mechanical behaviour of woven fabrics.....	20
Figure 2.12 Unit cell geometry of Grosberg's model.....	23
Figure 2.13 Bilinear response of a yarn to bending.....	24
Figure 2.14 Unit structure of Kawabata's model	25
Figure 2.15 Stress vs Strain A- from Biaxial theory B- Experimental results	26
Figure 2.16 Schematic representation of random and selective chain scission.....	29
Figure 2.17 Oxidation mechanism in a polymer structure	30
Figure 2.18 Formation of crosslinks in poly (ethylene terephthalate).....	30
Figure 2.19 Elimination of a side chain group from a polymer chain	31
Figure 2.20 The thermal degradation mechanism in polymer chains (a) Initiation and Propagation (b) Oxidative termination.....	32
Figure 2.21 The formation of "mechano-radicals" in a polymer structure under stress	35
Figure 2.22 (A) Flexural testing with a three point bend test (B) Flexural testing with a four point bend test.....	39
Figure 2.23 Flexural stress vs Flexural strain curve	40

Figure 2.24 (a) S-N curve for a flexural fatigue test (b) Type of Fatigue test introduced	41
Figure 3.1 Schematic representation of the tensile strength specimen.....	43
Figure 3.2 Oven utilised for hydrothermal ageing.....	44
Figure 3.3 Wetting tray used for wetting the fabric specimen with the roller.....	45
Figure 3.4 Conditioning racks for the fabric specimens.....	46
Figure 3.5 Yarn crimp tester equipment.....	48
Figure 3.6 Universal Testing Machine used for mechanical testing of the fabric and yarn specimens.....	49
Figure 3.7 Optical microscope Stermi 508 Setup.....	51
Figure 3.8 Film applicator used for the encapsulation of end of life sensors.....	52
Figure 3.9 Laser scribing equipment used to develop LIG sensors.....	53
Figure 3.10 Cellscale mechanical tester used for the bending test.....	55
Figure 4.1 Mechanical behaviour of Fabric MA in the unaged condition.....	59
Figure 4.2 Fabric MA specimen a) before and b) after testing.....	59
Figure 4.3 Mechanical behaviour of Fabric MB in the unaged condition.....	60
Figure 4.4 Fabric MB specimen (a) before and (b) after testing.....	61
Figure 4.5 Mechanical behaviour of Fabric MC in the unaged condition.....	62
Figure 4.6 Fabric MC specimens (a)before and (b)after testing.....	62
Figure 4.7 Mechanical behaviour of Fabric MD in the unaged condition.....	63
Figure 4.8 Fabric MD specimen (a)before and (b)after testing.....	64
Figure 4.9 Mechanical behaviour of Fabric ME in the unaged condition.....	65
Figure 4.10 Fabric ME specimens (a) before and (b) after testing.....	65
Figure 4.11 Mechanical behaviour of Fabric MF in the unaged condition.....	66
Figure 4.12 Fabric MF specimens(a) before and (b) after testing.....	67
Figure 4.13 Mechanical behaviour of Fabric MG in the unaged condition.....	67
Figure 4.14 Fabric MG specimen (a)before and (b)after testing.....	68
Figure 4.15 Mechanical Behaviour of Fabric MH in the unaged condition.....	69
Figure 4.16 Fabric MH specimen before and after testing.....	69
Figure 4.17 Mechanical behaviour of Fabric MA for (a) spun yarn (b) spun/filament yarn in the unaged condition.....	71

Figure 4.18 Mechanical Behaviour of Fabric MB for (a) spun yarn (b) spun/filament yarn in the unaged condition.....	72
Figure 4.19 Mechanical Behaviour of Fabric MC for (a) spun yarn (b) filament yarn in the unaged condition.....	73
Figure 4.20 Mechanical behaviour of Fabric MD for (a) spun yarn (Brown) (b) spun yarn (Black) in the unaged condition.....	75
Figure 4.21 Mechanical behaviour of Fabric ME for spun yarn in the unaged condition.....	76
Figure 4.22 Mechanical behaviour of Fabric MF for Spun yarn.....	77
Figure 4.23 Mechanical Behaviour of Fabric MG for (a) spun yarn (b) filament yarn in the unaged condition.....	79
Figure 4.24 Mechanical behaviour of Fabric MH for (a) spun yarn and (b) filament yarn in the unaged condition.....	80
Figure 4.25 Optical microscope image for yarns of Fabric ME.....	88
Figure 4.26 Mechanical performance of a) spun and b) filament yarns in Fabric MG and Fabric MH.....	89
Figure 4.27 Optical microscopy image of the two plies for the spun yarn from Fabric MF.....	91
Figure 4.28 Mechanical behaviour of Fabric MA under hydrothermal ageing after 50 days.....	92
Figure 4.29 Variation of the load at break as a function of the ageing temperature for Fabric MA.....	93
Figure 4.30 Variation of the load at break for Fabric MA as a function of the ageing temperature for (a) spun yarn (b) spun/filament yarn.....	94
Figure 4.31 Fabric MA specimens (a) before ageing and (b) after ageing for 50 days at 90 C.....	95
Figure 4.32 Mechanical behaviour of Fabric MB under hydrothermal ageing after 50 days.....	96
Figure 4.33 Variation of the load at break as a function of the ageing temperature for Fabric MB.....	97
Figure 4.34 Variation of the load at break for Fabric MB as a function of the ageing temperature for (a) spun yarn (b) spun/ filament (2-ply) yarn.....	98
Figure 4.35 Fabric MB specimens (a) before ageing and (b) after ageing for 50 days at 90 C.....	99
Figure 4.36 Mechanical Behaviour of the fabric MC under hydrothermal ageing after 50 days.....	100
Figure 4.37 Variation of the load at break as a function of the ageing temperature for Fabric MC.....	101
Figure 4.38 Variation of the load at break for Fabric MC as a function of the ageing temperature for (a) spun yarn (b) filament yarn.....	103
Figure 4.39 Fabric MC specimens (a) before ageing and (b) after ageing for 50 days at 90 C.....	104
Figure 4.40 Mechanical Behaviour of the fabric MD under hydrothermal ageing after 50 days.....	105
Figure 4.41 Variation of the load at break as a function of the ageing temperature for Fabric MD.....	106

Figure 4.42 Variation of the load at break for Fabric MD as a function of the ageing temperature for (a) spun yarn (b) filament yarn.....	108
Figure 4.43 Fabric MD specimens (a) before ageing and (b) after ageing for 50 days at 90 C.....	109
Figure 4.44 Mechanical Behaviour of the fabric ME under hydrothermal ageing after 50 days.....	110
Figure 4.45 Variation of the load at break as a function of the ageing temperature for Fabric ME.....	111
Figure 4.46 Variation of the load at break for Fabric ME as a function of the ageing temperature for (a) spun yarn (b) filament yarn.....	114
Figure 4.47 Fabric ME specimens (a) before ageing and (b) after ageing for 50 days at 90 C.....	114
Figure 4.48 Mechanical Behaviour of the fabric MF under hydrothermal ageing after 50 days.....	115
Figure 4.49 Variation of the load at break as a function of the ageing temperature for Fabric MF.....	116
Figure 4.50 Variation of the load at break for Fabric MF as a function of the ageing temperature for spun yarn.....	117
Figure 4.51 Fabric MF specimens (a) before ageing and (b) after ageing for 50 days at 90 C.....	118
Figure 4.52 Mechanical behaviour of Fabric MG under hydrothermal ageing after 50 days.....	119
Figure 4.53 Variation of the load at break as a function of the ageing temperature for Fabric MG.....	120
Figure 4.54 Variation of the load at break for Fabric MG as a function of the ageing temperature for (a) spun yarn (b) filament yarn.....	122
Figure 4.55 Fabric MG specimens (a) before ageing and (b) after ageing for 50 days at 90 C.....	122
Figure 4.56 Mechanical behaviour of Fabric MH under hydrothermal ageing after 50 days.....	123
Figure 4.57 Variation of the load at break as a function of the ageing temperature for Fabric MH.....	124
Figure 4.58 Variation of the load at break for Fabric MH as a function of the ageing temperature for (a) spun yarn (b) filament yarn.....	126
Figure 4.59 Fabric MH specimens (a) before ageing and (b) after ageing for 50 days at 90 C.....	126
Figure 4.60 Degradation behaviour in Kevlar/PBI and Kevlar/Nomex based fabrics with ageing temperature.....	128
Figure 4.61 Comparative behaviour of filament yarns in MC, MG and MH with ageing temperature...	129
Figure 4.62 Comparative loss in tensile strength between Fabric MG and Fabric MH with ageing temperature.....	130
Figure 4.63 SEM images of fibers in (a) Fabric MG (b) Fabric MH.....	131
Figure 4.64 Difference in the rate of loss of tensile strength in Fabric MD and ME with ageing temperature.....	132
Figure 5.1 Structural schematic of the end-of-life sensor	135

Figure 5.2 Schematic representation of the laser engraving process for the development of LIG sensors	136
Figure 5.3 (a) A typical Unreliability vs time curve (b) A typical Weibull plot to predict the failure probability	138
Figure 5.4 Schematic design of the end-of-life sensor.....	140
Figure 5.5 Schematic arrangement of sensors during the production process.....	140
Figure 5.6 Application of silver paste on the PEI sheet.....	142
Figure 5.7 Schematic representation of the sensors being popped out after encapsulation.....	142
Figure 5.8 Schematic representation of the mass production of the thermal sensor.....	143
Figure 5.9 Change in resistance with water immersion at 40 C.....	144
Figure 5.10 Schematic representation of the bending test.....	146
Figure 5.11 Flexural Stress vs strain for the two sets of epoxy sensors.....	147
Figure 5.12 Fatigue data of the sensors plotted against number of cycles.....	149

LIST OF TABLES

Table 2.1 Tensile properties of different grades of Kevlar fibers	7
Table 2.2 Tensile properties of commercially available Nomex fibers	8
Table 2.3 Tensile properties of Zylon® Fibers	12
Table 2.4 Mechanical properties of two different grades of LCP fibers	14
Table 2.5 Studies on Textile mechanics model in the literature.....	22
Table 2.6 Absorption spectra of UV radiation for different polymer grades	33
Table 3.1 List of the fabrics studied.....	42
Table 3.2 Inventory of the epoxy materials used.....	53
Table 4.1 Fabric characterisation of the tested fabrics.....	56
Table 4.2 Categorisation of different fabric mechanical behaviour.....	81
Table 4.3 Yarn crimp and crimp ratio for fabrics with two different yarns in their structure.....	83
Table 4.4 Difference in performance for Fabric MD and ME.....	83
Table 4.5 Categorisation of the spun yarn mechanical behaviour.....	85
Table 4.6 Filament yarn mechanical behaviour.....	86
Table 4.7 Spun/filament yarn mechanical behaviour.....	86
Table 4.8 Breaking strength and linear density of the two sets of yarns in Fabric ME.....	87
Table 4.9 Tensile strength and linear density for the two sets of yarns in Fabric MG and MH.....	89
Table 4.10 t-test analysis between relevant conditions for fabric MC.....	101
Table 4.11 t-test analysis between relevant condition for spun yarn in fabric MC.....	102
Table 4.12 t-test analysis between relevant conditions for fabric MD.....	105
Table 4.13 t-test analysis between relevant conditions for Kevlar/Nomex spun yarn in fabric MD.....	107
Table 4.14 t-test analysis between relevant conditions for Kevlar yarn of fabric MD.....	108
Table 4.15 t-test analysis between relevant conditions for fabric ME.....	111
Table 4.16 t-test analysis between relevant conditions for the thinner yarn in fabric ME.....	112
Table 4.17 t-test analysis between relevant conditions for thicker yarn in fabric ME.....	113

Table 4.18 t-test analysis between relevant conditions for fabric MF.....	116
Table 4.19 t-test analysis between relevant conditions for spun yarn in fabric MG.....	121
Table 4.20 Comparative differences in weight and fiber diameter between Fabric MG and Fabric MH.....	130
Table 5.1 Change in normalized resistance with increase in ageing time for each tested group.....	145
Table 5.2 Statistical analysis (ANOVA) within each group.....	145
Table 5.3 Flexural Modulus and resistance reading for the two sets of sensors.....	147

Chapter 1 Introduction

Firefighter bunker suits and other protective gear worn by the workers in the oil and gas industry are subjected to high heat, flame, and other severe conditions in their day-to-day application. Hence, garments are prepared with high performance fibers that have flame, heat, and chemical resistance and are mechanically robust [1].

Despite of all the advantages associated with high performance fibers, these materials do have a few weaknesses. When used for an extended period of time, these fibers show a decrease in performance due to the conditions they are exposed to [2]. This loss in performance can be attributed to the exposure of firefighter protective clothing to light, heat, moisture, and abrasion among others. Figure 1.1 shows two different levels of degradation. The performance limit defines the usability of the fabric until it no longer meets the criterion stated [3]. The visual limit states the change in the visual parameters like color until it no longer can meet the intended use. As illustrated in Figure 1.1, a major issue is that high performance fibers do not always exhibit visible changes before their performance have reached a very low level [4], potentially endangering the lives of the workers wearing these protective garments.

The NFPA 1971 (National Fire Protection Association) standard specification defines performance requirements that manufacturers shall meet before putting a firefighter protective garment in service [5]. In addition, the NFPA 1851 standard provides guidance about the maintenance of these garments and indicators of their condition [6]. However, there is still a lack of knowledge about the degradation behavior of high-performance fiber and a strong need for monitoring tools of their performance in service exists.

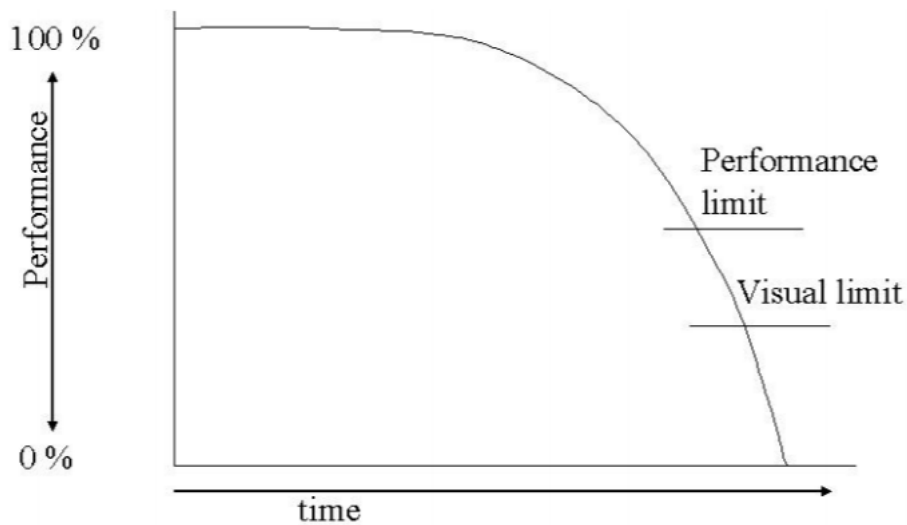


Figure 1.1 Textile performance as a function of time used. Reprinted from [7]

Hence, this thesis attempts to provide some information to help improve the safety of firefighters and others exposed to heat and flame. A first contribution relates to the need of characterizing the behavior of fabrics made with these high-performance fibers against ageing conditions like heat, UV and moisture. In particular, this thesis describes the effect of the exposure of firefighter suit outer shell fabrics to water at elevated temperatures (i.e., hydrothermal ageing). The residual condition of the fabrics is analysed in terms of loss in tensile strength of the aged specimens.

However, destructive testing cannot be used in service to assess the loss in performance of these protective garments. Thus, end-of-life sensors have been designed to monitor the ageing conditions sustained by the garments while in service [8]. They consist of a sacrificial polymer layer that mimics the behaviour of the fabric when exposed to the ageing condition. The loss in performance is monitored through the change in electrical conductivity of a conductive track imprinted on the surface of the sacrificial polymer layer. However, these sensors need to resist the regular use conditions of the fire protective clothing, which includes regular washing [9]. This thesis also reports on the work done to improve the manufacturing process and robustness of the end-of-life thermal sensors for fire protective fabrics.

The objectives of the thesis are:

- 1) Characterize the mechanical behaviour of outer shell fabrics and correlate it with their fiber content and fabric structure;
- 2) Study the effect of hydrothermal ageing on the mechanical behaviour of outer shell fabrics;
- 3) Develop strategies to produce mechanically robust end-of-life thermal sensors for fire protective fabrics that resist the regular laundering process.

The thesis is organised as follows: Chapter 2 discusses the background and literature review for fibers used in fire protective garments. It includes mechanical models of the behaviour of fabrics under tension and polymer/textile degradation fundamentals. Chapter 3 presents the materials and methods associated with the current thesis. Chapter 4 describes (i) the mechanical behaviour of the fabrics in the unaged condition and (ii) the effect of hydrothermal ageing on these fabrics. The results are analysed by considering the different fabric characteristics at the fabric, yarn, and fiber scale. Chapter 5 discusses the fabrication of the end-of-life thermal sensor and includes reliability studies and performance characterization. Chapter 6 summarises the conclusions and proposes avenues of future work.

Chapter 2 provides a literature review on fire protective fabrics, the concepts of fabric and yarn structures, textile mechanics, and degradation of textiles. This chapter also covers the degradation of polymer systems.

2.1 High performance textiles for protective clothing

Personal protective equipment (PPE) is defined as ‘any device or appliance designed to be worn or held by an individual for protection against one or more health and safety hazards’ [10]. The required functions of protective clothing, which are part of PPE, depend on three main factors [11]:

- Protection against health and safety hazards (e.g., heat, cold, fire, cuts)
- Comfort (thermal and tactile comfort properties such as heat and moisture management and softness)
- Ergonomics (e.g. mobility, flexibility, and tactile sensitivity)

The performance of protective clothing depends on many factors, including the structural parameters of the fabric [12] used as well as the fiber content [13]. The structural parameters include the fabric weave, fabric count, and type of yarns for instance. The characteristics of the fabric influence the physical and chemical properties of the protective clothing. In this chapter, we focus on fire protective clothing and the use of high-performance fibers to satisfy the requirements associated with their use.

2.2 Fire protective clothing

The life of firefighters is always under threat due to their hazardous working conditions. Hence ensuring their protection from heat, flame, abrasive objects, and chemical exposure is of utmost importance [6]. This is achieved in part with protective garments made of high-performance fibers capable of resisting flame and high temperatures [14]. Firefighter bunker suits generally comprise three layers: an outer layer, a moisture barrier, and a thermal liner, as illustrated in Figure 2.1 [15].

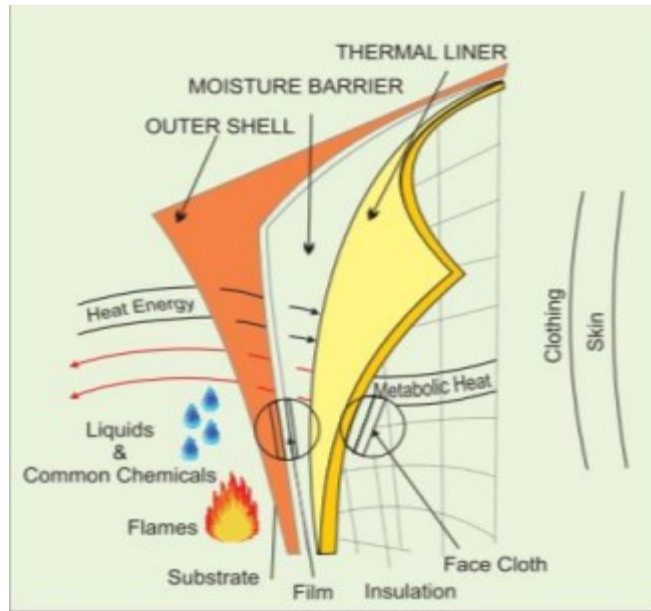


Figure 2.1 Layers of a fire protective clothing. Reprinted from [15]

The main function of the outer layer is to protect both the firefighter and the moisture barrier against the numerous mechanical hazards associated with the task [16]. It also has to resist exposure to heat and flame and be water repellent [17], [18]. Outer shell fabrics are generally made of blends of high performance fibers such as aramids, polybenzimidazole (PBI), and polybenzoxazole (PBO). These fabrics have a high tensile and tear strength and are inherently flame resistant. Section 2.3 presents different high-performance polymer fibers used in the manufacture of outer shell fabrics, which are the main topic of this thesis.

The moisture barrier is a laminate of a breathable film on a fabric substrate. The role of the moisture barrier is to block the entry of water and many common liquids inside the garment [11], while allowing water vapor to exit, thus reducing the risk of skin burns [17], [18]. This can be achieved using microporous membranes such as expanded polytetrafluoroethylene (ePTFE) [11].

The thermal liner is the innermost layer in the firefighter clothing. The role of the thermal liner is to limit skin exposure to the outside heat [17]. This layer generally consists of a nonwoven mat of flame-resistant fibers quilted on a substrate fabric [19]. Commercial thermal liners include AraliteGold (80% Kevlar and

20% PBI batting with 100% Nomex spun laced non woven face fabric) by Tencate and OMNIQuilt (100% Nomex batting with 1-layer, 2-layer, or 3-layer Basofil spun-laced non-woven face fabric) by Norfab [19].

2.3 High-performance polymer fibers

High performance polymers exhibit excellent mechanical properties along with good fire, heat and chemical resistance and have been utilised as fibers, films or membranes in the protective clothing industry [1]. In particular, the outer shell fabrics included in the study comprise different ratios of the following high-performance polymer fibers: para-aramid, meta-aramid, PBI, PBO, and liquid crystal polyester (LCP).

2.3.1 Para-aramid

Polyphenylene terephthalamide (or para-aramid) is prepared by the condensation reaction of p-phenylenediamine and terephthaloyl chloride, yielding sulphuric acid as a by-product [20]. Commercial names include Kevlar® and Twaron®. Figure 2.2 depicts the structure of para-aramid.

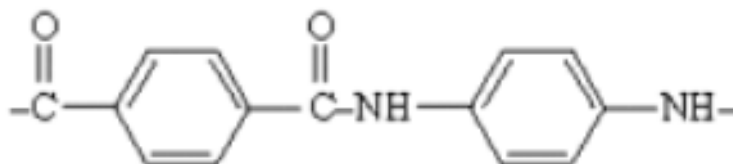


Figure 2.2 Chemical structure of p-aramid reprinted from [21]

The para-aramid polymer is converted to fibers using the process of wet spinning [21]. To be spun, the polymer is dissolved in concentrated sulphuric acid and extruded through a spinneret to make long, strong (through orientation), stiff fibers into an alkali bath to neutralise the effect of acid. The fibers formed are highly crystalline and are oriented in the fiber direction through mechanical drawing.

Due to their highly oriented structure, these fibers exhibit high tenacity and high modulus. When the fibers are spun, they show a tensile strength of 3.6 GPa and a relative density of 1.44 [22]. Different grades of

Kevlar® fibers with varying strength and modulus are produced by changing the orientation of the polymer molecules as shown in Table 2.1 [11].

Table 2.1 Tensile properties of different grades of Kevlar fibers [11]

Kevlar fiber grade	Young modulus (cN/tex)	Tensile strength (cN/Text)	Density (g/cm ³)
29	8,567.5	371.7	1.44
49	13,522.2	371.7-423.0	1.44
149	19,199.4	351	1.47

Para-aramid maintains its strength and performance at cryogenic temperatures (roughly around -196°C) [23]. It exhibits a glass transition temperature of 345°C [24]. The polymer melts at 560°C and shows a degradation temperature at 590°C in nitrogen [25]. This high thermal performance is attributed to the high dimensional orientation of the phenyl rings in the molecule. Because the melting and degradation temperatures are very close, this polymer does not exhibit the melt and drip behavior of thermoplastics, which makes it a choice material for protective clothing against high heat [1]. In addition, para-aramid is inherently flame resistant.

Because of the high degree of affinity of moisture for the amide group in the monomer structure, para-aramid fibers have a high sensitivity to moisture uptake [21]. However, the degree of moisture uptake is influenced by other characteristics such as crystallinity and molecular alignment. It generally ranges between 8% at 65% RH and 22 °C for Kevlar® 29 to 4.2% for Kevlar® 49 [26]. Kevlar® fibers also experience an easy uptake of solvents due to surface features such as the presence of microvoids on the surface of the fibers[27]–[29].

2.3.2 Meta-aramid

Poly (m-phenylene isophthalamide) is a meta aramid prepared by the condensation reaction of m-phenylenediamine and terephthaloyl chloride [30]. Commercial names are Nomex® and Conex®. In the case of meta-aramid, the amide group is formed at the 1,3 position whereas in case of para-aramid, the amide group is formed at the 1,4 position. Due to this meta-joined amide linkage, the polymer chains have the ability to bend and thus exhibit a reduced rigidity as compared to para-aramid [23]. Figure 2.3 depicts the chemical structure of meta-aramid.

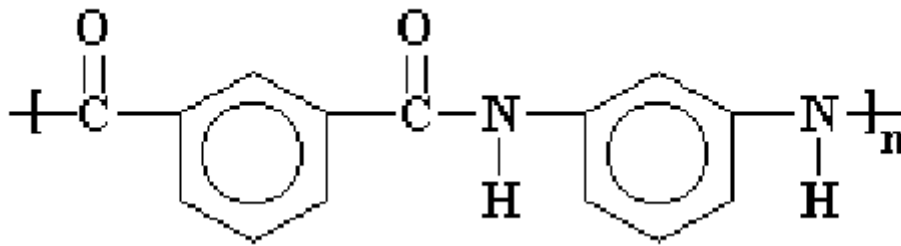


Figure 2.3 Chemical structure of m-aramid reprinted from [31]

Meta-aramid fibers are prepared by a wet spinning method similar to that of para-aramid. The meta-aramid family consists of staple fibers, continuous filaments, and paper. They have commercial applications for firefighter garments, thermal insulation apparel, and to protect against flash fire exposure [11]. Nomex® is available in various grades that have been approved for commercial use as listed in Table 2.2. Nomex® III and Nomex® IIIA are blends of Nomex® and Kevlar® fibers.

Table 2.2 Properties of commercially available Nomex® fibers [11]

Nomex fiber grade	Density (kg/m ³)	Tensile strength (MPa)	Tenacity (N/tex)
N301	-	340	0.247

Nomex 450	1370	349	0.256
Nomex 455 (Nomex III)	-	310	0.229
Nomex 430	1380	607	0.441

Meta-aramid fibers exhibit a lower strength compared to para-aramid fibers (e.g. 340 MPa for Nomex® [32] vs. 3.6 GPa for Kevlar® [22]) because of the flexible backbone structure created by the amide linkages joining at the 1,3 position. Due to the flexible structure of the polymer, it also shows a higher extensibility, around 19% for Nomex® fibers [32] compared to 3.6% for Kevlar® fibers [23]. Nomex® fibers retain their tensile performance when exposed to 250°C over short periods of time [33].

Meta-aramid exhibits excellent thermal properties [34]; it does not melt when heated but shows a weight loss (~1%) until a temperature of 350-400°C and then shows a maximum loss in weight around 450 °C in air [25]. It also has self-extinguishing properties and is inherently flame resistant. When a meta-aramid fabric is exposed to high heat fluxes, the fabric chars and thickens rather than melting, and is thus a choice material for fire protective clothing.

Meta-aramid has a relatively good resistance to moisture and only shows a moisture regain of 4.5% at ambient conditions [33]. This is a major advantage of meta-aramid over para-aramid. Meta-aramid also exhibits an excellent chemical resistance to acids and bases at ambient conditions. However, it shows some degradation when exposed to alkalis at elevated temperatures [33].

2.3.3 Polybenzimidazole (PBI)

The PBI polymer (2,2-m-phenylene-5,5-dibenzimidazole) is formed by condensation between tetraaminobiphenyl (TAB) and diphenylisophthalate (DPIP) in an inert atmosphere with a two step high temperature reaction process[35], [36]. Figure 2.4 depicts the structure of PBI.

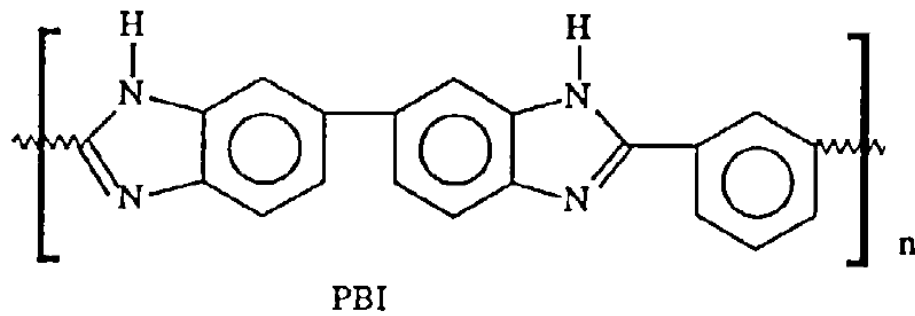


Figure 2.4 Chemical structure of PBI reprinted from [35]

PBI fibers are prepared by dissolving the polymer at high pressure in a dimethylacetamide (DMAc) solvent [37]. The solution is filtered, and fibers are prepared by a high temperature dry spinning process. The fibers are ultimately drawn at elevated temperatures to acquire the desired mechanical properties. The formed fibers are sulfonated, and then made into staple fibers using conventional crimping and cutting techniques. Figure 2.5 shows the flowchart for the preparation of PBI fibers. PBI fibers are used to manufacture staple yarns and processed into woven and knitted fabrics.

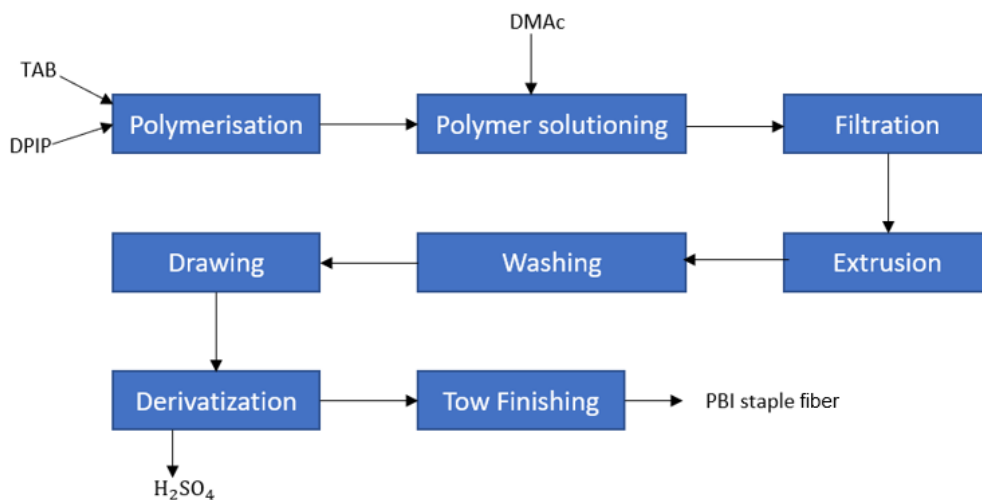


Figure 2.5 Flowchart depicting the procedure of formation of PBI fibers adapted from [37]

PBI fibers offer a very good combination of thermal, chemical, and mechanical properties. They exhibit a tensile strength of 160 MPa with an elongation at break of 3% [35]. They also have a high tensile modulus at 5.9 GPa.

In terms of thermal properties, they can withstand very high temperatures without degrading or burning [36]. With a limiting oxygen index of greater than 41%, PBI fibers are inherently flame resistant. In addition, they do not melt and decompose directly at 580 °C in air and their dimensional stability remains intact when exposed to high temperatures and heat fluxes. They retain their tensile properties at high temperatures up to 371°C and show no embrittlement at a temperature as low as -73 °C.

PBI fibers also exhibits exceptional resistance against chemicals [37]. These include acids, bases, and high-pressure steam. They do not show any loss in tensile performance through continuous exposure to steam at 150 °C at 50 psig after 3 hours. When exposed to organic chemicals, the tensile performance remains unchanged. When in contact with strong acids and bases, their strength remains unaffected. For instance, they preserved ~95% of their original strength when exposed to sodium hydroxide at room temperature for 168 hours [37].

2.3.4 Polybenzoxazole (PBO)

Poly(p-phenylene-2,6-benzobisoxazole) (PBO) was developed by Toyobo Co. Ltd and is commercialised under the name of Zylon® [38]. It is formed by the self-condensation reaction of 4,6-diaminoresorcinol and terephthalic acid in phenylpropanolamine (PPA) as a solvent. Figure 2.6 depicts the structure of PBO [38].

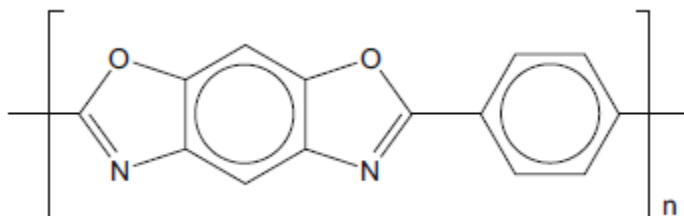


Figure 2.6 Chemical structure of PBO reprinted from [38]

PBO fibers are formed by extruding the polymer solution through capillaries to form filaments [38]. The filaments are then drawn in one direction to increase the mechanical strength of the fibers. Once the required strength is reached, the fibers are allowed to coagulate with an intent to solidify them [39]. Finally, the fibers are washed and soaked in a base bath to neutralize the acid content present in the fibers [40].

There are two types of Zylon® fibers commercially available: Zylon® HM and Zylon® AS [41], [42]. Zylon® HM exhibits a higher tensile modulus and lower moisture regain compared to Zylon® AS (Table 2.3). Zylon® fibers are 1.6 times stronger than Kevlar® fibers (5.8 GPa for Zylon® and 3.6 GPa for Kevlar®). The chemical structure of PBO is responsible for its outstanding thermal and mechanical performance.

Table 2.3 Tensile properties of Zylon® fibers [43]

Property	Zylon® HM	Zylon® AS
Density (g/cm ³)	1.54	1.56
Moisture Regain (at 65% RH)	2.0	0.6
Tensile strength (GPa)	5.8	5.8
Tensile Modulus (GPa)	180	270
Elongation at break (%)	3.5	2.5

In addition, the excellent thermal behaviour of PBO makes it an ideal candidate for fire protective clothing. It has excellent heat oxidation tolerance and is not combustible [1]. It also has low smoke emission and high pyrolysis resistance. It shows a decomposition temperature of 650°C in air, which is higher than p-aramids. These fibers also show a limiting oxygen index of 68%, which contributes towards its resistance to flame in air and makes it an inherent flame resistant fiber [38].

However, these high-performance fibers have been reported as highly sensitive to moisture [48], chemicals [44], and UV [38]. For instance, a decrease in strength of the Zylon® fibers was observed under exposure

to high temperature, high humidity, and UV [45]. This reduction in strength was associated with the presence of the oxazole ring in the chemical structure, which is highly sensitive to moisture[44]–[46]. When exposed to sunlight for a total duration of six months, PBO fibers showed a reduction of 35% in tensile strength [38].

2.3.5 Liquid crystalline polyester fibers

Liquid crystalline polyester (LCP) fibers were developed with the objective of allowing high temperature applications while preserving melt processability [47]. When monomers in the liquid state can move around, they join in a random fashion resulting in a random co-polymer. The ability of these polyester monomers to form crystals in the liquid state is why they are called liquid crystal polyesters.

The thermotropic LCP polymer is formed by polycondensation reaction of 6-hydroxy naphthoic acid and 4-hydroxy benzoic acid[47], [48]. The reaction is conducted in an inert atmosphere at a temperature 50-80°C higher than the melting point of the monomers. Catalysts are usually added to speed up the reaction. Vacuum is introduced into the system to drive the reaction forward towards a higher molecular weight product. The final product thus obtained can be extruded and used for fiber production.

The LCP fibers are prepared by common melt spinning techniques [47]. But these fibers cannot be drawn the conventional way. As a result, it is difficult to control the fiber diameter. Because of this, LCP fibers require specially designed spinnerets and melt extruders. The obtained fibers undergo solid-state polymerisation, thus increasing the molecular weight of the polymer and hence, the mechanical properties of the fibers. The resulting fibers have high ordered crystalline domains within the structure, which contributes towards enhanced physical properties comparable to that of p-aramid[49]–[51].

Two grades of LCP fibers are commercially available: LCP standard modulus and LCP high modulus. The properties of these two grades are listed in Table 2.4.

Table 2.4 Properties of the two different grades of LCP fibers [47]

Property	LCP standard modulus	LCP high modulus
Density (g/cm ³)	1.4	1.4
Tensile strength (GPa)	3.2	3.0
Tensile Modulus (GPa)	75	103

The highly oriented structure of LCP fibers results in an excellent mechanical performance as shown in Table 2.4. Figure 2.7 depicts the molecular and crystal orientation in standard polyester and LCP fibers. Moreover, LCP fibers exhibit excellent yarn to yarn abrasion resistance, which improves in the wet condition [47].

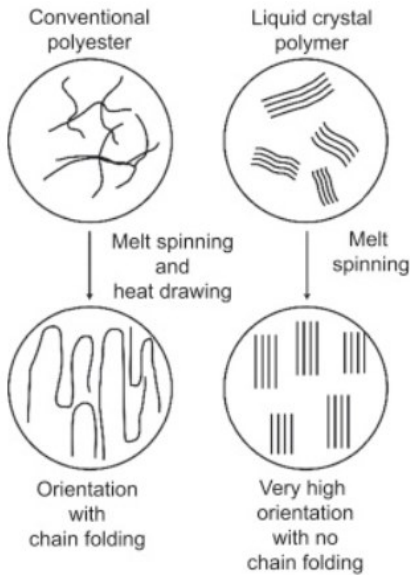


Figure 2.7 Schematic representation of the chain orientation in (a) conventional polyester (b) LCP fibers reprinted from [52]

Due to the unique production process of LCP fibers, their thermal properties are a combination of both thermoplastics and thermosets. With a limiting oxygen index of 30%, LCP fibers have a high resistance to burning in air [47]. They show a melting point at 350°C [47], which is lower than that of Kevlar®.

Thermogravimetric analysis (TGA) of LCP fibers shows that there is a 20% loss in weight when the temperature exceeds 450°C. With increasing temperature, LCP fibers exhibit a decrease in tensile strength at a rate that is higher than that of aramids [47].

LCP fibers show a strong resistance when exposed to chemicals and moisture [47]. They have a very low equilibrium moisture adsorption, which prevents a significant amount of moisture uptake. However, the continued exposure to moisture leads to microcracking issues similar to that seen in aramids. As they are constituted of a polyester-based polymer, the fibers are resistant to weak acids and bases but tend to show degradation when exposed to highly concentrated acids and bases.

2.4 Fabric characteristics relevant to fire protective clothing outer shell fabrics

The fibers formed from processes such as wet spinning and melt spinning are then converted into yarns by the process of spinning [53]. Spinning is defined as the process that binds many fibers together to form yarns of varying strength by the application of twist. There are two types of twist which are generally applied to the yarns. If the direction of the twist is to the right, it is termed as a Z twist and if the direction of the twist is to the left it is an S twist. There are three types of yarn structures which are present in the fabrics studied i.e., spun yarns, filament yarns, and spun/filament yarns (Section 2.4.2). After the process of twisting, yarns are generally converted into a fabric either by weaving or knitting. After the formation of the fabric, the final apparel is prepared by the process of dyeing, finishing, cutting and sewing. This process of manufacturing is shown in Figure 2.8. Due to the various components or processes introduced in its manufacture, fabrics are termed multiscale structures. This comprises of fibers, yarns and then the fabric scale. The mechanical performance of the fabric is governed by each scale; thus measuring the performance at each scale gives us an entire picture of how the fabric behaves when tension is applied.

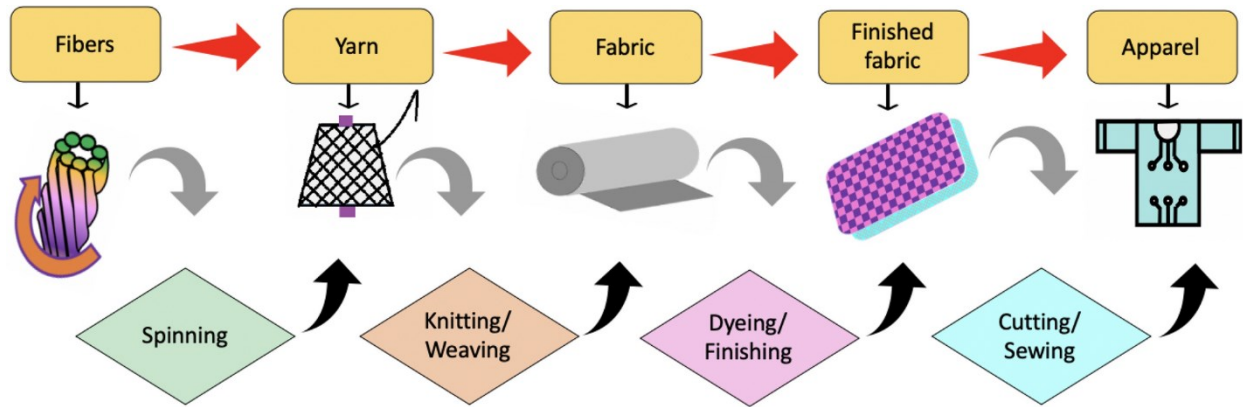


Figure 2.8 Fiber to fabric manufacturing process reprinted from [54]

The performance of fire protective clothing is affected by its fiber content [13]. Aside from the fiber content, the main parameters that influence the performance of a fabric are its fabric count, type of weave, and type of yarn [12]. This thesis only covers woven fabrics and their corresponding textile characteristics since this is the structure used for outer shell fabrics in fire protective clothing.

2.4.1 Woven fabric structures

A woven fabric is characterized by two sets of orthogonal yarns, namely the warp and weft yarn, which are interlaced by weaving [55]. The warp yarns are positioned length wise and the weft yarns are inserted transversally under and over the warp yarns (Figure 2.9). Different types of arrangements of the yarns lead to different types of weave constructions. This thesis focuses on the plain weave and twill weave structures as they are the ones generally encountered in outer shell fabrics for fire protective clothing.

Plain weave fabrics are made by passing each warp yarn over and under each weft yarn, leading to a high number of intersections between the orthogonal yarns [56]. On the other hand, twill weave fabrics are made by passing each warp yarn under two or more weft yarns, leading to a reduced number of intersections.

In the typical graphical representation of the plain and twill weaves shown in Figure 2.9, the black squares indicate where the warp yarn appears on the upper surface of the fabric and the white blocks indicate where the weft yarn appears on the fabric surface [55]. There is thus the same number of warp and weft yarns at

the fabric surface in a plain structure but twice as much weft yarns in a twill weave. As a result, these fabric structures have different surface properties, such as the resistance to abrasion [57].

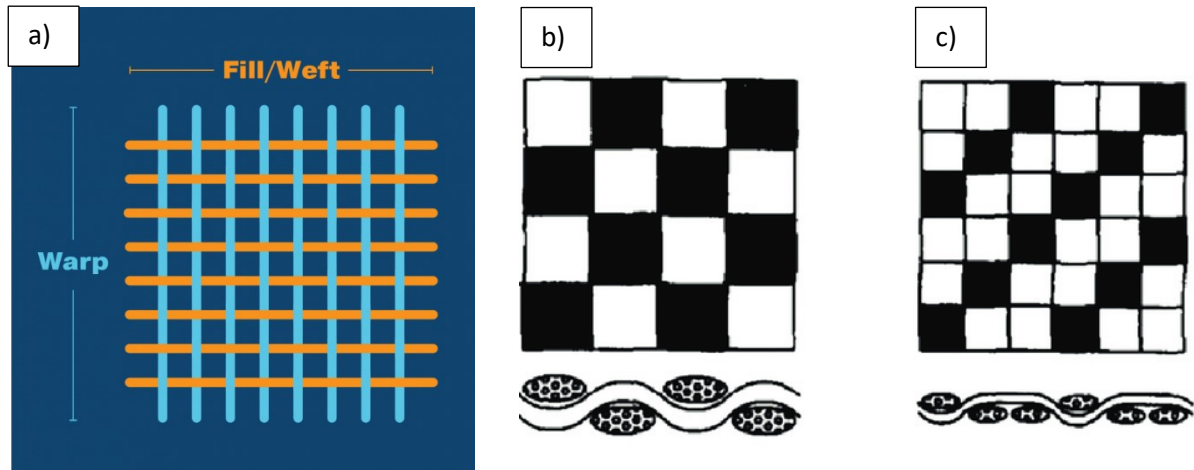


Figure 2.9 (a) Schematic representation of the warp and weft yarn orientation [58]; Schematic representation of (b) the plain weave (c) 2/1 twill weave reprinted from [59]

The mechanical performance of fabrics is also affected by their structure. In particular, plain weave fabrics have a higher tensile strength compared twill weave fabrics because of the higher number of interlacements between the yarns [60]. On the opposite, twill weave fabrics have a higher resistance to tearing due to the larger yarn mobility associated with the lower number of yarn interlacements.

In addition to the standard plain and twill weave structures, some outer shell fabrics included in this study present variations of these structures. This includes the broken twill weave structure, in which the direction of the twill line is changed at regular intervals [61], and the rip-stop, where a stronger yarn, for instance a filament yarn, is inserted at regular intervals between the regular yarns to increase the mechanical performance of the fabric [62].

2.4.2 Fabric count and yarn characteristics

Fabric count is defined by the number of yarns per unit length in the warp and weft direction. Fabric count is calculated according to Equation 2-1.

Fabric Count = Warp count (number of yarns/cm) x Weft count (number of yarns/cm) (equation 2-1)

Yarns in a fabric can be made using staple fibers or filaments. Spun yarns are produced with short staple fibers to form a continuous assembly of overlapping fibers which are bound together by twisting [53]. Spun yarns are characterised by a non lustrous appearance and are hairy in nature as shown in Figure 2.10(a), with small fibers protruding out of the surface [63]. They are softer than filament yarns.

Filament yarns are prepared using continuous fibers [64]. Filament yarns have a lustrous appearance and a smoother surface as compared to spun yarns [63]. Due to the continuity of the fibers in filament yarns, they tend to be stronger than spun yarns. Figure 2.10(b) represents an image of a filament yarn.

Crimp interchange is defined as the transfer of crimp (the waviness of a yarn in the fabric) from the yarn direction under tension to the other direction because of the increasing load [65]. Crimp interchange leads to a slipping motion between the yarns at the crossover points, which causes an increase in extension with no change in stress value. The crimp (C) of a yarn is calculated using equation 2-1.

$$C = \frac{L_{yarn} - L_{fabric}}{L_{fabric}} \quad (\text{equation 2-1})$$

Where L_{fabric} is the length of the yarn in the fabric and L_{yarn} is the length of the yarn after it is extracted from the fabric and straightened out.

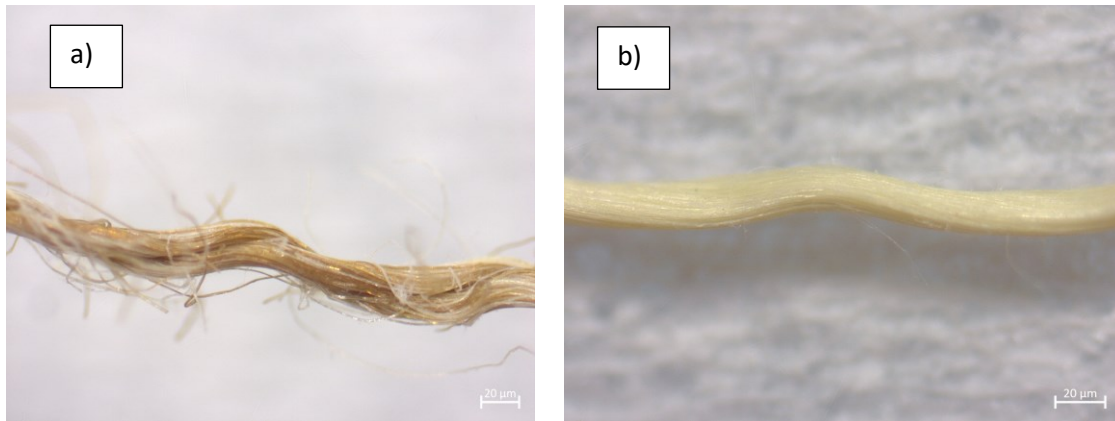


Figure 2.10 Microscopy image (a) a spun yarn, (b) a filament yarn

2.4.3 Mechanical behavior of fabrics relevant to firefighter outer shell

The short and long-term performance of a firefighter clothing is estimated based upon many factors such as mechanical behaviour of the fabric, flame resistance, water repellency and many more. The standard specification NFPA 1971 [5] details the requirements that these bunker suits must pass as a material and a system before being put into service. The mechanical strength of all three layers of the fire protective clothing are assessed based upon their tensile and tear strength. This thesis focusses on tensile strength and tensile behaviour of fabrics used in the firefighter protective clothing outer shell. These fabrics are generally woven fabrics.

2.4.4 Tensile behaviour of woven fabrics

Mechanical behaviour is one of the most important way to study the performance of woven fabrics. However, this mechanical behavior is complex due to the multi scale nature of fabrics. From fiber to yarn to fabric, each component at every level contributes to the global fabric behavior and any slight change in the fabric structure within the fabric leads to a unique behavioural characteristic [66]. This leads to the non-Hookean behaviour of fabrics and yarns with increasing strain [67].

Figure 2.11 shows the typical stress vs strain curve for a woven fabric under tension. The initial region is characterised by a low slope, i.e. with no appreciable increase in stress with strain. It is due to the phenomenon of crimp interchange (Phase I), which corresponds to the decrimping of the loaded yarns.

After the crimp has been taken out, the stress increases with increasing strain during Phase II. The yarns are stretching due to the applied load on the fabric. These yarns continue extending until the fabric reaches its breaking strength (Phase III), which is identified as the peak in the curve in Figure 2.11.

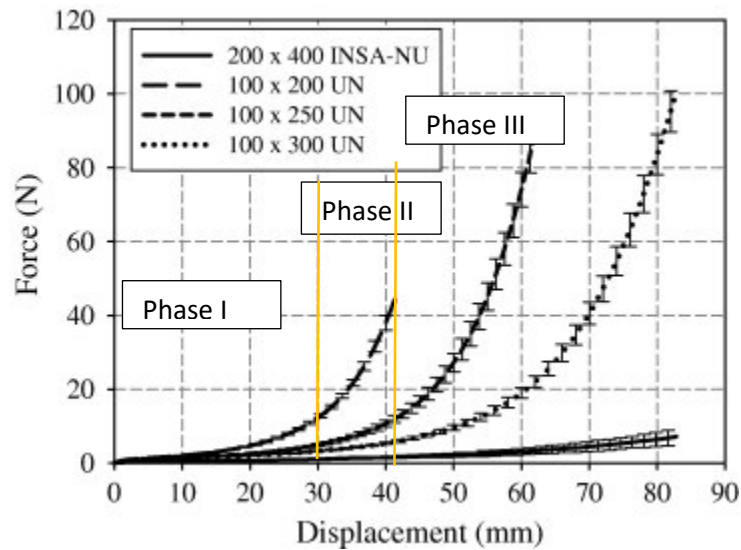


Figure 2.11 Example of distinction of different phases in the mechanical behaviour of woven fabrics (200x400 INSA-NU fabric) [68]

2.4.5 Effect of textile parameters on woven fabric strength

The dependence of breaking strength, elongation, fabric assistance, tear strength, crimp and air permeability on fabric weave, twist level, and weight per area of fabrics has been studied by Schiefer and co-workers [69]–[71]. Firstly, they studied the effect of weave on the properties of fabrics with same weight but different types of weave: Plain, twill, rib, mock leno, basket, and satin. They defined a term “fabric assistance” as:

$$\text{Fabric assistance} = \frac{(\text{Strength of fabric})}{(\text{Strength of Yarn})} - 1 \quad (\text{equation 2-2})$$

The following parameters were observed as having a major effect on the fabric strength [69]–[71]:

- Yarn strength
- Manner of interlacing of two orthogonal yarns (weave construction)
- Twist of the yarn (degree of interaction between fibers)

The plain weave construction resulted in a fabric having the highest strength amongst all the types of weave constructions studied [69]–[71]. The strength was observed to increase with the number of yarn interlacing per unit length if the repetition of the yarns was regular.

Scheifer at al. also stated that the weft yarns were weaker because of a lower degree of twist [69]–[71]. The strength however improved when the yarns were closely interlaced together, which would bring them in close contact. This apparent increase in the fabric strength brought about by interlacing is termed as fabric assistance. The case is quite opposite for the warp yarns. Due to the presence of a higher level of twist, the fibers in the yarn are already in close contact with each other. Therefore, the weave construction has no effect on the tensile strength of the yarn. The increase in the yarn strength caused by the increase in twist is not sufficient to overcome the loss in performance from abrasion occurring between two orthogonal yarns during weaving. This behaviour is termed as negative fabric assistance.

They also analysed the effect of twist in the tensile strength of the yarns [69]–[71]. They found that the increase in twist causes an increase in the tensile strength value. However, there is a threshold value above which the increase in twist does not influence the tensile strength.

2.4.6 Mechanics models of woven fabrics

Geometry-based models have been proposed to describe the mechanics of woven fabrics. The sections below present two of them. Their main features are summarized in Table 2.5.

Table 2.5 Textile mechanics models of woven fabrics

Model	Main characteristics
Grosberg (1966) [72]	<ul style="list-style-type: none"> - Explained the fabric behaviour under stress for extremely large deformations. - The failure of the fabric was analysed based on the average breaking load of the fabric component. - Considered the initial geometry of the yarn and the change in geometry with loading - Studied the bending response of the yarn
Kawabata (1973) [73], [74]	<ul style="list-style-type: none"> - Defined a fabric model for biaxial and uniaxial deformations considering small to large deformations. - For uniaxial model, postulated that the compressive forces arise due to resistance of yarn to bending and shearing. - Did not consider the change in yarn diameter with increase in loading. - The uniaxial model works best for larger deformations

Grosberg's model (1966)

Grosberg developed a geometry-based model for the stress strain behaviour of plain weave fabrics [55], [72]. His model states that when a fabric is under load F , a force V acts on the intersection region as a result of the crimp interchange in the fabric cross section as shown in Figure 2.12.

In his model, Grosberg considered the following parameters:

- The initial geometry of the fabric at the yarn level;
- The change in geometry during loading;
- The bending response of the yarns;
- The change in yarn diameter;

- The failure calculated from the average load value.

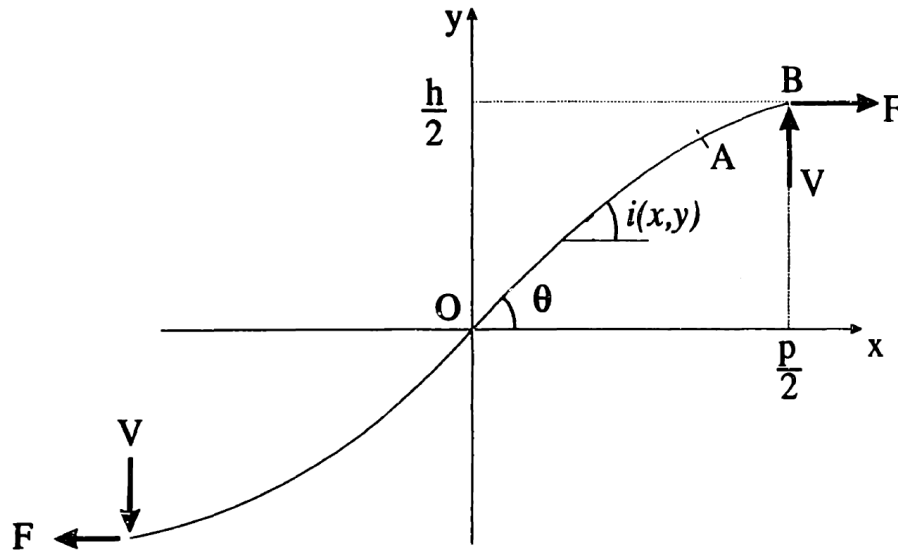


Figure 2.12 Unit cell geometry of Grosberg's model reprinted from [55]

During low extensions, this force V tends to increase because of the contact resistance between the two orthogonal yarns [72]. Grosberg predicted that the bending response of a yarn is bilinear (Figure 2.13): the initial slope is due to the force V dominating the applied load F with no fiber slippage whereas the gradual softening is linked to the applied load F progressively dominating the force V because of fiber slippage. Fiber slippage is defined as the relative fiber motion between different fibers brought about by the increasing tension or force applied to a yarn or fabric.

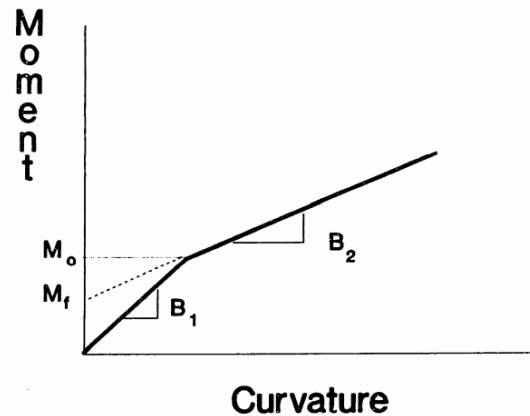


Figure 2.13 Bilinear response of a yarn to bending reprinted from [55]

He expressed the value of the tension (T) in terms of both F and V as follows [59]:

$$T = F \cos i + V \sin i \quad (\text{equation 2-3})$$

He also expressed the change in diameter of the yarn Δd during loading as follows:

$$\Delta d = K(\Delta V)^c \quad (\text{equation 2-4})$$

Where K and c are constants and ΔV is obtained experimentally by comparing the yarn contraction due to bending to the theoretically predicted contraction when it was assumed that there is no change in diameter. This contraction observed in the warp yarns is due to the crimp interchange occurring in woven fabrics with increase in loading force. To take into account the fracture of yarns within fabric, he used the average breaking load and extension of the yarns.

Kawabata (1973)

Kawabata et al. drew up a model for biaxial extension (warp and weft direction) (Figure 2.14), uniaxial extension, and shear deformation (at the intersecting points in a plain weave fabric) of a woven fabric dependent on the variation in geometry (different types of weave construction, fabric count) of the fabric structure [73], [74]. Kawabata's model is similar to Grosberg's model. However, they suggested a different

treatment for the bending response for the fabric. In addition, they didn't include the failure of the fabric since they wanted to describe fabrics at low deformations. Figure 2.13 shows the mechanical model as developed by Kawabata.

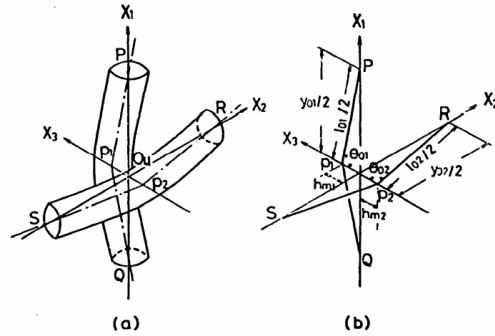


Figure 2.14 Unit structure of Kawabata's model reprinted from [73]

Kawabata et al. defined the crimp S using the following relation [73]:

$$S_1 = \frac{l_{01} - y_{01}}{y_{01}} \quad S_2 = \frac{l_{02} - y_{02}}{y_{02}} \quad (\text{equation 2-5})$$

Where l_{01} corresponds to the length of the yarn in the unit cell and y_{01} is inversely proportional to the number of yarns per millimeter. S_1 and S_2 are the crimp values in each orthogonal direction.

First considering a biaxial deformation, the normal force at the point of contact between the two orthogonal yarns F_c is given by [73].

$$F_c = 2F_{T1} \cos \theta \quad (\text{equation 2-6})$$

Where F_{T1} is the warp yarn tension, F_c is the compressive force acting on the yarn at the interlacement point and θ is the angle between the yarn axis and the neutral axis X_1 shown in Figure 2.14. Further simplification led to the force F_1 corresponding to the biaxial extension of the fabric for any fabric geometry and yarn deformation:

$$F_1 = g_1(\lambda) \sqrt{1 - \left(\frac{2C_0 + C_1 l_{01} \cos \theta}{4g_1(\lambda) + C_1 l_{01} \lambda} \right)^2} \quad (\text{Equation 2-7})$$

Where C_0 and C_1 are constants and λ is the extension along the yarn axis. The term $g_1(\lambda)$ function corresponds to the mechanical properties of the warp yarn.

From the theoretical model Kawabata et al. developed, they postulated that the normal compressive force arises because of the fiber resistance to bending and shearing during the extension and bending of the fabric. When extending the biaxial model to uniaxial deformation, Kawabata et al. introduced the effect of bending of the transverse yarn. They obtained a good agreement with experimental results (Figure 2.15). A deviation from the experimental curve observed in some instances at higher deformations, i.e., in the yield region, was attributed to the linear approximation of the compression force in the development of the uniaxial model. A small deviation was also obtained at low extension due to the bending of the yarn in the loaded direction being neglected. Finally, another factor leading to the difference between the theoretical and experimental results is the consideration of the diameter of the yarn, which was assumed to be constant for the entire loading process. Thus, this theory best describes deformations above 1.03-1.05. It also gives a reasonable approximation for the fabric behaviour in the lower extension range.

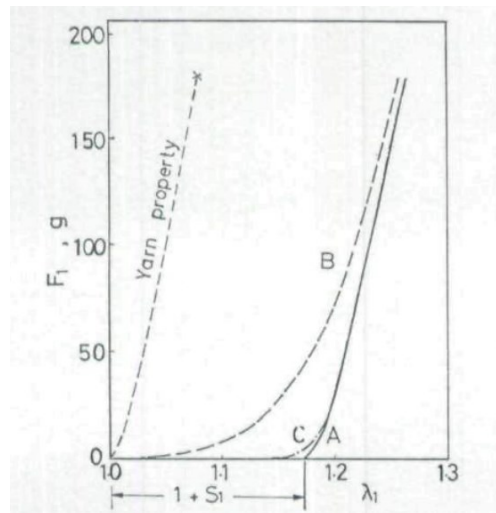


Figure 2.15 Stress vs strain curve: A- from the biaxial model; B- Experimental results; C- correction due to straightening of the yarn crimp reprinted from [74]

2.5 Loss in performance in firefighter protective garments

Studies have shown that firefighter protective garments experience a loss in performance over time. For instance, assessments conducted on retired and in-service firefighter suits revealed significant mechanical losses among other factors [75]. In addition, Makinen reported that protective clothing over 10 years old and soiled are at a risky condition [76]: the tensile strength showed a loss of 40% in aramid-based suits after use and laundering. Additionally, the use of PBO has been barred from ballistic protective clothing due to its high sensitivity to moisture leading to extensive mechanical loss [77]. As a precaution, NFPA 1851 states that no firefighter protective garment shall be used for more than a period of 10 years [6]. However, the results by McQuerry et al. show that outer shell fabrics may go below the tear strength requirement of 22 Lbf well before that time [75].

This loss in performance is associated with the degradation occurring in textiles because of the ageing process [78], [79]. In the case of firefighter garment outer shell fabrics, it can be related to the processes undergone by the polymers of the high-performance fibers because of the ageing conditions experienced by the protective clothing. These ageing conditions include a variety of factors such as mechanical action, ultra-violet (UV) radiation, heat and moisture [7]. For instance, Day et al. simulated the ageing of outer shell fire protective clothing against light and heat exposure [80]. The outer shell fabrics were exposed to UV light at 0.75 W/m^2 at 420 nm for 40 hours at 60 °C and 42 °C. The same fabrics were exposed to heat at temperatures ranging from 250 °C for 7 minutes to 150 °C for 7 days. The specimens exposed to light showed color fading and a loss in tear strength of more than 33%. This large loss in mechanical performance raises some concerns about safety hazards such as puncture and tears. The specimens exposed to heat also showed a high tear strength reduction. For instance, the reduction in tearing strength was higher than 23% when exposed at 180 °C for 24 h. A reduction in thermal performance was also recorded after heat exposure.

This degradation can be identified with a variety of visual and nonvisual indicators [3], [17]. Visual signs may include a change in color, generally fading. The fabric may also become more brittle. However, Slater suggested that the actual degradation might begin even before the visual indicators are visible [3]. This was

confirmed by Rossi et al. who showed that a significant decrease in the mechanical strength of outer shell fabrics exposed to a combination of a convective heat and UV was observed before any visual indicators (i.e, discoloration) was exhibited by the sample [4]. There is thus a risk that a firefighter is not aware that their protective garment is not able to protect them any more from the hazards associated with their tasks because of ageing.

2.6 Degradation of polymers

All commercially available fire protective clothing are made of high-performance polymers like aramids, PBI, and PBO. The loss in performance by outer shell fabrics can be associated to the degradation of polymers. This section discusses the different causes of degradation in polymers and the mechanisms associated with them.

2.6.1 Mechanisms of chemical degradation

The process of degradation may involve the loss in physical and chemical properties due to a chemical modification in the polymer under the influence of heat, light, chemical or mechanical stress [81]. This section discusses the different mechanisms involved in polymer chemical degradation.

Backbone chain scission

There are two types of chain scission mechanisms, i.e. random scission and selective scission [82]. Random scission occurs randomly throughout the polymer backbone when the sensitivity of all groups is equal. Selective scission happens at sites having higher reactivity. Figure 2.16 depicts the difference between random and selective scission. In long duration hydrolytic and oxidative ageing, random scission predominates over selective scission [82].

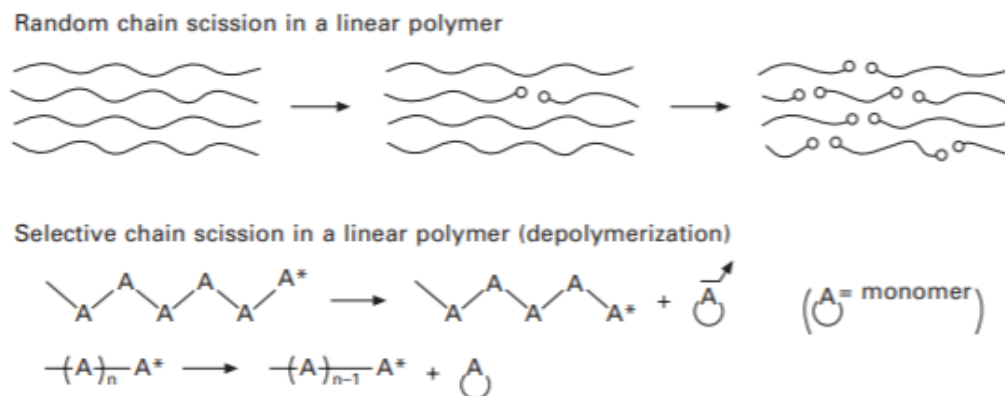


Figure 2.16 Schematic representation of random and selective chain scission reprinted from [82]

Depolymerization

Depolymerization is defined as the conversion of macromolecules into monomer units or oligomeric units [83]. Depolymerization begins with the formation of free radicals in the backbone chain by random scission. This is followed by propagation by three possible methods: intra molecular hydrogen transfer, inter molecular hydrogen transfer or unzipping [84]. Unzipping leads to the formation of monomer units whereas the other two methods lead to the formation of oligomeric units.

Oxidation

This is defined as the breaking of macromolecules into smaller oligomeric units by the action of oxygen [85]. Figure 2.17 represents the mechanism of oxidation in polymeric materials. Free radicals are formed and react with oxygen to form oxy and peroxy radicals. The formation of free radicals is initiated by the exposure to light, heat or through mechanical stress [86].

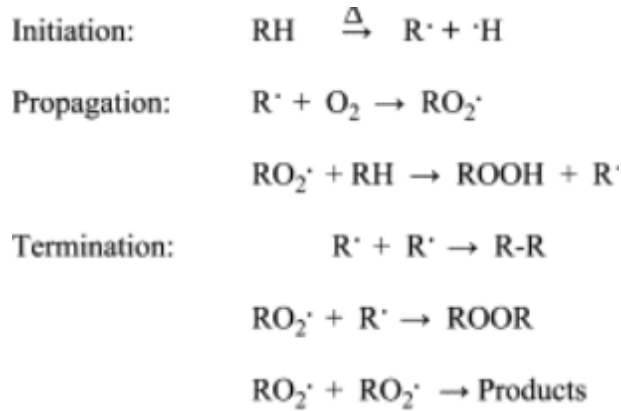


Figure 2.17 Oxidation mechanism in a polymer structure reprinted from [87]

Crosslinking

During the degradation process, the free radicals formed can form crosslink junctions at the free radical sites between different chains, which leads to a reduced mobility between the polymer chains [88]. Figure 2.18 illustrates the formation of crosslinks in a poly (ethylene terephthalate) structure. Such a reaction leads to an increased modulus and a decreased elongation at break.

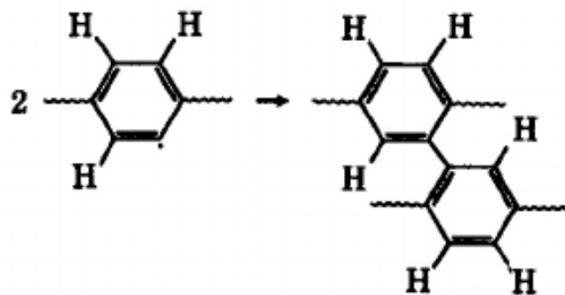


Figure 2.18 Formation of crosslinks in poly (ethylene terephthalate) reprinted from [88]

Side group cleavage

Side group cleavage or side group reactions occur prior to the chain scission process. These reactions can follow an elimination mechanism [89]. Figure 2.19 represents the process of the elimination mechanism.

The by-products from these reactions are generally short oligomeric units and hence, do not have an overall effect in the backbone of the polymer or its mechanical behaviour.

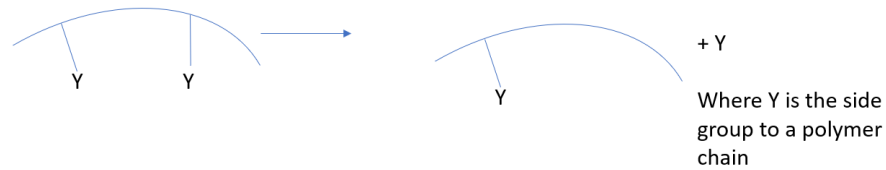


Figure 2.19 Elimination of a side chain group from a polymer chain

2.6.2 Degradation classified according to the environmental causes

Thermal degradation

Thermal degradation can occur in the presence or absence of oxygen. Degradation occurring in the absence of oxygen is termed pyrolysis [7]. Degradation occurring in the presence of oxygen is called thermally induced oxidation reaction [90]–[92]. Since ageing and weathering generally occur in the presence of oxygen, this section will focus on thermo-oxidative degradation [93], [94].

Thermo-oxidation involves oxygen as a catalyst and heat as a facilitator [95]. It comprises two different reactions [96]. One reaction involves the random scission of polymer chains induced by the formation of free radicals in the system. It leads to a loss in mechanical performance and molecular weight. The second reaction consists of chain end scission leading to the generation of volatile by-products. Figure 2.20 illustrates the thermo-oxidative degradation of hydrocarbon polymers. The first step leads to the formation of peroxide radicals by the application of heat in the system. The peroxide radical formed attacks the main backbone and generates free radicals that lead to random scission in the polymer chain. There is also a possibility of crosslinks formed by the free radicals. Eventually, the process of termination occurs by coupling or disproportionation.

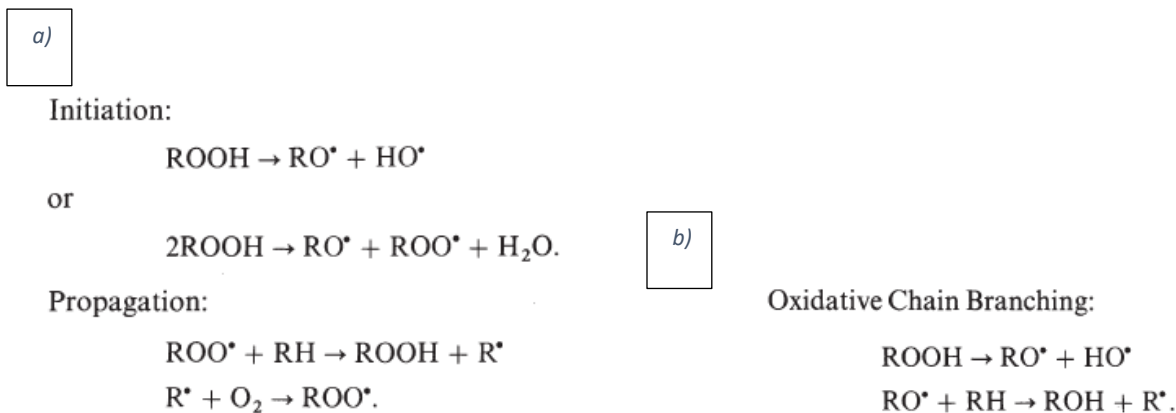


Figure 2.20 The thermal degradation mechanism in polymer chains: (a) Initiation and propagation (b) Oxidative termination reprinted from [90]

Thermo-oxidation is a bulk phenomenon where oxygen permeates into the bulk of the polymer [96]. However, this movement of oxygen can be influenced by the chain flexibility on the surface thus altering the rate of oxidation in the bulk [90].

Photochemical degradation

Photochemical degradation occurs following the absorption of UV radiation by the polymer structure [90]. UV radiation expands over a wavelength spectrum of 100 nm to 400 nm. However, radiation with a wavelength below 290 nm is screened by the ozone layer. Thus, UV radiation with wavelengths from 290 nm to 400 nm is primarily responsible for photo-oxidation reactions on earth [90].

UV susceptible polymers usually contain functional groups that are sensitive to UV absorption [90]. However, structural irregularities or impurities introduced into the structure can also lead to an increased sensitivity to UV [90]. Table 2.6 highlights the activation range of different classes of polymers.

Table 2.6 Main absorption wavelengths of UV radiation for different polymer grades [95]

Polymer	Absorption wavelength
Polyesters	325 nm

Polystyrene	318 nm
Polyethylene	300 nm
Polypropylene	310 nm
Poly (vinyl chloride)	320 nm
Poly (vinyl acetate)	280 nm
Polycarbonate	295 nm
Poly (methyl methacrylate)	290-315 nm
Polyoxymethylene	300-320 nm
Cellulose Acetate Butyrate	295-298 nm

The first step in the photo-oxidation mechanism involves the absorption of radiation, which leads to the formation of free radicals [97,99], similarly to what happens in thermal degradation. Thermal degradation and photodegradation are similar in many ways, but there are some differences. Photo-oxidation is a surface phenomenon; the radiation does not penetrate in the polymer bulk. On the other hand, thermal degradation is a bulk phenomenon as mentioned previously.

After the formation of free radicals in the polymer structure, the reaction proceeds by the traditional free radical chain mechanism [93]. The free radicals formed show a propagation mechanism leading to many short chain free radicals in the structure. This continued generation of free radicals leads to a lower molecular weight as well as poor mechanical performance.

Hydrolytic degradation

Hydrolytic degradation occurs upon exposure of polymer systems to water and moisture [7]. Polymers prepared by polycondensation reactions are the most sensitive to this type of degradation. Those containing functional groups such as ester, amides or ethers are highly sensitive to hydrolysis. Hydrolytic degradation happens in two steps. It begins by the hydrolysis of the moisture-sensitive group in the polymer backbone.

Then, it is followed by the random scission of the polymer chains, ultimately leading to a loss in molecular weight and mechanical performance [98].

The rate of hydrolysis is influenced by various structural parameters [99]. For instance, in the case of Nylon, which is hydrophilic in nature, Nylon 11 shows a higher stability to hydrolysis than Nylon 66 due to longer hydrocarbon chains. In addition, the hydrolysis affects more the amorphous regions than in crystalline regions due to a disordered nature of polymer chains in the amorphous regions [90], [100]. Surface characteristics can also play a vital role in polymer sensitivity to hydrolysis. The absorption of water or moisture is affected by the flexibility of chains at the surface [90]; rigid chains do not allow the easy permeation of water into the structure hereby, improving the resistance to hydrolysis.

Mechanical degradation

Mechanical degradation is induced by the presence of shearing forces and stresses applied on the system leading to a loss in mechanical properties and molecular weight [101], [102]. Many factors such as the degree of crystallinity and the presence of impurities and defects in the structure influence the rate of mechanical degradation [103]. “Mechano-radicals” are created when external mechanical stress is applied to the system [103], [104]. In semi-crystalline solid polymers, the movement of chains is highly restricted. As a result, the phenomenon of chain scission is highly localised. Due to the lack of mobility of chains in the structure, chain termination occurs by the abstraction of hydrogen from the neighbouring molecule thus leading to the propagation of the formed radicals and hence the formation of sub microcracks as shown in Figure 2.21. The overall loss in performance is attributed to the formation of these localised microcracks in the structure, leading to a loss in physical and chemical properties.

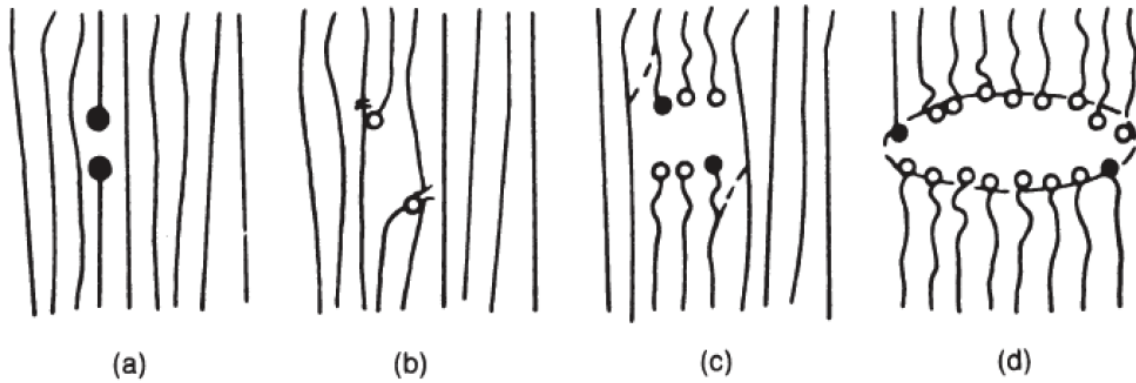


Figure 2.21 The formation of "mechano-radicals" in a polymer structure under stress reprinted from [104]

Biological degradation

Biodegradation involves the action of microbial species to convert organic molecules to low molecular weight species with the formation of carbon dioxide and water [105]–[107]. The first step involves the colonisation by the microbial species, which is highly influenced by the amount of exposed surface and the deterioration caused by weathering on the surface of the polymer systems. The backbone chain undergoes a biochemical transformation reducing the polymer substrate to simpler systems, which results in discoloration and loss in mechanical strength [108].

The surface properties of the polymer play an important role in the colonization by the microbial species [96]. Factors such as the molecular weight and crystallinity highly influence the degree of colonization by the microbial species.

2.7 Hydrothermal ageing of high-performance polymer fibers

Exposure of firefighter clothing to water may result from the water medium used to extinguish fires, steam, weather, laundering, and firefighter perspiration [109]. Mandal et al. studied the performance of fire protective clothing when exposed to hot water and steam [110]. Standard tests exist to evaluate the transmission of heat through the fire protective clothing in the case of hot water splashes [111] and

immersion in hot water [112]. In terms of laundering, the current version of the NFPA 1851 standard recommends subjecting firefighter bunker gear to advanced cleaning at least twice a year [6]. It involves machine washing with a mild detergent in water at a temperature not exceeding 40°C.

Studies have also investigated the hydrothermal ageing of high-performance polymer fibers, in particular those used in firefighter clothing outer shell fabrics. Arrieta et al. studied the effect of hydrolytic ageing on a Kevlar®/PBI blend fabric [113]. This study exposed yarns taken from a fabric made of 60-40 wt% of Kevlar® and PBI staple fibers reinforced with Kevlar® filaments to relative humidity of 65 and 80% at three different temperatures (50, 60 and 80°C). The yarns showed a consistent decrease in strength with an increase in temperature. However, the loss in strength appeared to be independent of the relative humidity levels used in the study. The authors reported an Arrhenius behavior for the yarn strength loss, similarly to what had been observed previously for the hydrolysis of polycondensates [114], [115]. Based on the absence of effect of the moisture ratio on the loss in performance, they also concluded that the absorption of water in Kevlar® occurs faster than the hydrolysis reaction. Energy Dispersive X-ray (EDX) analysis identified the presence of traces of sulfuric acid in the yarns which are believed to act as a catalyst for the hydrolysis reaction of Kevlar®.

Aidani et al. studied the hydrolytic degradation of moisture barriers used in fire protective clothing [116]. The moisture barriers studied were composed of an e-PTFE film laminated on a Nomex® woven fabric. The fabric specimens were exposed in a humidity chamber at a temperature of 50, 70, and 80°C at a relative humidity varying between 60% to 100% for times between 1 and 600h. ATR-FTIR (Attenuated total reflectance-Fourier transform infrared spectroscopy) was run to identify the changes occurring the Nomex® fibers with an increase in exposure time. A new band at 1725 cm⁻¹ was observed for the aged specimens. It indicates the presence of carbonyl groups. The authors attributed it to the hydrolysis of the amide bond in the Nomex® molecule. EDX analysis shows the presence of traces of sulphur in the Nomex® fabric which is introduced as a solvent during the manufacturing of Nomex® fibers and would act as a catalyst for the hydrolysis reaction. SEM analysis was performed on the unaged and aged specimens. It revealed physical

changes on the surface of the fibers in the form of cavities, thus corroborating the occurrence of hydrolytic ageing. The water vapor permeability of the ePTFE layer was studied to analyse the degree of hydrolytic degradation. Water vapor permeability showed a consistent decrease with increase in ageing time which was attributed to the closure of pores on the ePTFE layer. A possible reason for this closure was attributed to the degradation of the PU adhesive.

Wiggans et al. studied the effect of elevated temperature and humidity on 5-amino-2-(p-aminophenyl) benzimidazole (PBIA) [117]. Two different copolymer yarns on smooth bobbins were aged in an environmental chamber at temperatures varying from 25°C to 70°C with a relative humidity ranging from 41% to 76%. Tensile measurements were performed to investigate the effect of ageing on the fibers. Both sets of copolymer yarns showed limited loss in tensile strength throughout the exposure time, i.e. 11-13% after 303 days at 70°C and 76% RH. The Young's modulus and elongation at break remained unchanged for the yarns. ATR-FTIR hinted at a few changes in the chemical structure, but no distinct degradation mechanism could be deciphered. Both types of fibers showed a higher resistance to hydrolytic exposure as compared to PPTA(p-phenylene terephthalamide) fibers.

Mead et al. studied the effect of accelerated ageing on Nylon 66 and Kevlar® 29 at elevated temperatures and humidity [118]. The yarns were exposed at 50% RH at temperatures of 110°C, 130°C and 150°C for a period of six months. The test was conducted on two types of yarns: 210 denier Nylon 66 yarns and 1500 denier Kevlar® 29 yarns. The Nylon yarns showed a 40% loss in strength at 110°C and 85% loss at 150°C. On the other hand, the Kevlar® yarns showed a loss of 10% at 130°C and 32% at 150°C. This difference in moisture sensitivity of the two yarns was attributed by the authors to the presence of aromatic rings in the backbone structure for Kevlar®, which has a high resistance to thermo-oxidative degradation.

Auerbach studied the dependence of the tensile strength of Nylon and Kevlar® yarns to lower and elevated temperatures at varying degrees of relative humidity [119]. The study was performed for two different types of yarns: 210 denier Nylon 66 and 1500 denier Kevlar® 29 yarns. The samples were placed in an environmental chamber with varying temperatures and humidity levels. A first set of yarns were exposed

to relative humidity levels of 0, 10, 50, and 90% at 25°C. The other set of yarns were exposed to different temperatures at a 100% relative humidity. The study revealed that at lower humidity levels, the degradation proceeded through a thermo-oxidative process, which transitioned to a moisture-induced degradation as the relative humidity level increased. Moreover, Nylon resisted degradation at the lowest temperatures whereas Kevlar® showed a consistent reduction in tensile strength with increasing temperature.

Davis et al. studied the effect of moisture and UV ageing on the performance of outer shell fire protective clothing [120]. Two different fabrics were used for this study: a 60-40% of Kevlar®/PBI rip-stop weave fabric and a Nomex®, Kevlar® and carbon fibers (Nomex® IIIA) plain weave fabric. The hydrothermal aging involved a temperature of 50°C at a 50% relative humidity. The two fabrics did not show any statistically significant change in the tear strength after an exposure duration of 56 days. The yarns were also tested and showed a similar response to that of fabrics. On the other hand, when the fabrics were simultaneously exposed to UV, they showed a consistent decrease in tear strength. The Kevlar®/PBI rip-stop fabric showed a higher resistance to UV as compared to the Nomex® IIIA plain weave fabric, which can be attributed to the higher sensitivity of Nomex® to UV.

2.8 Mechanical testing of polymers

For polymeric materials, mechanical properties are important in all applications. In case of degradation studies, the loss in strength can reveal the occurrence of ageing processes in progress.

Various parameters are analysed to characterize the mechanical behaviour of polymeric materials. These include Young's modulus, elongation at break, and flexural modulus. Polymer mechanical testing can be conducted at different loading configurations, to simulate what is experienced in real life service. Two tests, which have been used to characterize the performance of the end-of-life sensors (Chapter 5), are described below: the static bending test and the fatigue test.

2.8.1 Static bending testing of polymers

Flexural testing involves measuring the force required to bend a polymeric part and gathers information on the resistance to flexing, i.e. the stiffness of a material [121]. The flexural modulus indicates the degree of flexing a material can undergo before permanent deformation. This measurement can be done with a three point bending test or a four point bending test (Figure 2.22). In most applications, a three point bending test is used with the exception of textile fiber reinforced plastics, where a four-point bending test is preferred [122]. Flexural tests are however not suited for rubbers since these tests are applicable for rigid to semi rigid plastics and are difficult to perform for low modulus applications.

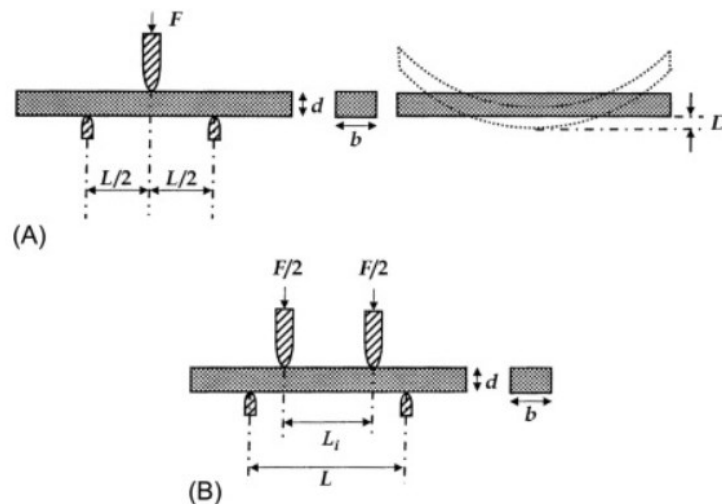


Figure 2.22 (A) Flexural testing with a three point bend configuration (B) Flexural testing with a four point bend configuration reprinted from [122]

Several standard test methods have been developed to characterize the flexural modulus of plastics. This thesis uses the standard test method ASTM D790-03 [123] for measuring the flexural modulus at small and large deformations. A rectangular test specimen is positioned on a support span of varying lengths. It is loaded with an overhead nose midway between the supports. The strain rate is determined on the basis of how fast or slow the material takes to break. For materials that break at a slower rate, the strain rate is 0.1

min^{-1} , whereas for materials that break at a faster rate (brittle materials), the strain rate is 0.01min^{-1} . A typical flexural stress vs flexural strain curve is shown in Figure 2.23.

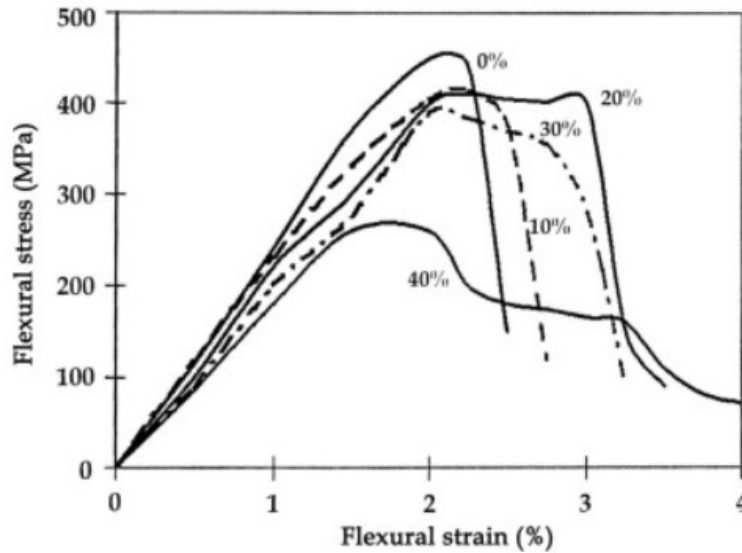


Figure 2.23 Flexural stress vs flexural strain curve reprinted from [122]

For 3-point bending tests, the flexural modulus E_b is calculated using equation 2-8.

$$E_b = \frac{L^3 m}{4bd^3} \quad (\text{equation 2-8})$$

Where L is the support span length, m is the slope of the initial linear portion of the curve, b is the width of the beam tested and d is the depth (thickness) of the beam.

2.8.2 Fatigue testing of polymers

Fatigue testing involves the repetitive loading of a polymeric material to study the effect of these loading cycles on the long term performance of the material and make sure that they are safe for the intended application or will be replaced before failure [124]. Fatigue tests usually involve recording the S-N curve (i.e., applied stress vs the number of cycles prior to failure). A typical S-N curve is shown in Figure 2.24.

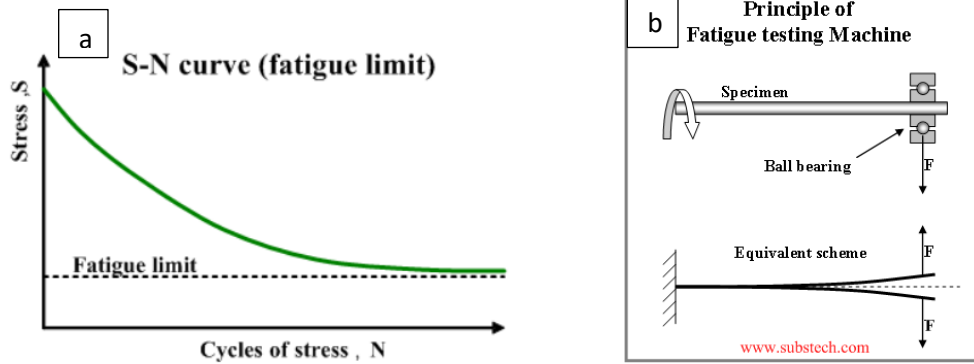


Figure 2.24 (a) S-N curve for a flexural fatigue test (b) Examples of fatigue tests reproduced from [125]

In the case of deformation-controlled tests, the material undergoes softening due to repetitive loading [124]. However, this does not lead to the ultimate failure of the specimen. This is the opposite of load-controlled tests, which lead to eventual failure. Thus, the need to define a failure criterion is of paramount importance before starting a load-controlled fatigue test. This criterion depends on the application the material is intended for. For the current thesis, the failure criterion is set at two orders of magnitude from the original condition.

Various test standards have been developed to measure the fatigue response of polymeric materials. This thesis uses ASTM D7774-17 for measuring the fatigue response of the material [126]. A rectangular test specimen is kept on two supports with varying length and loaded with an overhead nose midway between the supports. The specimen is then cyclically loaded at a uniform frequency ranging from 1 Hz to 25 Hz until the specimen ruptures, yields or the required number of cycles have been completed. The data is reported in the form of an S-N curve.

Chapter 3 Materials and Methods

3.1 MATERIALS TESTED

Eight different fire-resistant woven fabrics used in outer shell for fire fighter protective clothing have been selected for the study. All the fabrics studied are listed down in Table 3.1. They were characterised based on fiber content, fabric count, weave construction, yarn type and linear density (Section 4.1).

Table 3.1 List of the fabrics studied

FABRIC CODE	FABRIC COMPOSITION*
Fabric MA	PBI/Kevlar®
Fabric MB	PBI/Kevlar®/LCP
Fabric MC	Kevlar®/Nomex®
Fabric MD	Kevlar®/Nomex®
Fabric ME	Kevlar®/Nomex®/PBO
Fabric MF	Kevlar®/Nomex®/Antistat
Fabric MG	Kevlar®/PBI
Fabric MH	Kevlar®/PBI

*Information provided by the manufacturer

3.2 SPECIMEN PREPARATION

The specimens were prepared according to ASTM D5035 [127] to measure the initial and residual tensile strength of the fabrics in the warp direction. The specimen is rectangular in shape with dimensions of 15cm x 3.5cm as shown in Figure 3.1.



Figure 3.1 Schematic representation of the tensile strength specimen

Each specimen was raveled to 2.5 cm (See Figure 3.1). Raveling consists in taking out a number of yarns from a woven fabric with the objective of ensuring that the yarns run the full length of the specimen, i.e., are held in the lower and upper grips of the tensile tester [128].

After raveling, the specimens were placed in a conditioning room at 21°C and 65% relative humidity for at least 24 hours before testing according to the standard test method (ASTM D5035). Sample conditioning

is an important element to obtain measurement repeatability with textiles as temperature and moisture content strongly affect the performance of fibers (ASTM D1776) [129].

3.3 HYDROTHERMAL AGEING

The hydrothermal ageing was done at three different ageing temperatures, i.e. 60°C, 80°C and 90°C, for up to 50 days. Specimens were immersed in water and collected at 5-day intervals.

3.3.1 Starting the oven

An oven (Heratherm OGH 60, ThermoFisher Scientific) was used to keep the immersed specimens at the designated temperature (see Figure 3.2). The oven was initially preheated to the set temperature for 1 hour. Then, 500-ml glass flasks filled with reverse osmosis (RO) water preheated at the same temperature as the oven were left in the oven while the specimens were being wetted (section 3.3.2).



Figure 3.2 Oven utilised for hydrothermal ageing

3.3.2 Wetting the specimens

The raveled specimens were wetted with RO water in a tray using a roller (Figure 3.3) before being inserted into the flasks contained in the oven. After wetting, the specimens were rolled in groups of five specimens corresponding to the five replicates measured for each condition. The specimen rolls were inserted into the preheated water flasks. The flasks were capped with a temperature resistant rubber stopper with two holes to limit the amount of evaporation while avoiding the buildup of pressure inside the flasks.



Figure 3.3 Wetting tray used for wetting the fabric specimen with the roller

3.3.3 Collecting specimens.

Specimens were collected every 5 days. The maximum ageing time was 50 days. RO water preheated at the required temperature using a kettle was added into the flasks at regular intervals to compensate for evaporation so that the fabric specimens remain immersed in water.

3.3.4 Drying and conditioning specimens

After the specimens were taken out from the water, they were allowed to dry flat on a drying rack. This usually lasted for 5 days. After the specimens were dry, they were moved to the conditioning room and left to condition for at least 24h (Figure 3.4).



Figure 3.4 Conditioning racks for the fabric specimens

3.4 YARN CRIMP AND LINEAR DENSITY MEASUREMENT

The crimp and linear density of the different fabric yarns were measured according to the standard test method ASTM D3883-04 [130]. Fabric specimens with dimensions of 310 mm x 25 mm were cut in the warp direction. Two marks spaced at 250mm apart were made on the fabric specimen. This distance is the initial length of the yarn, i.e., with crimp. Before measuring the initial length, the specimens were conditioned at 21°C and 65% RH for at least 24 hours.

Fabric specimens were raveled to obtain 310mm warp yarns. A crimp tester (Figure 3.5) was used to straighten out each yarn and determine the true yarn length after removing the crimp. One side of the yarn was fixed to an immovable edge of the crimp tester by locating the mark at the set position. The other end of the yarn was fixed to the movable edge of the twist tester which was connected to weights by a string.

After fixing the yarn to the equipment, the crimp in the yarn was slowly taken out by adding weights to the movable end until the entire crimp in the yarn was removed. When the yarn stopped extending, the reading on the scale was recorded. This value corresponds to the change in length of the yarn introduced because of crimp.

Then, the yarns were cut at the 250mm spaced apart marks made when they were in the fabric and weighed. The experiment was repeated for 10 different yarns for each yarn type in each fabric.

The crimp and linear density were calculated using the equations below.

$$\% \text{ crimp} = \frac{\text{Average change in length } (\Delta L)}{\text{Initial length}} \times 100 \quad (\text{equation 3-1})$$

$$\text{Linear density (in tex (g/km))} = \frac{\text{Total mass of 10 yarns (g)}}{\text{Total yarn length (cm)}} \times 100,000 \quad (\text{equation 3-2})$$

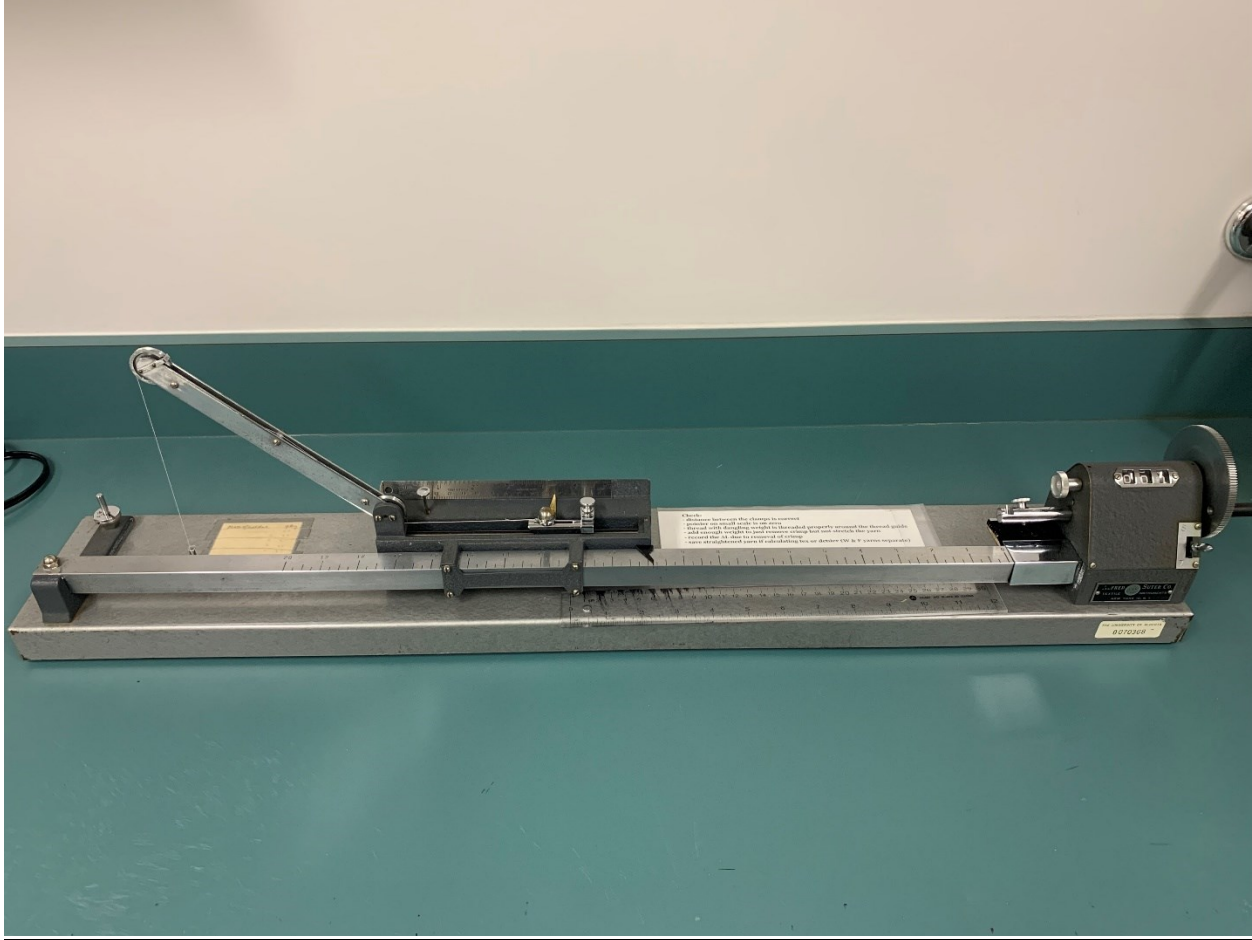


Figure 3.5 Yarn crimp tester equipment

3.5 RESIDUAL STRENGTH MEASUREMENT

The strength of the specimens was measured in the initial condition as well as after ageing. The specimens were conditioned before testing. The test was performed both on yarns and fabrics. The sections below describe individually the measurement protocol for the fabrics and the yarns.

3.5.1 Fabrics

The tensile strength of the fabrics was measured according to the ASTM D5035 test method [127] using the raveled strip procedure in the warp direction. A Universal Testing machine (Model 5565, Instron Corporation, USA) shown in Figure 3.6 equipped with a load cell of 10kN was used to deform the fabric

specimens at a speed of 100 mm/min. The fabric specimens were gripped at both ends using pneumatic grips with rubber faces. The fabric specimens were deformed until they failed. The data were obtained as load vs extension for each of the specimens. Five specimens were tested for each condition.

Besides this, the fabrics were deformed at a reduced speed and observed using a portable microscope to see changes occurring at the microscopic scale with increasing tension. The tests were conducted at 30mm/min. The slow-motion video of the fabric under deformation produced was synchronized with the recording of the stress vs strain curve.

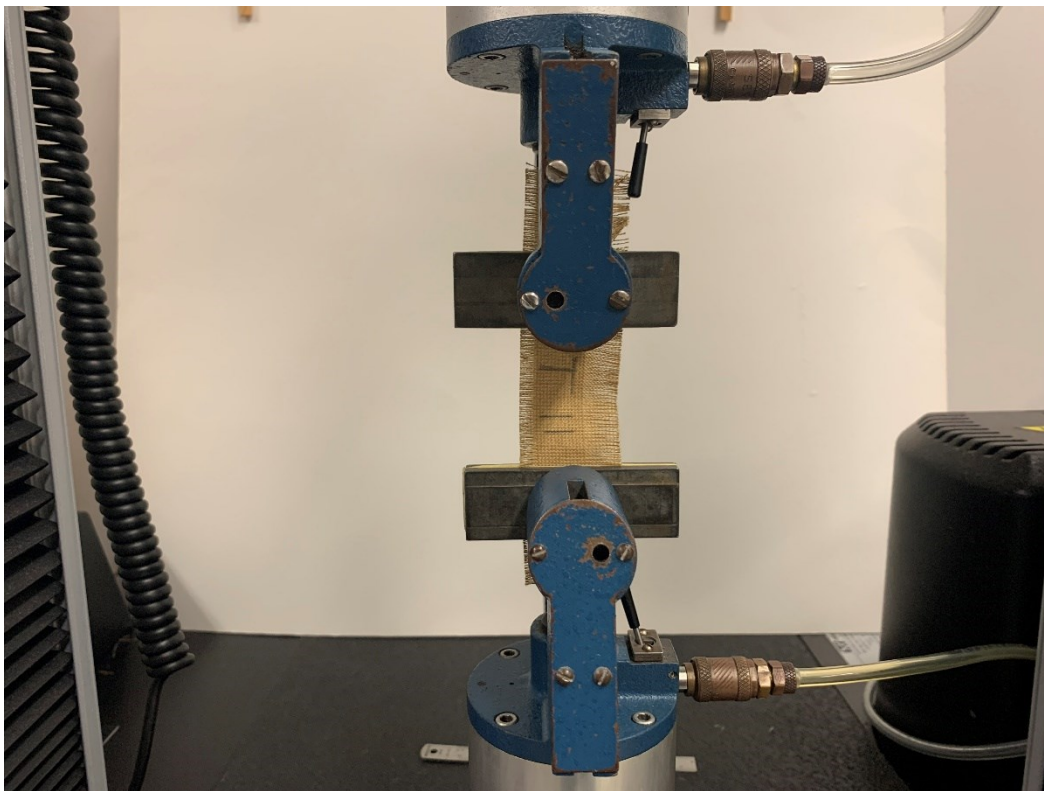


Figure 3.6 Universal Testing Machine used for mechanical testing of the fabric and yarn specimens

3.5.2 Yarns

The tensile strength of yarns taken out from the fabric specimens was also assessed. The same Universal Testing Machine was used to stretch the 150mm long yarns until failure. The test was performed on one yarn at a time. Grips with sandpaper were used to hold the yarn specimens. The yarn specimens were tested at a speed of 30mm/min with a gauge length of 50mm. The results were reported as load vs elongation curves for each specimen. 12 replicates were tested for spun yarns. In the case of filament yarns, the number of replicates depended on their availability in the structure of the fabric. In general, it was possible to measure seven replicates. However, in the case of some filament yarns, the number of yarns available in the specimen was lower.

Similar to what was done with fabrics, a slow-motion video using a portable microscope was produced for some of the yarns to see the changes occurring with increasing tension.

3.6 OPTICAL MICROSCOPY

A stereomicroscope (Stemi 508 Optical microscope (Figure 3.7)) with a magnification ranging from 2x to 50x and equipped with an eye lens with a fixed magnification of 10x, was used to analyze the effect of ageing on the microstructure at the fabric and yarn scale.

A portable microscope, having a single lens with magnification ranging from 2x to 56x was used to observe the specimen during mechanical testing at low speed to observe intricate changes to the specimen structure when deformed (Section 3.5.1 and 3.5.2).



Figure 3.7 Optical microscope Stemi 508

3.7 SENSOR FABRICATION AND TESTING

This section discusses the experimental tools and the materials explored for the fabrication of end-of-life sensor as described in Chapter 5.

3.7.1 Film Applicator

Epoxy film encapsulation was performed with an Elcometer 4340 motorized film applicator and an Elcometer 3570/2 micrometric film applicator (Figure 3.8), which are used for a uniform film deposition on a variety of substrates such as steel sheets, plastic foils, glass slabs, and polymer substrates. The equipment can apply films of thickness ranging from 10 μm to 1mm. The flat bed, on which the substrate is kept, is vacuum controlled allowing a proper grip of the substrate and ensuring uniform film thickness. The Elcometer 3570/2 micrometric film applicator was used to control the thickness of the film being

applied on whereas the speed settings were optimised using the controller on the equipment in such a way so that uniform film thickness could be obtained throughout the polymer substrate.



Figure 3.8 Film applicators used for the encapsulation of end of life sensors

3.7.2 Laser Engraver

A 70 W 10.6 μ m CO₂ laser scribing system (PLS 6.150D, Universal laser system Inc.) designed for patterning (Figure 3.9) was used to print the graphene tracks on the polymer substrate. Before starting the experiment, the power, speed, and the pulses per inch value are optimised based upon the material on which the tracks were being printed on. Once, the settings are optimised, the material is installed on the printing table, and the process starts based upon the input design given by the user. Once the printing is completed, the material is left in place for some time to allow for the gases to vent out.

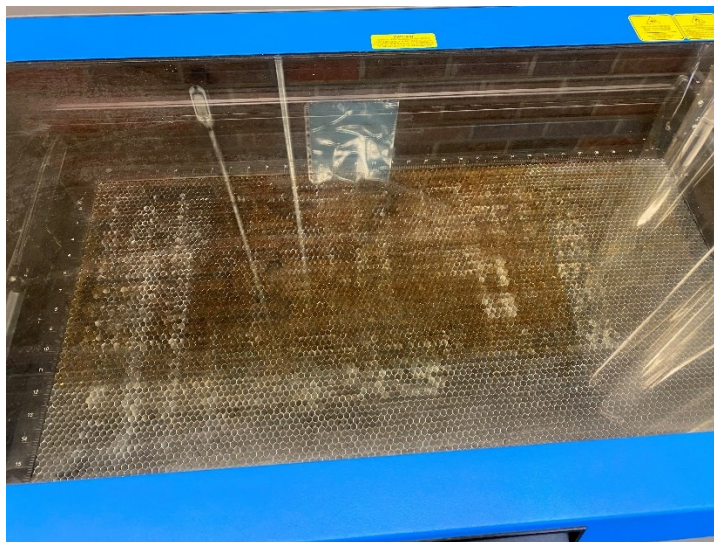


Figure 3.9 Laser scribing equipment used to develop LIG sensors

3.7.3 Epoxy Materials

Candidate materials for the sensor encapsulation were chosen on the basis of the parameters listed below:

- High mechanical performance, including abrasion resistance
- High thermal resistance
- Good processing conditions (low curing temperatures, lower viscosity)

On the basis of the above parameters, epoxy resins were chosen as an ideal candidate for the encapsulation of the sensor. The epoxy resins used in the current thesis are listed in Table 3.2.

Table 3.2 Inventory of the epoxy resins used

Epoxy candidate	Thermal properties	Mechanical Properties	Processing Conditions
EpoxAmitte HT	Provides high temperature resistance up to 149 °C	- Tensile strength: 32100 psi - Tensile modulus: 2,150,000 psi	- Viscosity: 650 Cps - 24 hour curing time

		- Elongation at Break: 2.3%	
Epox Acast 670 HT	Provides high temperature resistance up to 177°C	- Tensile strength: 4500 psi - Tensile modulus: 332,000 psi – - Elongation at Break: 0.65%	- Viscosity: 6000 Cps - 24 hour curing time

3.7.4 Bending Tester

A Cellscale Univert mechanical tester, with a load cell of 200 N, is used for performing the bending and fatigue tests on the sensors produced (Figure 3.10). A 3-point bending test setup with a support span of length 2 cm was used in its operation. The sensors were mounted on the setup and the load was applied midway through the nose overhead. The strain rate was predetermined accordingly using the standard ASTM D790-03 (for static bending) and ASTM D7774-17 (for flexural fatigue test). For each test, three sensors were tested.

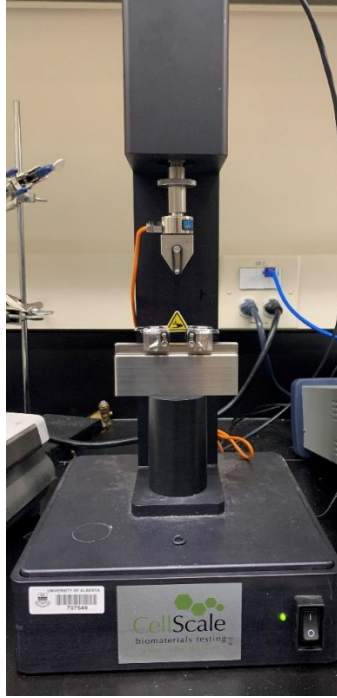


Figure 3.10 Cellscale mechanical tester used for the bending test

3.8 STATISTICAL ANALYSIS

For the ageing studies performed, statistical analysis tools have been employed to study significant difference in the extent of degradation with each measured value. These tools include a paired t-test, which checks for the statistical difference between two groups of data having the same type of data. The obtained p-value from the test is used to determine whether to accept or reject the null hypothesis. A p-value of greater than 0.5 indicates that there is no significant difference between the two groups of data.

Moreover, ANOVA (Analysis of Variance) tool also has been used in the ageing study to determine significant difference in the entire ageing study. ANOVA is usually employed when multiple groups of data exist (more than 2) and we need to know whether or not there is statistical difference between these specific groups. Again, a p-value of 0.5 also indicates that there is no statistical difference between these groups or in other words these groups are statistically identical.

4.1 FABRIC CHARACTERISATION

The fabrics were characterised in terms of crimp and linear density (see table 4.1). Table 4.1 also includes other characteristics of these fabrics such as the weave, fabric count, and type of yarn obtained by another student [131]. The information in terms of fiber content was obtained from the fabric manufacturers.

Table 4.1 Fabric characteristics of the tested fabrics

	Fiber Content # Weight**	Weave**	Warp x Weft** (Nb./cm)	Type of Yarn**	Yarn Content**	Linear Density (tex)	Crimp
Fabric MA	36% PBI and 64% Kevlar®, 234 g/m ²	Twill Weave	18 x 17	Spun Yarn	PBI & Kevlar® staple fiber	93	5%
				2 ply Spun/ Filament Yarn	PBI & Kevlar® staple fiber	68	3%
					Kevlar® filament		
Fabric MB	55% Kevlar® 37% PBI 8% LCP, 246 g/m ²	Plain Weave	16 x 15	Spun Yarn	PBI & Kevlar® staple fiber	100	7%
				Spun Yarn	PBI & Kevlar® Staple fiber	78	6%
				Filament Yarn	LCP		
Fabric MC	65% Kevlar® with 35%	Plain and Twill Weave	24 x 24	Spun Yarn	Kevlar® and Nomex® staple fiber	56	6%

	Nomex, 222 g/m ²			Filament Yarn	Kevlar® filament yarn	48	4%
Fabric MD	60% Kevlar and 40% Nomex 227 g/m ²	Twill Weave	19 x 18	Spun Yarn	Kevlar® and Nomex® staple fiber	109	4%
				Spun Yarn	Kevlar® staple fiber	59	3%
Fabric ME	60% Kevlar 20% Nomex and 20% PBO 226 g/m ²	Twill Weave	19 x 18	Spun Yarn	Kevlar®, Nomex®, PBO staple fiber	62	6%
Fabric MF	93% Nomex, 5% Kevlar & 2 % Anti stat 257 g/m ² *	Plain Weave	28 x 17	Spun Yarn	Kevlar® and Nomex® staple fiber	51	16%
Fabric MG	65% Kevlar 35% PBI, 214 g/m ²	Twill Weave	24 x 22	Spun Yarn	PBI & Kevlar® staple fiber	53	5%
				Filament Yarn	Kevlar® filament yarn	46	2%
Fabric MH	65% Kevlar 35% PBI, 247 g/m ²	Twill Weave	19 x 20	Spun Yarn	PBI & Kevlar® staple fiber	79	3%
				Filament Yarn	Kevlar® filament yarn	66	1%

Data obtained from fabric manufacturers

** Data from [131]

These eight woven fabrics have a fabric content comprised mostly either of Kevlar® and Nomex® (MC, MD, ME, MF) or Kevlar® and PBI (MA, MB, MG, MH). Fabric ME also includes 20% of PBO fibers in addition to the Kevlar® and Nomex®. Fabric MF includes 2% of antistat fibers (carbon fibers). Fabric MB includes LCP filament yarns.

The fabrics have different structures including plain weave (MB, MF), twill weave (MA, MD, ME, MG, MH) and a combination of plain and twill weave (MC). The structure of Fabrics MC, MG and MH involves a matrix of filament yarns with spun yarns in between. They have varying fabric counts (number of yarns per cm) with Fabric MB having the lowest fabric count (16 yarns per cm) in the warp direction and Fabric MF having the highest fabric count (28 yarns per cm) in the warp direction. Fabrics MD, ME, MF only include spun yarns whereas Fabrics MA and MB involve a unique arrangement of a 2-ply spun yarn and a 2-ply spun/filament yarn.

4.2 MECHANICAL BEHAVIOUR OF THE UNAGED FABRICS

The mechanical behaviour of the eight different fabrics was analysed in the initial condition both at the fabric and yarn scale.

4.2.1 FABRIC SCALE

The mechanical behaviour of the fabrics was tested according to the method described in Section 3.5.1. The results for each individual fabric are depicted below.

a. Fabric MA

Figure 4.1 shows the load extension curve for Fabric MA with the five replicates tested. Fabric MA exhibits the typical three-part behaviour when tension is applied (See section 2.4.4). First, it shows a very low increase in load with increasing deformation, which corresponds to crimp interchange. Above an extension

of 3.8mm, the load starts increasing significantly. The Young's modulus measured in the phase 2 region is equal to 197 ± 8 N/mm. The breaking strength is 1020 ± 40 N and the maximum extension at break is 9.0 ± 0.4 mm. The coefficient of variation of the three parameters is in the range of 4%; the degree of variability between the specimens is quite low. Figure 4.2 shows an example of the specimens before and after mechanical testing.

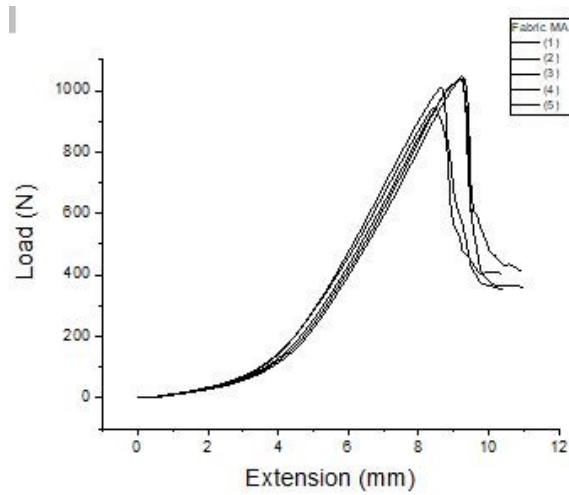


Figure 4.1 Mechanical behaviour of Fabric MA in the unaged condition

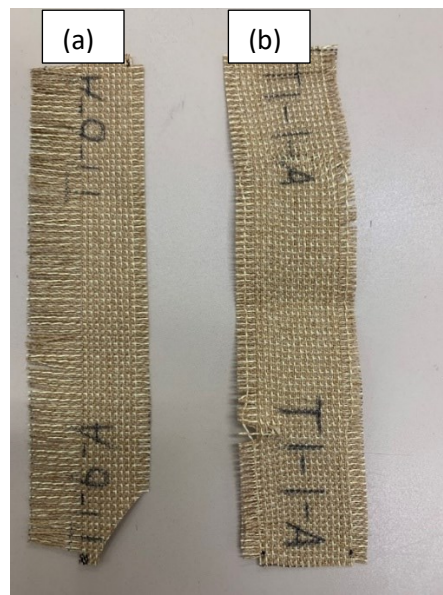


Figure 4.2 Fabric MA specimen a) before and b) after testing

b. Fabric MB

Figure 4.3 shows the load extension curve for Fabric MB with the five replicates tested. Fabric MB shows the typical three-part behaviour when tension is applied. First, it shows a very low increase in load with increasing tension, which corresponds to crimp interchange. Above an extension of 6mm, the load starts increasing significantly. The Young's modulus in the phase 2 region is equal to 160 ± 8 N/mm. The breaking strength is 1230 ± 30 N and the maximum extension is 13.7 ± 0.5 mm. The coefficient of variation for these three parameters lies in the range of 9%. Figure 4.4 shows an example of the specimens before and after testing.

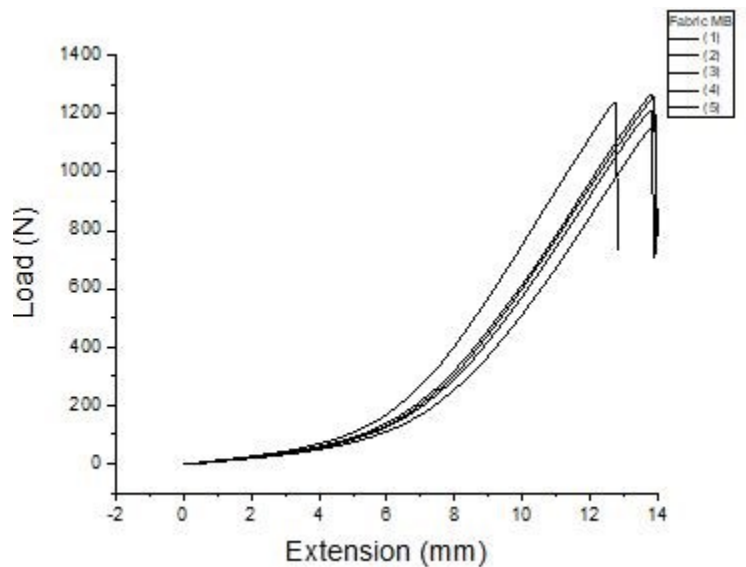


Figure 4.3 Mechanical behaviour of Fabric MB in the unaged condition

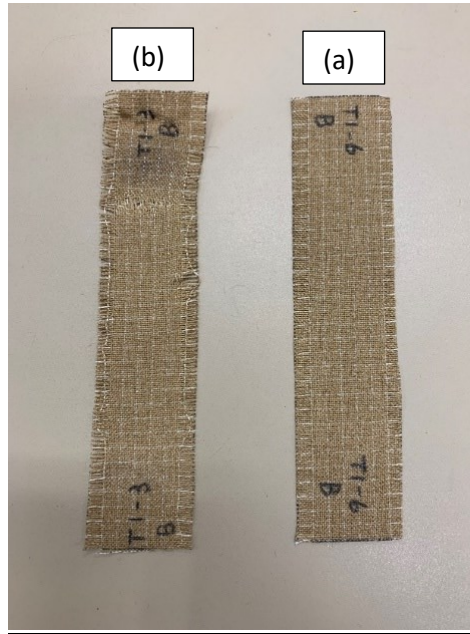


Figure 4.4 Fabric MB specimen (a) before and (b) after testing

c. Fabric MC

Figure 4.5 shows the load extension curve for Fabric MC with the five replicates tested. Fabric MC shows the typical three-part behaviour when tension is applied. Initially, it shows a very low increase in load with increasing strain, which corresponds to crimp interchange. Above an extension of 4.5mm, the load starts increasing significantly as the strain increases. The Young's modulus of the phase 2 region is equal to 158 ± 6 N/mm. The breaking strength is 1230 ± 40 N and the maximum extension at break is 12.3 ± 0.6 mm. The coefficient of variation for these three parameters lies in the range of 4%; the degree of variability between the specimens is quite low. Figure 4.6 shows an example of the specimens before and after testing.

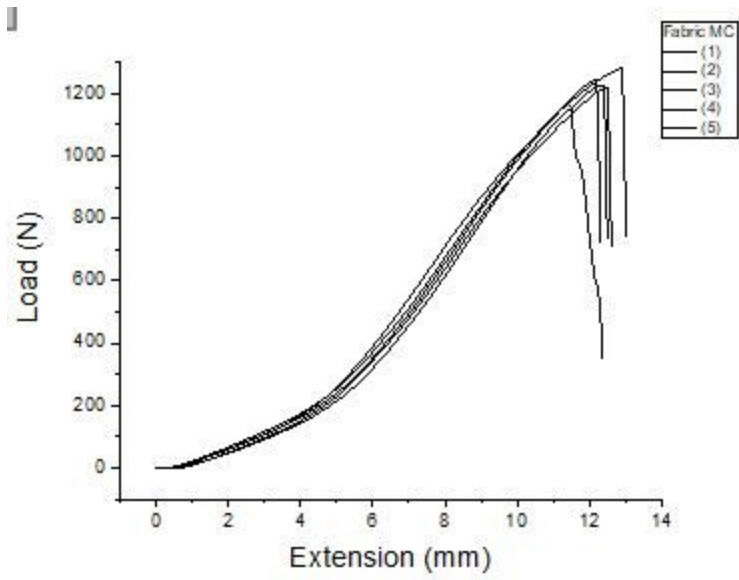


Figure 4.5 Mechanical behaviour of Fabric MC in the unaged condition

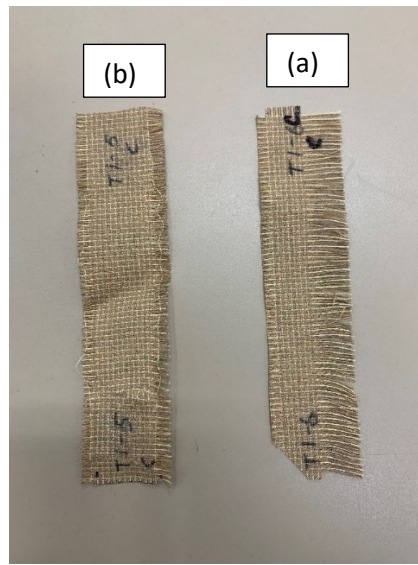


Figure 4.6 Fabric MC specimens (a) before and (b) after testing

d. Fabric MD

Figure 4.7 shows the load extension curve for Fabric MD with the five replicates tested. Fabric MD shows the typical three-part behaviour when tension is applied. First, it shows a very low increase in load with increasing strain, which corresponds to crimp interchange. Above an extension of 3.5mm, the stress value starts increasing with increasing tension. The Young's modulus of the phase 2 region is equal to 234 ± 4 N/mm. The breaking strength is 1290 ± 20 N and the maximum extension at break is 9.0 ± 0.2 mm. The coefficient of variation for these three parameters lies in the range of 2%; the degree of variability between the specimens is quite low. Figure 4.8 shows an example of the specimens before and after testing.

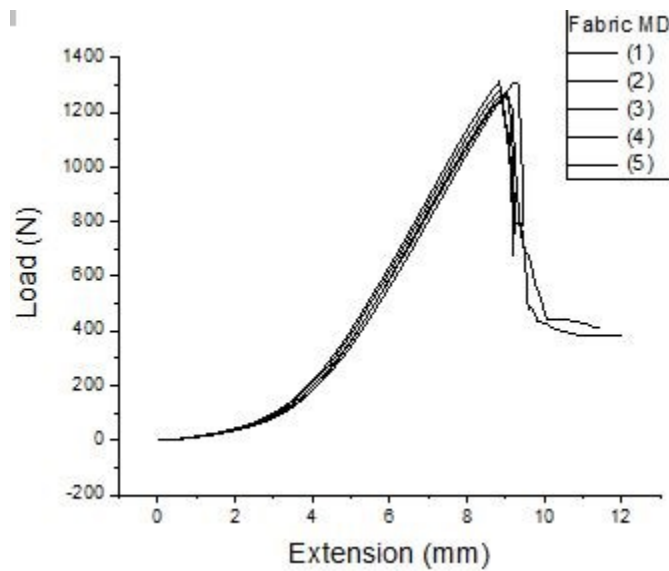


Figure 4.7 Mechanical behaviour of Fabric MD in the unaged condition



Figure 4.8 Fabric MD specimen (a) before and (b) after testing

e. Fabric ME

Figure 4.9 shows the load extension curve for Fabric ME with the five replicates tested. Fabric ME shows the typical three-part behaviour when tension is applied. First, it shows a very low increase in stress with increasing strain, which corresponds to crimp interchange. Above an extension of 3mm, the stress increases with increasing strain. The Young's modulus in the phase 2 region is equal to 213 ± 5 N/mm. The breaking strength is 1537 ± 53 N and the maximum extension at break is 10.2 ± 0.2 mm. The coefficient of variation for these three parameters lies in the range of 3%; the degree of variability between the specimens is quite low. Figure 4.10 shows an example of the specimens before and after testing.

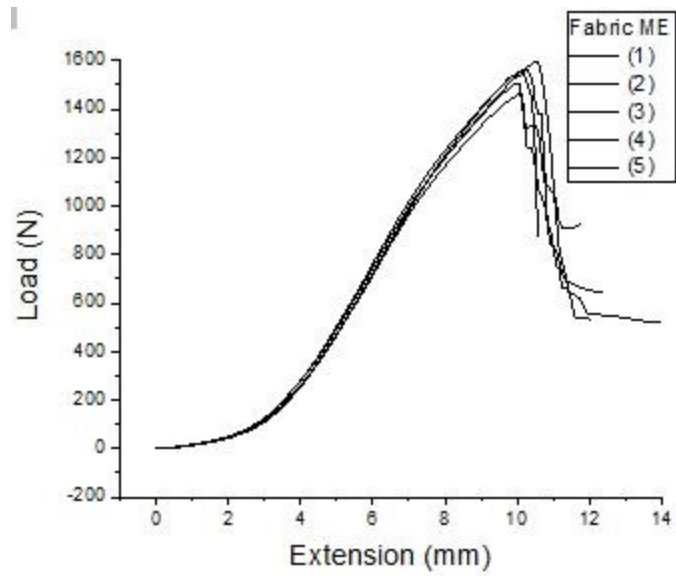


Figure 4.9 Mechanical behaviour of Fabric ME in the unaged condition

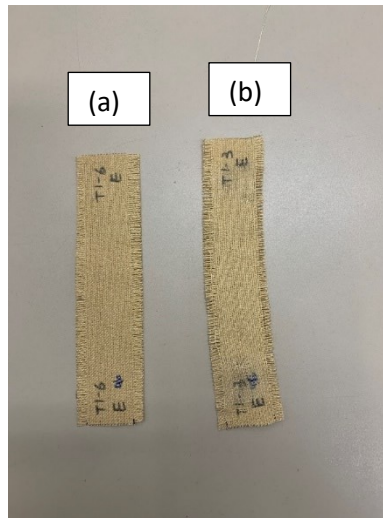


Figure 4.10 Fabric ME specimens (a) before and (b) after testing

f. Fabric MF

Figure 4.11 shows the load extension curve for Fabric MF with the five replicates tested. Fabric MF does not show the typical three-part behaviour when tension is applied. First, there is no crimp interchange region. The fabric shows an increasing stress with increasing strain from the beginning. Also, there is a

change in the slope observed about halfway between the beginning of the test and the failure point. This hump in the load-extension curve corresponds to a transition in the value of Young's modulus from 16.4 ± 0.2 N/m to 9.4 ± 0.3 N/mm at an extension of 22 ± 0.2 mm. The breaking strength is 624 ± 9 N and the maximum extension is 50 ± 2 mm. The coefficient of variation for these three parameters lies in the range of 4%; the degree of variability between the specimens is quite low. Figure 4.12 shows an example of the specimens before and after testing.

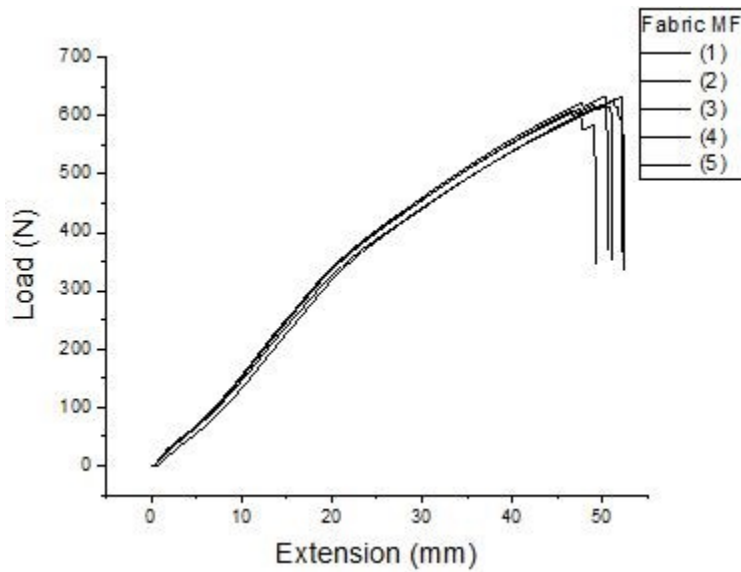


Figure 4.11 Mechanical behaviour of Fabric MF in the unaged condition

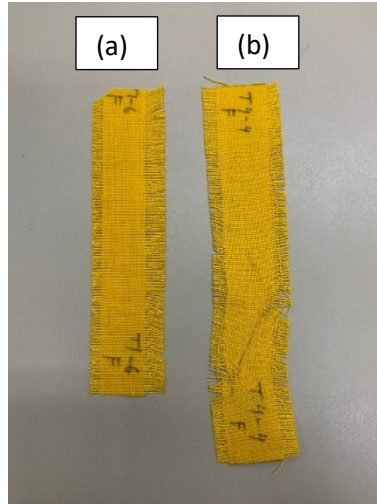


Figure 4.12 Fabric MF specimens (a) before and (b) after testing

g. Fabric MG

Figure 4.13 shows the load extension curve for Fabric MG with the five replicates tested. Fabric MG exhibits a four-part behaviour when tension is applied. Initially it shows the typical crimp interchange. It enters the Phase 2 regime above an extension of 2.8mm. However, contrary to the Phase 2 behavior typically exhibited by woven fabrics (Section 2.4.4), Fabric MG exhibits a hump characterized by a change in slope at an extension of 6.5 ± 0.2 mm, similarly to Fabric MF. The value of the Young's modulus changes from 171 ± 3 N/mm to 90 ± 3 N/mm at an extension of 6.5 mm. The breaking strength is equal to 950 ± 10 N and the extension at break is 8.27 ± 0.3 mm. The coefficient of variation for these three parameters lies in the range of 4%; the degree of variability between the specimens is quite low. Figure 4.14 shows an example of the specimens before and after testing.

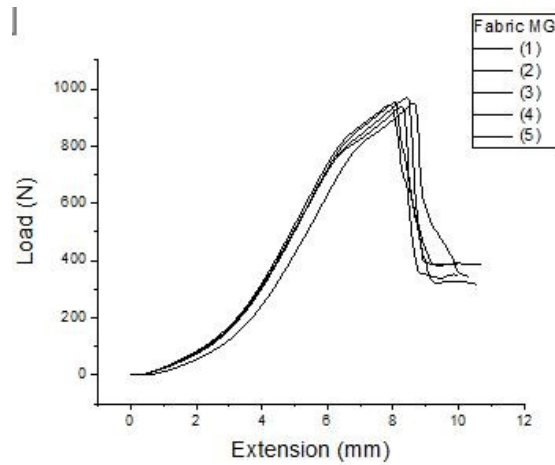


Figure 4.13 Mechanical behaviour of Fabric MG in the unaged condition



Figure 4.14 Fabric MG specimen (a) before and (b) after testing

h. Fabric MH

Figure 4.15 shows the load extension curve for Fabric MH with the five replicates tested. Fabric MH exhibits the same behavior as Fabric MG, with crimp interchange and a hump. Two values of the Young's modulus are 200 ± 20 N/mm below an extension of 3.75 ± 0.07 mm and 121 ± 3 N/mm. A breaking strength of 1030 ± 20 N and a maximum extension of 7.5 ± 0.4 mm were recorded. The coefficient of variation of

these three parameters lies in the range of 8%. Figure 4.16 shows an example of the specimens before and after testing.

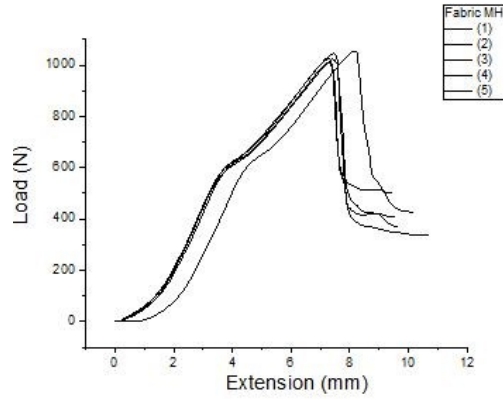


Figure 4.15 Mechanical behaviour of Fabric MH in the unaged condition



Figure 4.16 Fabric MH specimen before and after testing

4.2.2 YARN SCALE

The mechanical behaviour of the yarns was tested according to the method mentioned in Section 3.5.2. The results for each individual type of yarn are provided below.

a. Yarns in Fabric MA

Figure 4.17 depicts the mechanical behaviour of the constituent yarns for Fabric MA. Figure 4.17(a) represents the mechanical behaviour of the spun yarn and Figure 4.17(b) represents the mechanical behaviour of the spun/filament yarn.

The spun yarn, which is made of Kevlar and PBI, depicts a three-phase behaviour when tension is applied. Initially it shows a very low increase in stress with increasing strain, which corresponds to the removal of crimp since the yarn was extracted from the fabric. Above an extension of 1mm, the stress increases significantly with strain. The Young's modulus of the second region is equal to 8.4 ± 0.9 N/mm. The spun yarn exhibits a breaking strength of 18 ± 2 N and a maximum extension of 3.2 ± 0.3 mm. The degree of variability for these three parameters lies in the range of 10%.

The spun/filament yarn, which contains Kevlar filaments and Kevlar/PBI staple fibers, also depicts a three-phase behaviour when tension is applied. Firstly, it shows a small increase in load with increasing extension, which corresponds to crimp being taken out of the yarn. However, the time to straighten the filament yarn is longer than for the spun yarn. Above an extension of 1.75mm, the stress increases significantly with increasing strain. The Young's modulus of the second phase is equal to 31 ± 5 N/mm. The spun/filament yarn has a breaking strength of 50 ± 4 N and a maximum extension of 3.4 ± 0.2 mm. The degree of variability for these three parameters lies in the range of 15%.

The spun/filament yarn is much stronger than the spun yarn and shows a higher Young's modulus. The higher strength can be attributed in part to the fact that the spun/filament yarn includes continuous fibers as compared to only short staple fibers in the case of the spun yarn. The higher Kevlar fiber content in the spun/filament yarn compared to the spun yarn also contributes to the higher strength of the spun/filament yarn as Kevlar fibers have a higher strength compared to PBI fibers (see section 2.3). The higher Kevlar fiber content in the spun/filament yarn can also explain its higher Young's modulus as Kevlar fibers also have a higher modulus compared to PBI fibers (see section 2.3).

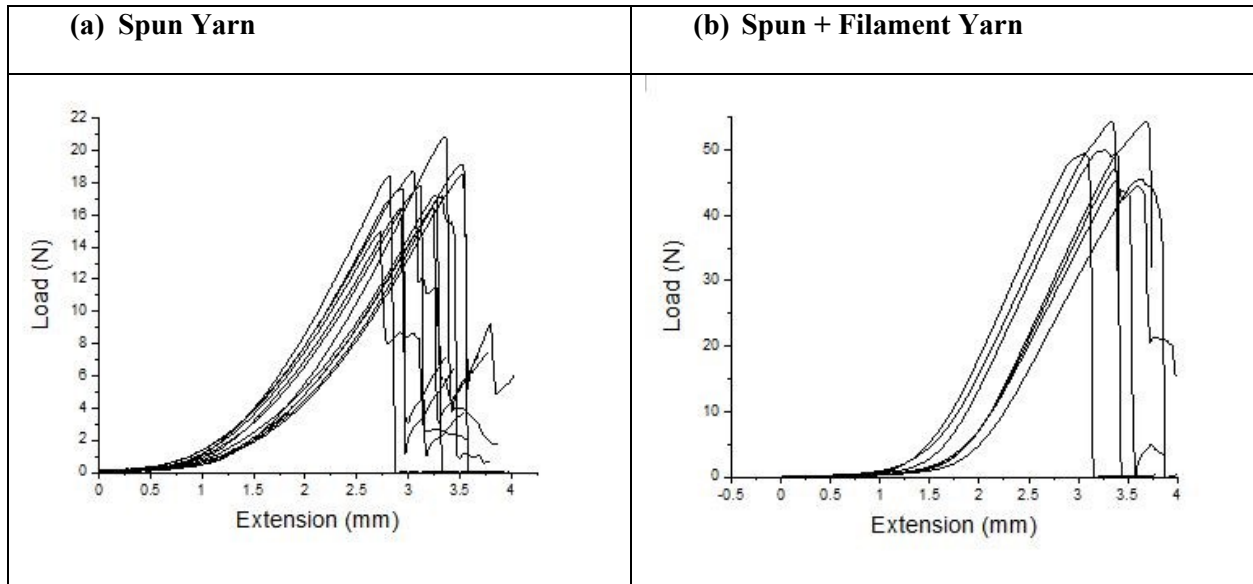


Figure 4.17 Mechanical behaviour of the (a) spun yarn and (b) spun/filament yarn in Fabric MA for the unaged condition

The mechanical performance measured on the individual yarns shows a much higher variability compared to the fabric scale. This could be attributed to the difference in the gauge length during testing at the yarn and fabric scale (50cm for the yarn and 75cm for the fabrics). Realf et al. observed an increase in the variability in the strength results of the yarns with decreasing the gauge length [55]. If a larger length of specimen is tested, there is a better chance to capture the full extent of the variability in the specimen, which as a whole is highly variable since it involves textiles.

b. Yarns in Fabric MB

Figure 4.18 depicts the mechanical behaviour of the constituent yarns for Fabric MB. Figure 4.18(a) represents the mechanical behaviour of the spun yarn and Figure 4.18(b) represents the mechanical behaviour of the spun/filament yarn.

The spun yarn, which is made of Kevlar® and PBI, depicts a three-phase behaviour when tension is applied. Initially it shows a very small increase in load with increasing strain, which corresponds to crimp being taken out, since the yarn was extracted from the fabric. Above an extension of 2.1mm, the increase in stress is significant with increasing strain. The Young's modulus of the second phase region is equal to 12 ± 3

N/mm. The spun yarn exhibits a breaking strength of 28 ± 2 N and a maximum extension of 4.5 ± 0.4 mm. The coefficient of variation for these three parameters lies in the range of 22%.

The spun/filament yarn, which contains Kevlar filaments and Kevlar®/PBI staple fibers, also depicts a three-phase behaviour when tension is applied. Initially it shows a very small increase in load with increasing strain, which corresponds to crimp being taken out. However, the time to straighten this yarn is much longer as compared to the spun yarn. Above an extension of 2.4mm, the increase in stress is significant with increasing strain. The Young's modulus of the second phase region is equal to 29 ± 7 N/mm. The spun/filament yarn exhibits a breaking strength of 56 ± 3 N and a maximum extension of 4.3 ± 0.3 mm. The coefficient of variation for these three parameters lies in the range of 23%.

The mechanical performance measured on the individual yarns show a much greater variability between the specimens compared to the fabric scale.

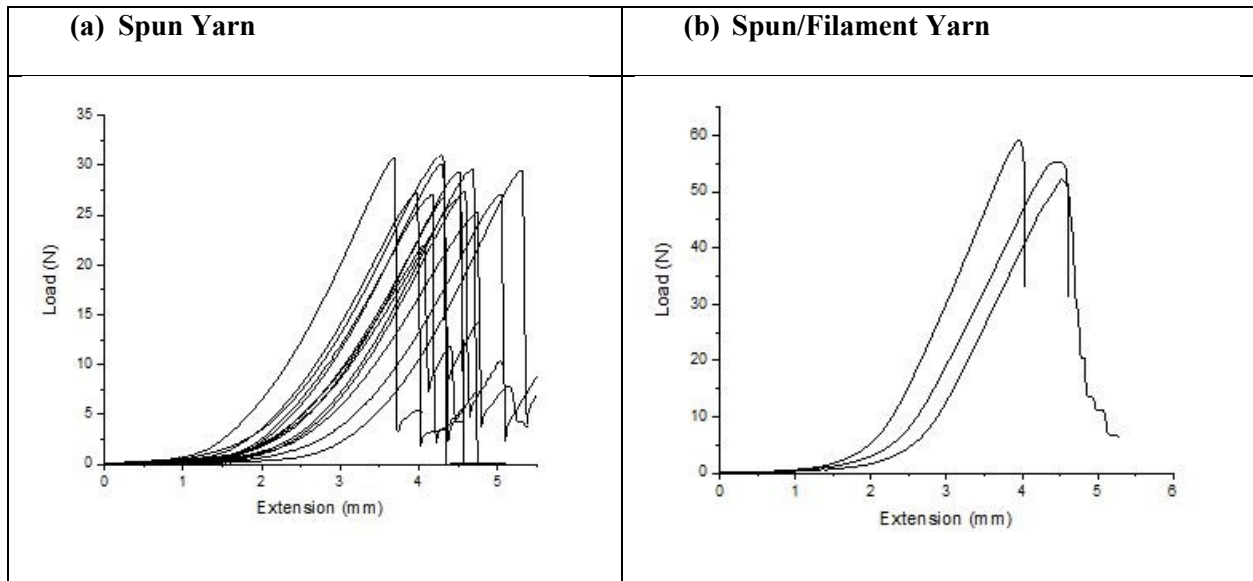


Figure 4.18 Mechanical behaviour of the (a) spun yarn and (b) spun/filament yarn in Fabric MB for the unaged condition

c. Yarns in Fabric MC

Figure 4.19 depicts the mechanical behaviour of the constituent yarns for Fabric MC. Figure 4.19(a) represents the mechanical behaviour of the spun yarn and Figure 4.19(b) represents the mechanical behaviour of the filament yarn.

The spun yarn, which contains Kevlar and Nomex staple fibers, depicts a three-phase behaviour when tension is applied. Initially it shows a very small increase in load with increasing strain, which corresponds to the crimp being taken out, since the yarn is extracted from the fabric. Above an extension of 1.7mm, the increase in stress is significant with increasing stress. The Young's modulus of the second phase region is equal to 9 ± 2 N/mm. The spun yarn shows a breaking strength of 18 ± 2 N and a maximum extension of 3.7 ± 0.4 mm. The coefficient of variation for these three parameters lies in the range of 21%.

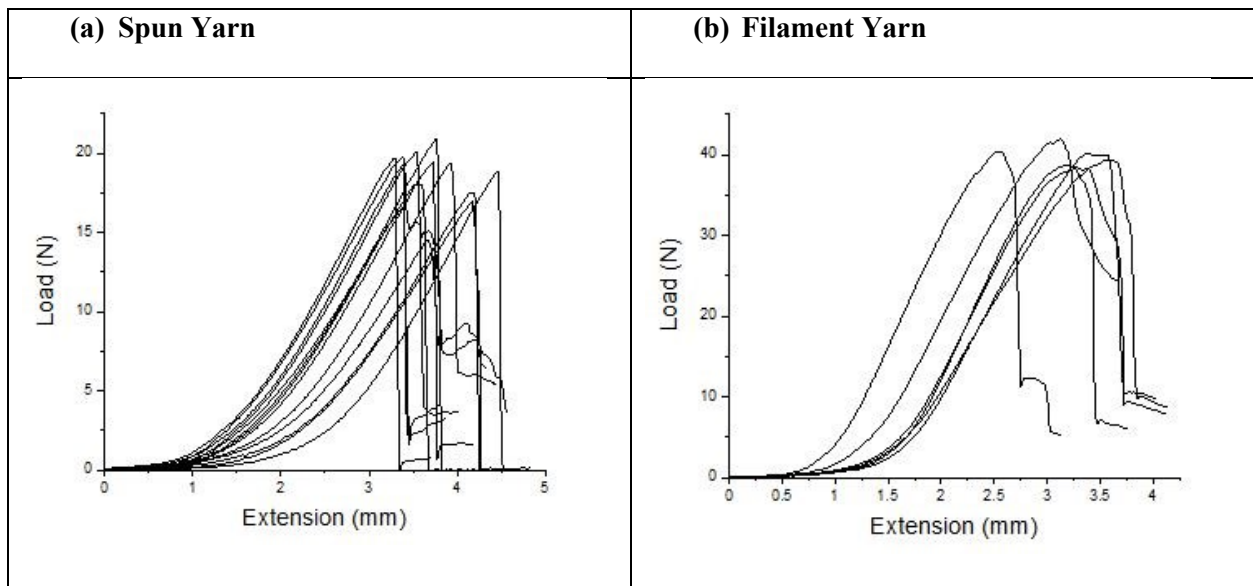


Figure 4.19 Mechanical behaviour of the (a) spun yarn and (b) filament yarn for Fabric MC in the unaged condition

The filament yarn, which contains Kevlar® filaments, also depicts a three-phase behaviour when tension is applied. Initially it shows a very small increase in load with increasing strain, which corresponds to crimp being taken out. However, the filament yarn straightens faster than the spun yarn. Above an extension of 1.4mm, it shows a significant increase in stress with strain. The Young's modulus of second phase region

is equal to 23 ± 6 N/mm. The filament yarn exhibits a breaking strength of 40 ± 1 N and a maximum extension of 3.2 ± 0.4 mm. The coefficient of variation for these three parameters lies in the range of 27%.

Both yarn specimens show a greater degree of variation within the same class as compared to the fabric specimens.

d. Yarns in Fabric MD

Figure 4.20 depicts the mechanical behaviour of the constituent yarns for Fabric MD. Figure 4.20(a) represents the mechanical behaviour of the brown spun yarn and Figure 4.20(b) represents the mechanical behaviour of the black spun yarn.

The brown spun yarn, which contains Kevlar® and Nomex® staple fibers, depicts a three-phase behaviour when tension is applied. Initially it shows a very small increase in load with increasing strain, which corresponds to the crimp being taken out, since the yarn is extracted from the fabric. Above an extension of 1mm, the increase in stress is significant with increasing strain. The Young's modulus of second phase region is equal to 12 ± 1 N/mm. The brown spun yarn shows a breaking strength of 25 ± 3 N and a maximum extension of 3.2 ± 0.2 mm. The coefficient of variation for these three parameters lies in the range of 12%.

The black spun yarn, which contains Kevlar® staple fibers, also depicts a three-phase behaviour when tension is applied. Initially it shows a very small increase in load with increasing strain, which corresponds to crimp being taken out. In this case, the black spun yarn has more crimp as compared to the brown spun yarn. Above an extension of 1.5mm, the increase in stress is significant with increasing strain. The Young's modulus of second phase region is equal to 27 ± 6 N/mm. The spun yarn shows a breaking strength of 42 ± 3 N and a maximum extension of 3.1 ± 0.4 mm. The coefficient of variation for these three parameters lies in the range of 22%. Both yarn specimens show a much higher degree of variation than the specimens at the fabric scale.

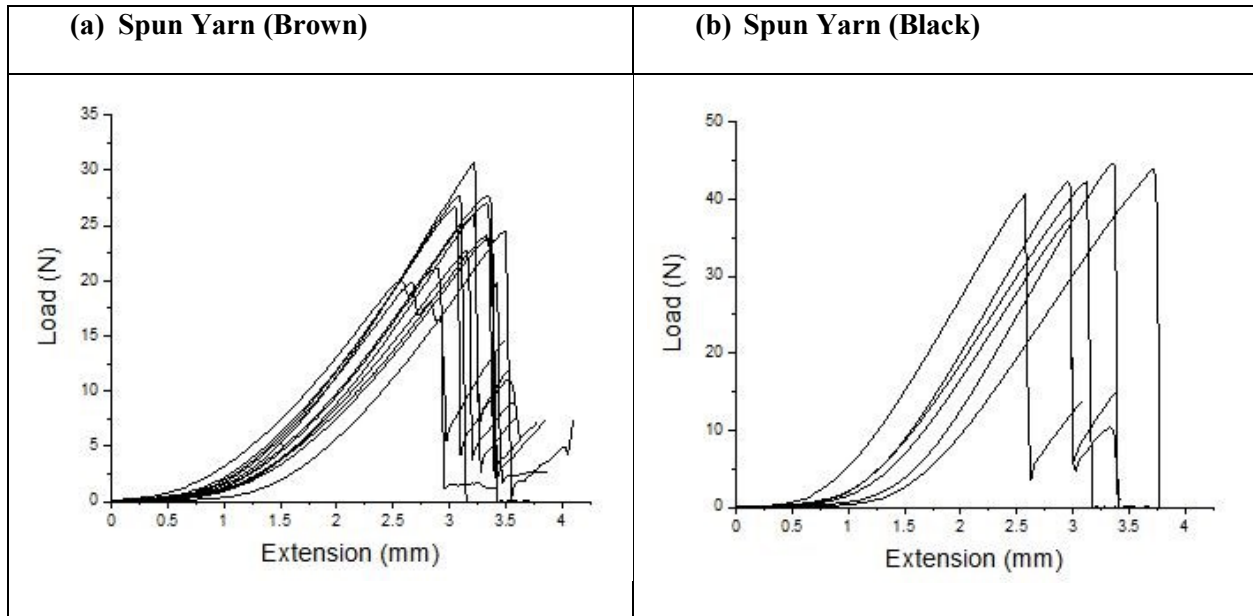


Figure 4.20 Mechanical behaviour of the (a) brown spun yarn (b) black spun yarn in Fabric MD in the unaged condition

e. Yarns in Fabric ME

Figure 4.21 depicts the mechanical behaviour of the constituent spun yarns for Fabric ME. Although only one type of yarn was observed in Fabric ME, the 20 specimens of yarn tested showed two levels of performance.

The yarns, which contains Kevlar®, Nomex® and PBO, show the three-phase behaviour when tension is applied. Initially there is a very small increase in load with increasing strain, which corresponds to the crimp being taken out. All yarn specimens exhibited the same crimp removal distance of 0.7mm, beyond which a significant increase in stress with strain was observed. But 13 of the 20 yarns have a Young's modulus of 11.32 ± 3 N/mm in the phase two region. This group showed a breaking strength of 34.5 ± 3 N and a maximum extension of 3.8 ± 0.3 mm. The coefficient of variation for these three parameters lies in the range of 30%. The second group of seven of the 20 yarns have a modulus in the phase two region equal to 25 ± 2 N/mm. The breaking strength of these yarns was recorded as 58 ± 3 N and the maximum extension was 3.1 ± 0.2 mm. The coefficient of variation for these parameters lies in the range of 8%. Again, the

degree of variation in the yarn specimens appears to be more than what is observed for the specimens at the fabric scale.

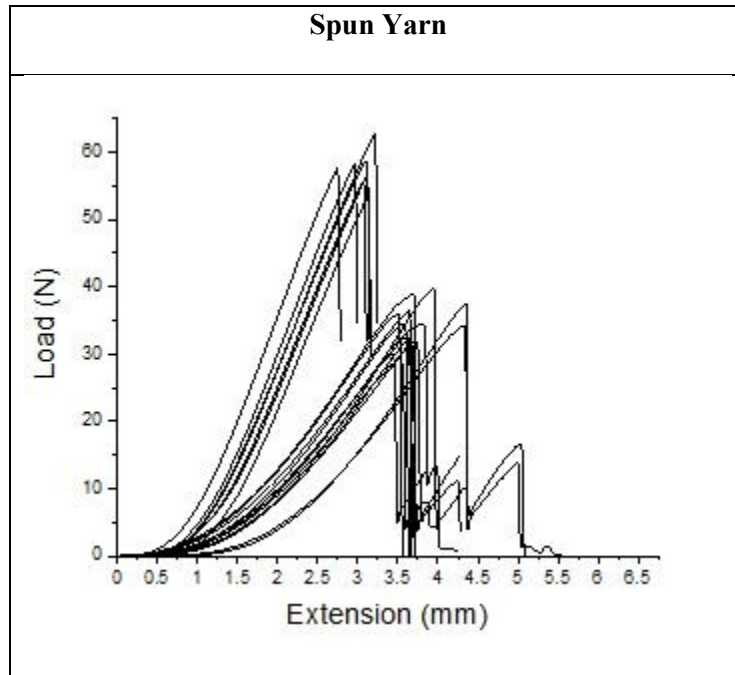


Figure 4.21 Mechanical behaviour of the spun yarns in Fabric ME in the unaged condition

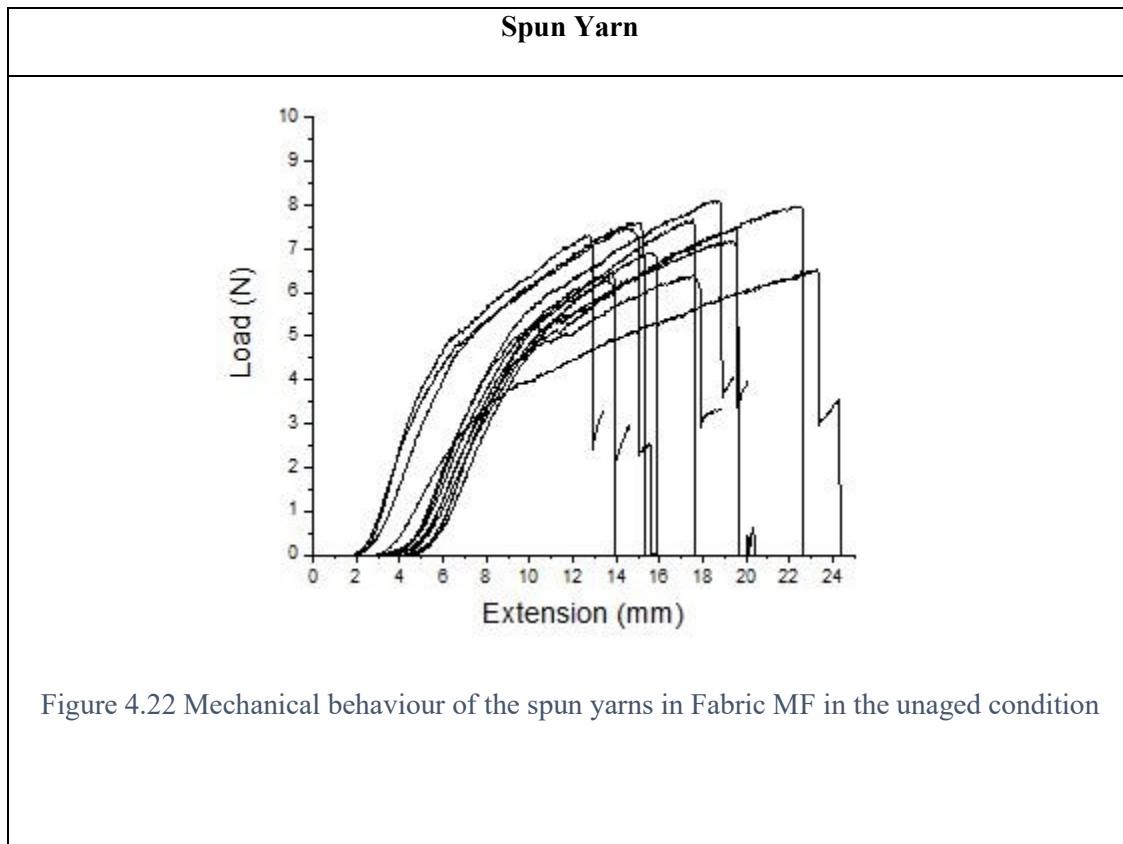
No difference in fiber content was observed between the two groups of yarns. However, a difference in diameter and linear density was measured between the two groups of yarns. The yarns with the larger diameter and higher linear density are the ones which showed a higher strength and a lower elongation at break.

f. Yarns in Fabric MF

Figure 4.22 depicts the mechanical behaviour of the constituent spun yarns for Fabric MF. The spun yarn, which contains Kevlar®, Nomex® and antistat fibers, depicts a four-phase behaviour when tension is applied. Initially it shows a very small increase in load with increasing strain, which corresponds to the crimp being taken out. Yarn MF records the largest crimp among all the yarn specimens. Above an extension of 5.5mm, the increase in stress is significant with increasing strain. The yarn exhibited two different values for the modulus in the phase two region (i) 0.8 ± 0.1 N/mm up to an extension of 10.8mm

mm and (ii) 0.27 ± 0.06 N/mm up to the breaking point. Such a hump in the load extension curve was also observed at the fabric scale.

The yarn shows a breaking strength of 7.2 ± 0.6 N and a maximum extension of 17 ± 3 mm. The coefficient of variation for the parameters lies in the range of 22%. It is greater at the yarn scale than at the fabric scale.



g. Yarns in Fabric MG

Figure 4.23 depicts the mechanical behaviour of the constituent yarns for Fabric MG. Figure 4.23(a) represents the mechanical behaviour of the spun yarn and Figure 4.23(b) represents the mechanical behaviour of the filament yarn. It can be noted that the hump behaviour that was recorded at the fabric scale isn't observed at the yarn scale.

The spun yarn, which contains Kevlar® and PBI staple fibers, depicts a three-phase behaviour when tension is applied. Initially it shows a very small increase in load with increasing strain, which corresponds to the crimp being taken out, since the yarn is extracted from the fabric. Above an extension of 0.6mm, the increase in stress is significant with increasing strain. The Young's modulus of the second phase region is equal to 4.8 ± 0.6 N/mm. The spun yarn shows a breaking strength of 11 ± 1 N and a maximum extension of 3.0 ± 0.2 mm. The coefficient of variation for these three parameters lies in the range of 12%.

The filament yarn, which is made of Kevlar® filaments, also depicts a three-phase behaviour when tension is applied. Initially it shows a very small increase in load with increasing strain, which corresponds to crimp being taken out. Above an extension of 1.4mm, the increase in stress is significant with increasing strain. The Young's modulus of the second phase two region is equal to 26 ± 7 N/mm. The filament yarn shows a breaking strength of 42 ± 2 N and a maximum extension of 3.1 ± 0.4 mm. The coefficient of variation for these three parameters lies in the range of 28%.

Both yarn specimens show a much greater degree of variation as compared to the fabric specimens.

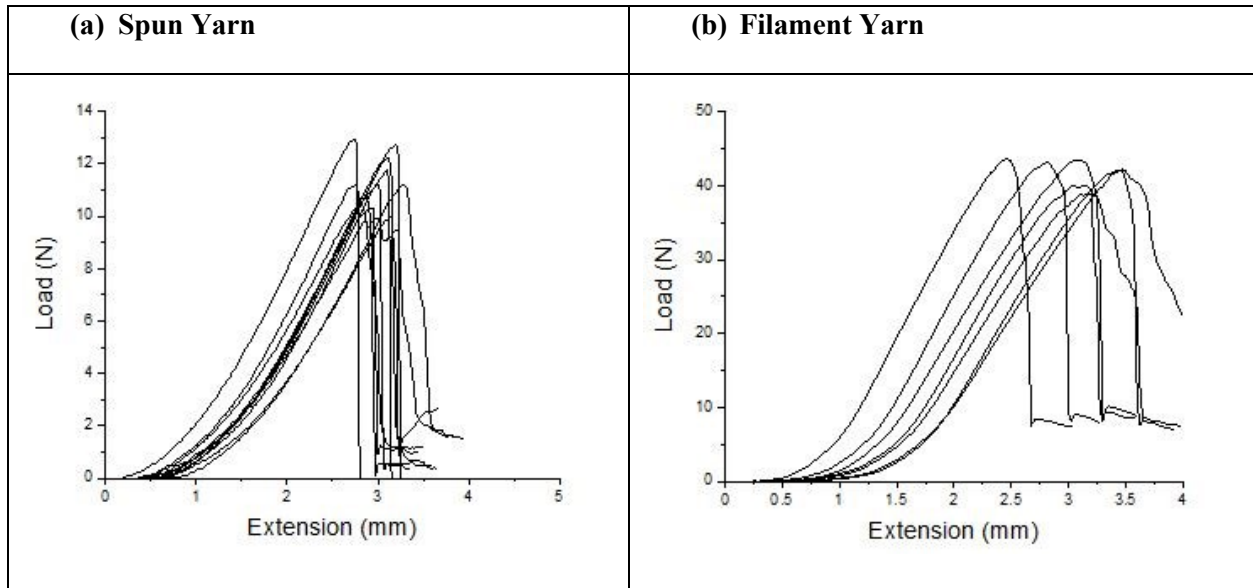


Figure 4.23 Mechanical Behaviour of the (a) spun yarn and (b) filament yarn for Fabric MG in the unaged condition

h. Yarns in Fabric MH

Figure 4.24 depicts the mechanical behaviour of the constituent yarns for Fabric MH. Figure 4.24(a) represents the mechanical behaviour of the spun yarn and Figure 4.24(b) represents the mechanical behaviour of the filament yarn. It can be noted that the hump behaviour that was recorded at the fabric scale isn't observed at the yarn scale.

The spun yarn, which contains Kevlar® and PBI staple fibers, depicts a three-phase behaviour when tension is applied. Initially it shows a very small increase in load with increasing strain, which corresponds to the crimp being taken out, since the yarns are extracted from the fabric. Above an extension of 0.7mm, the increase in stress is significant with increasing strain. The Young's modulus of the second phase region is equal to 9.1 ± 0.6 N/mm. The spun yarn shows a breaking strength of 20 ± 2 N and a maximum elongation of 2.9 ± 0.2 mm. The coefficient of variation of these three parameters lies in the range of 9%.

The filament yarn, which contains Kevlar® filaments, also depicts a three-phase behaviour when tension is applied. Initially it shows a very small increase in load with increasing strain, which corresponds to crimp being taken out. Above an extension of 0.5mm, the increase in stress is significant with increasing strain.

The Young's modulus of the second phase region is equal to 29 ± 1 N/mm. The filament yarn shows a breaking strength of 65 ± 2 N and a maximum extension of 2.7 ± 0.1 mm. The coefficient of variation for these three parameters lies in the range of 5%.

Both types of yarn show a much greater degree of variation within the yarn specimens as compared to the fabric specimens.

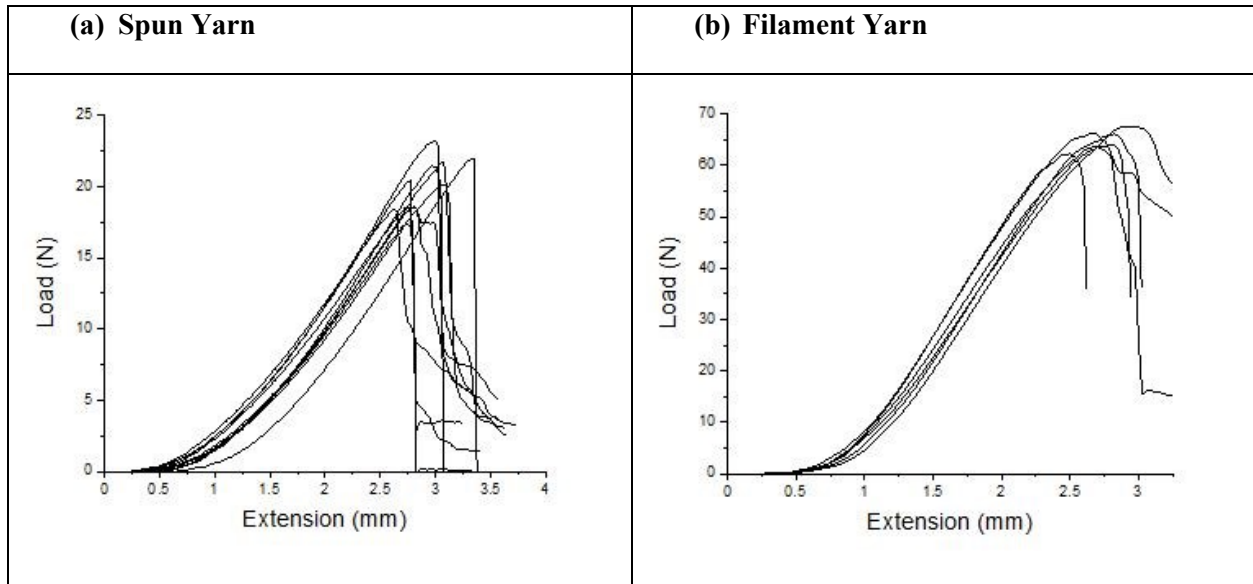


Figure 4.24 Mechanical behaviour of the (a) spun yarn and (b) filament yarn in Fabric MH in the unaged condition

4.2.3 DISCUSSION

It was mentioned earlier that fabrics are multiscale structures with each scale contributing towards the mechanical behaviour of the fabric specimen (Section 2.4). Thus, this section studies some unique behaviours exhibited by the fabrics in the unaged condition at the fabric and yarn scale.

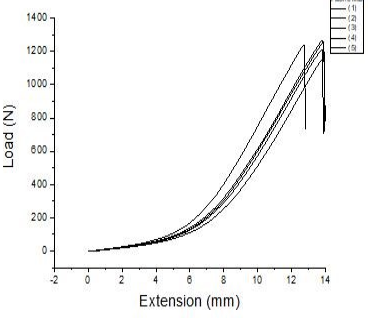
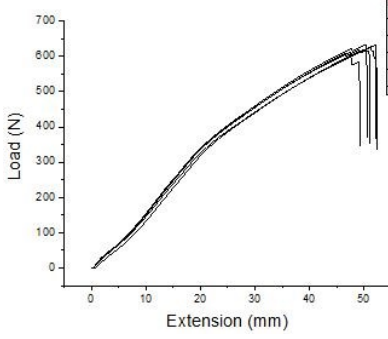
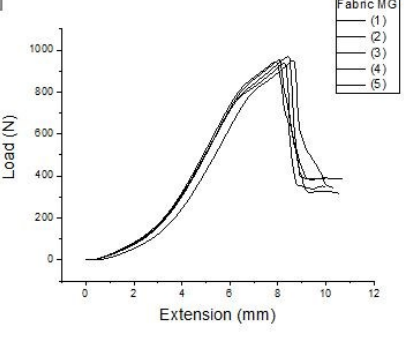
FABRIC SCALE

Categorisation of the fabric mechanical behaviour

Some distinct trends in the load-extension curves have been observed for the different fabrics. They can be identified as the standard behavior generally described in the literature (Section 2.4.4), the absence of crimp

interchange, and the presence of a hump. Table 9 lists the fabrics pertaining to each specific behavior. The sections below discuss the possible reasons for these deviations from the standard behavior.

Table 4.2 Categorisation of different fabric mechanical behaviours

Standard behaviour	No crimp interchange	Hump characteristic
		
<p>Shown by</p> <ul style="list-style-type: none"> • Fabric MA • Fabric MB • Fabric MC • Fabric MD • Fabric ME 	<p>Shown by</p> <ul style="list-style-type: none"> • Fabric MF 	<p>Shown by</p> <ul style="list-style-type: none"> • Fabric MF • Fabric MG • Fabric MH

Absence of crimp interchange

As mentioned in Section 2.4.4, the mechanical behaviour of woven fabrics is usually associated with three different phases: Crimp interchange, increase in stress, and mechanical failure. For Fabric MF, we observed that the region of crimp interchange was completely absent. This could be attributed to the fact that Fabric MF had the highest fabric count in the warp direction, which was the direction in which the fabric was tested. As a result, the structure was much stiffer, and the yarns had a very limited possibility to adjust their level of crimp when the fabric was stretched.

Fabric MF also showed the lowest breaking strength among the eight different fire protective fabrics studied. This can potentially be attributed to the fiber content of the fabric. Fabric MF contains the highest Nomex fiber content with 93%, the complement being 5% Kevlar® and 2% Antistat (carbon fibers). Previous authors have reported that Nomex® fibers have a strength of 340 MPa, which is about 10 times lower than Kevlar® fibers [32]. Fabric MF also exhibited the highest extension at break at 50 mm. This can be potentially attributed the high degree of extension of Nomex fibers [32] due to its relatively flexible structure as compared to Kevlar® fibers [23].

Hump in the fabric

In section 4.2.1, we reported the presence of a hump for three different fabrics: Fabric MF, Fabric MG, and Fabric MH. In the case of Fabric MF, a hump was also observed at the yarn scale and will be further discussed later in the thesis. It can be hypothesized that the hump observed in the mechanical behavior at the fabric scale originated from the hump occurring at the yarn scale.

Regarding Fabric MG and MH, they have the same fiber content, i.e. 65% Kevlar® and 35% PBI, and a similar weave construction. In order to try explaining the hump behaviour observed at the fabric scale, a video of the fabric specimen being stretched at a slow speed was made and compared to the behavior of fabrics having similar fiber content (Fabric MA and Fabric MB). However, no specific difference between the samples was observed. In particular, they all showed some slipping of the fringe yarns while the warp yarns were stretched.

As another possible cause for the hump in the force-extension curve of Fabric MG and MH, we looked at the difference in crimp between the yarns for the five fabrics that include two different yarns in their structure. This includes Fabric MA and MB, with a spun and a spun/filament yarn, and Fabric MC, MG and MH with a spun and a filament yarn. The ratio in the crimp between the two yarns was calculated for each of these fabrics. The values are listed in Table 4.3.

Table 4.3 Yarn crimp and crimp ratio for fabrics with two different yarns in their structure

Fabric	Crimp in the spun yarn	Crimp in the filament or spun/filament yarn	Ratio of yarn crimp
Fabric MA	4.6%	3.3%	1.4
Fabric MB	7.2%	5.6%	1.3
Fabric MC	6.5%	4.5%	1.46
Fabric MG	5.2%	1.7%	3.1
Fabric MH	3.3%	0.9%	3.6

It can be observed in Table 4.3 that the ratio in the crimp for the two yarns composing Fabric MG and MH is very high, twice as much as the ratio observed for the three other fabrics. This difference in the crimp between the two yarns in Fabric MG and MH could possibly be due to a difference in compliance between the spun and filament yarns. It is possible that, because of this large crimp difference between the spun and filament yarns in Fabric MG and MH, the contributions of both series of yarns to the different phases of the fabric deformation are out of phase, which generates the formation of the hump in the load extension of Fabric MG and MH.

Effect of the fiber content on the fabric mechanical behaviour

Fabric MD and ME exhibit the same weave construction, type of yarns (i.e. comprised entirely of spun yarns), and fabric count in both warp and weft directions. However, these two fabrics show a large difference in the breaking strength and extension at break (Table 4.4).

Table 4.4 Difference in performance for Fabric MD and ME

Fabric	Breaking strength	Extension at break
Fabric MD	1290 ± 20 N	8.9 ± 0.2 mm
Fabric ME	1540 ± 50 N	10.2 ± 0.2 mm

Since, the fiber content in fabrics generally plays a crucial role in their strength [13], an analysis was done to see if this difference in breaking strength could be traced back to the difference in the fiber content between the fabrics. Fabric MD comprises 60% Kevlar® and 40% Nomex®. Fabric ME is made of 60% Kevlar®, 20% Nomex®, and 20% PBO. PBO fibers have a tensile strength of 5.8 GPa [38], which is 1.6 times that of Kevlar®, whereas it is 17 times that of Nomex® [43]. This difference in strength at the fiber level can lead to a change in mechanical performance at a fabric scale. Therefore, the higher strength of Fabric ME can potentially be attributed to the presence of the PBO fibers in the fabric.

YARN SCALE

Categorisation of the yarn mechanical behaviour

Table 4.5 shows the two types of behaviours observed for the spun yarns of the different fabrics. Most yarns exhibited the traditional behavior already reported in the literature [132] while the spun yarn in Fabric MF showed a hump. In the case of the filament and spun/filament yarns, only the traditional behavior was observed (Table 4.6 and 4.7). An analysis is provided in the following sections about the different parameters affecting the modulus, breaking strength, and extension at break of these yarns as well as the presence of the hump.

Table 4.5 Categorisation of the spun yarn mechanical behaviour

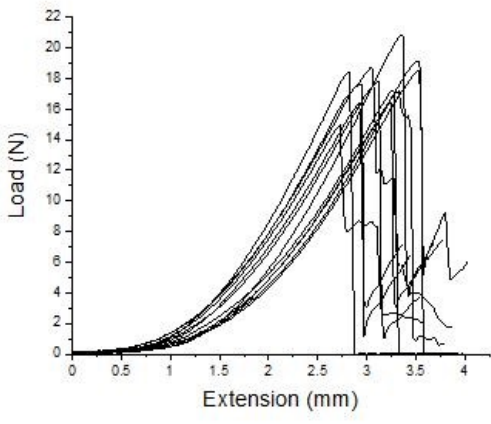
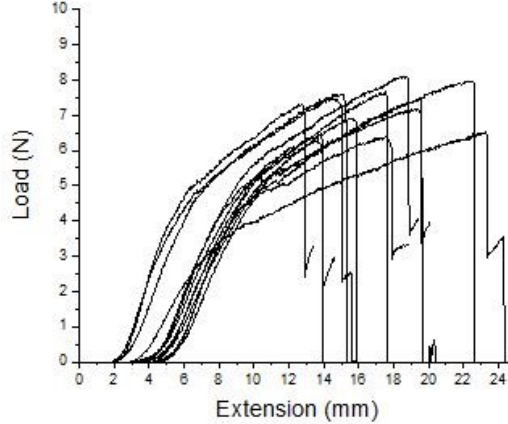
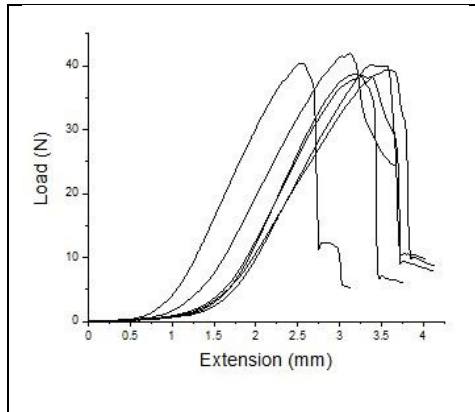
Traditional behaviour	Hump behaviour
	
<p>Shown by:</p> <ul style="list-style-type: none"> • Yarn from Fabric MA • Yarn from Fabric MB • Yarn from Fabric MC • Yarn from Fabric MD • Yarn from Fabric ME • Yarn from Fabric MG • Yarn from Fabric MH 	<p>Shown by:</p> <ul style="list-style-type: none"> • Yarn from Fabric MF

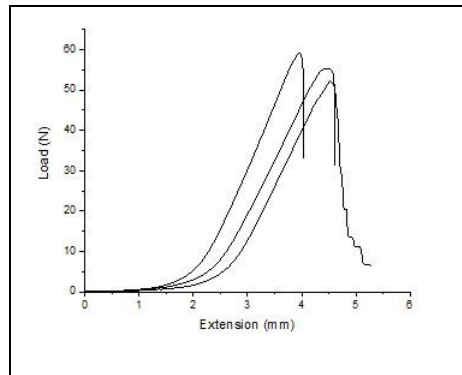
Table 4.6 Filament yarn mechanical behaviour



Shown by:

- Yarn from Fabric MC
- Yarn from Fabric MG
- Yarn from Fabric MH

Table 4.7 Spun/filament yarn mechanical behaviour



Shown by:

- Yarn from Fabric MA
- Yarn from Fabric MB

Effect of the yarn characteristics on their modulus, breaking strength, and extension at break

a. Difference in the yarn mechanical performance within a series of yarns

Fabric ME only includes spun yarns consisting of Kevlar®, Nomex® and PBO. However, the yarns showed a bimodal distribution of their breaking strengths (see Fig 4.21). A first group of yarns (13 yarns over 20 successive yarns) had an average tensile strength of 34 N whereas the second set of yarns (the 7 remaining yarns) had an average tensile strength of 58 N (Table 4.8). The difference in strength between these two groups of yarns is statistically significant (t-test, $p = 4 \times 10^{-10}$).

Table 4.8 Breaking strength and linear density of the two sets of yarns in Fabric ME

# of yarns	Strength of the different groups of yarns (N)	Linear density (tex)
13	34 ± 3	59
7	58 ± 3	62

The characteristics of the yarns were examined to look for a possible reason for this difference in strength. It was observed by optical microscopy that the two groups of yarns have a different diameter (Figure 4.25). The linear density was calculated for each group of yarns (Table 4.8). It confirms the observation by optical microscopy about the difference in diameter. Since a lower linear density in yarns has been associated with a lower strength [133], this can potentially explain why the spun yarns in Fabric ME exhibited two different breaking strengths.



Figure 4.25 Optical microscope image of examples of yarns of Fabric ME having a different strength

b. Comparison between the yarns of two fabrics only differing by their weight

Fabric MG and Fabric MH have a twill weave structure and the same fiber content (i.e., 65% Kevlar® and 35% PBI). In both cases, they include spun yarns, made of Kevlar® and PBI, and filament yarns, which only include Kevlar®. However, the two fabrics have a different weight: Fabric MG has a weight of 214 g/mm², and Fabric MH has a weight of 247 g/mm².

Different mechanical strengths were observed for each series of yarns between the two fabrics as shown in Figure 4.26. The spun yarns from Fabric MG showed a maximum strength of 11 N whereas the spun yarns from Fabric MH showed a maximum strength of 20 N. The same trend was observed for the filament yarns (42 N for the filament yarns from Fabric MG and 65 N for the filament yarns from Fabric MH).

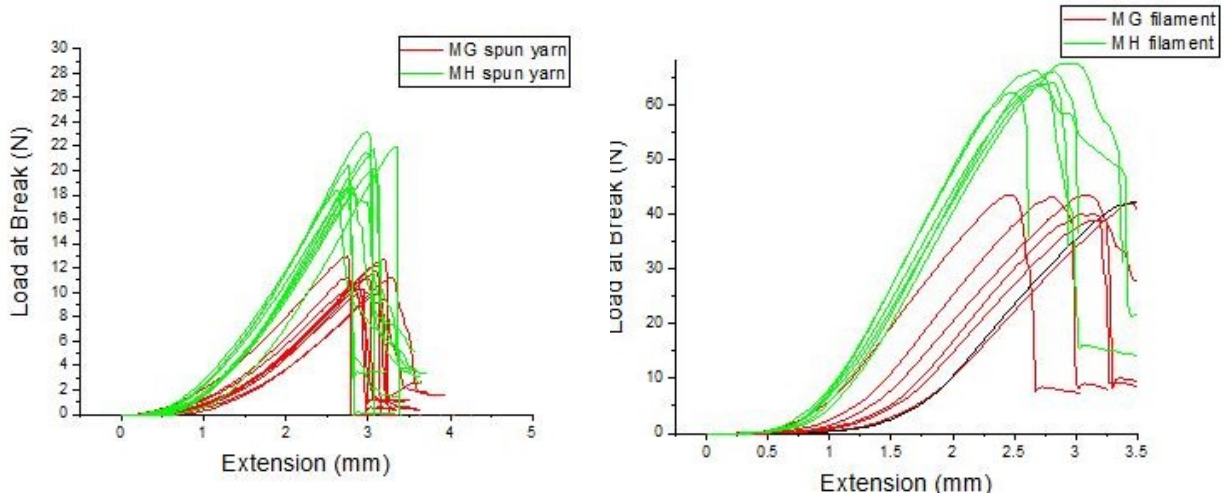


Figure 4.26 Mechanical performance of the a) spun and b) filament yarns in Fabric MG and Fabric MH

As a way to uncover where this difference in strength in the yarns is coming from, the yarn linear density was measured. The values are provided in Table 4.9. It shows that both the spun and filament yarns in Fabric MH have a higher linear density compared to MG. Previous literature suggests that yarns with a higher linear density, thus a larger diameter, have a higher strength [133]. The difference in yarn strength observed for the two fabrics can thus be attributed to the difference in the linear density of the two series of yarns.

Table 4.9 Tensile strength and linear density for the two sets of yarns in Fabric MG and MH

	Spun yarn		Filament yarn	
	Breaking strength (N)	Linear density (tex)	Breaking strength (N)	Linear density (tex)
Fabric MG	11 ± 1 N	53	42 ± 2 N	46
Fabric MH	20 ± 2 N	79	65 ± 2 N	66

Hump behaviour in yarns

The spun yarns from Fabric MF exhibited a hump-like characteristic in the load-extension curve (see Fig. 4.22). These yarns are composed of two plies and contain Kevlar®, Nomex® and antistat fibers. In an attempt to try explaining this unique feature, we did a video of the yarn while it was being stretched at a low speed and compared it to the slow-motion videos of spun yarns with similar structure and fiber content (from Fabric MC, MD and ME).

A first observation is that the yarns from Fabric MF take a long time to loose their crimp compared to the other yarns. This behavior can be attributed to their very high degree of crimp, at least twice as much compared to the other yarns (Table 4.1). However, it does not explain the reason behind the hump.

A second observation is that there was a rotation in the yarn from Fabric MF when it was stretched, which was not observed in the other similar yarns. This was also attributed to its very high degree of crimp. However, it does not explain either the reason behind the hump.

We looked for a difference in the degree of compliance between the two plies of the yarn, e.g. if one of the ply contained carbon fibers and not the other, which could explain the presence of the hump. Figure 4.27 shows the optical microscope image of the two plies of the yarn. Both plies show a few carbon fibers. Therefore, the potential explanation based on a difference in the degree of compliance caused by an inhomogeneous distribution of the carbon fibers between the two plies was not validated.

So far, no explanation has been found for the hump observed in the load-extension curve of the spun yarn in Fabric MF.

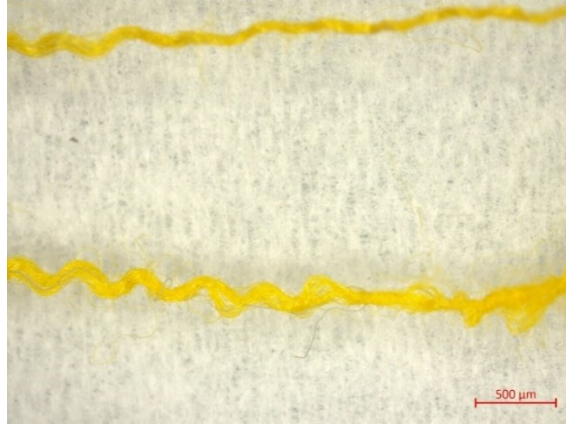


Figure 4.27 Optical microscopy image of the two plies of the spun yarn from Fabric MF

4.3 HYDROTHERMAL AGEING OF THE FABRICS

The following sections report the study of the effect of hydrothermal ageing on the mechanical behaviour of the fabrics at both the fabric and the yarn scale.

4.3.1 Results

Fabric MA

Figure 4.28 shows the load extension curve of the Fabric MA fabric specimens after hydrothermal ageing for 50 days at three different temperatures. The results for the unaged condition are also included. The aged specimens show the same typical three-part behaviour as the control specimens. In particular, there is no reduction in the crimp interchange due to hydrothermal ageing. However, the aged specimens exhibit a gradual decrease in the load and extension at break with increasing hydrothermal ageing temperature. The same behaviour was observed for the other ageing times.

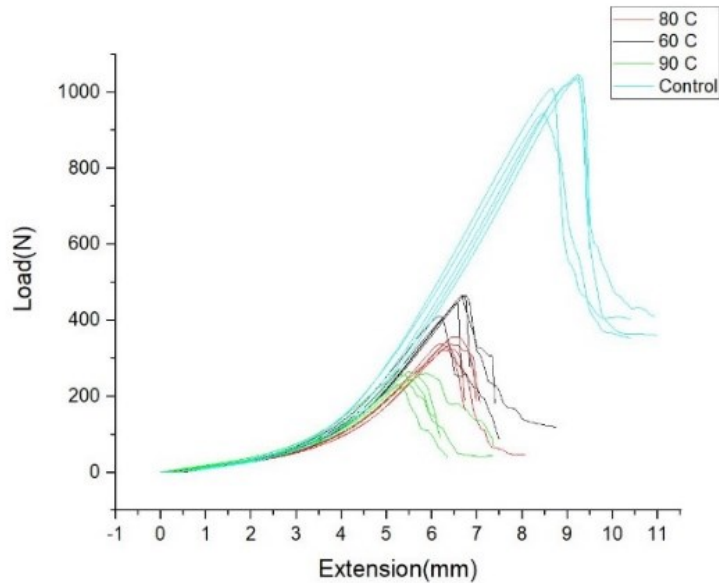


Figure 4.28 Mechanical behaviour of Fabric MA at the fabric scale under hydrothermal ageing after 50 days

The values of the load at break after 25 and 50 days of ageing are plotted in Figure 4.29 as a function of the ageing temperature. The individual data points corresponding to the different specimens tested are also included. The load at break follows a decreasing trend with increasing temperature. After 25 days of ageing at 90°C, the load at break reached 320 ± 20 N compared to 1020 ± 40 N for the unaged specimens, corresponding to a loss of 68% in the load at break. The load at break decreased to 250 ± 20 N for the fabric specimens aged at 90°C for 50 days, corresponding to a loss of 75% compared to the unaged specimens. A paired t-test was performed between the load values for the unaged condition and after ageing at 90°C for 50 days. A p value of 0.000005 was obtained indicating that significant degradation has occurred for the fabric specimen. A t-test was also performed between ageing at 25 and 50 days conducted at 90°C. A p value of 0.007 was obtained. This indicates that the extent of degradation between the two times is different.

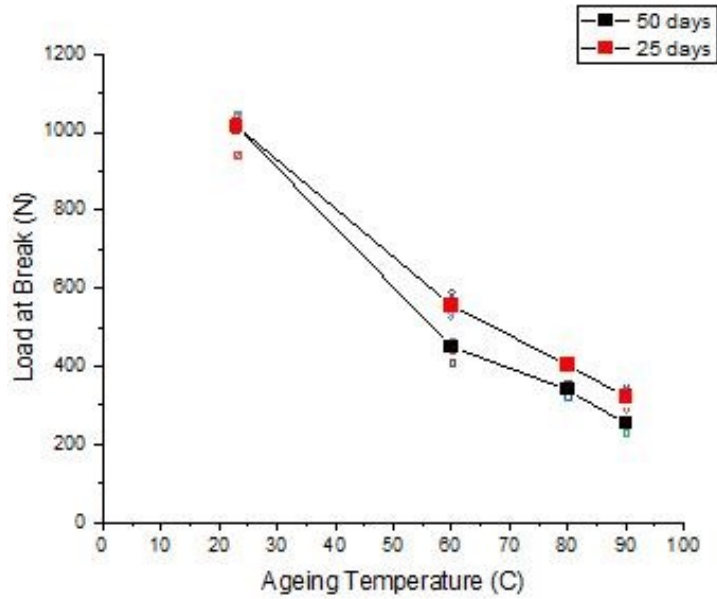


Figure 4.29 Variation of the load at break of the fabric specimens as a function of the ageing temperature for Fabric MA. The individual data points corresponding to the different specimens tested are also included (open symbols) in the graph.

The values for the load at break for the two types of yarns composing Fabric MA are plotted in Figure 4.30 as a function of the ageing temperature. Figure 4.30(a) corresponds to the spun yarn and Figure 4.30(b) corresponds to a 2-ply spun/filament yarn. The individual data points corresponding to the different specimens tested are also included. Both yarns show a decrease in the load at break with increasing temperature.

The spun yarn had a strength of 18 ± 2 N in the unaged condition. The strength progressively reduced to 5.5 ± 0.7 N after ageing for 25 days at 90°C ; it corresponds to a loss of 69% in the load value. The yarns aged for 50 days show a similar trend in degradation characterised by the yarn having a residual load at break of 5.0 ± 0.4 N after ageing at 90°C , corresponding to a total loss of 72%. A paired t-test was performed between the load values at unaged condition and after ageing at 90°C for 50 days. A p value of 5×10^{-11} was obtained, indicating that the spun yarn has undergone significant degradation. A t-test was also

performed between the load values at 25 and 50 days for 90°C. A p value of 0.002 was obtained. This indicates that the extent of degradation between 25 and 50 days is different.

The spun/filament yarn showed a load at break of 50 ± 4 N at the unaged condition. It progressively decreased to 7 ± 2 N after hydrothermal ageing for 25 days at 90°C, corresponding to a loss of 85% in the load at break. When aged for 50 days, the yarns showed a similar response to the increase in the ageing temperature. The load at break reduced to 5.0 ± 1.3 N after ageing at 90°C, corresponding to a loss of 90% in the load value. A p value of 0.0000001 between the data points at unaged condition and after ageing at 90°C for 50 days indicates that the yarn experienced significant degradation due to hydrothermal ageing.

The difference between the loads at break after 25 and 50 days of ageing decreased when the ageing temperature increased. A statistical comparison between the load values at 25 and 50 days for 90°C shows a statistical difference (p value of 0.008). This indicates that the extent of degradation is different for the two times.

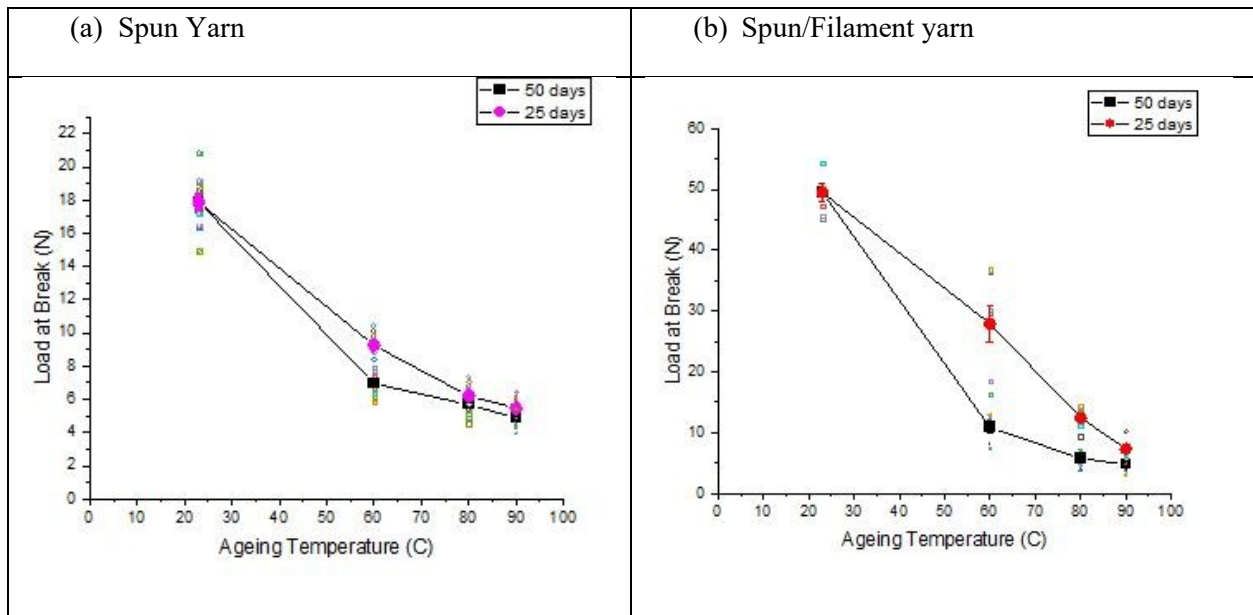


Figure 4.30 Variation of the load at break for the (a) spun yarn and (b) spun/filament yarn from Fabric MA as a function of the ageing temperature. The individual data points corresponding to the different specimens tested are also included (open symbols) in the graph.

Figure 4.31 compares the visual aspect of specimens of Fabric MA before ageing and after ageing for 50 days at 90°C. A strong change in the specimen color is visible.

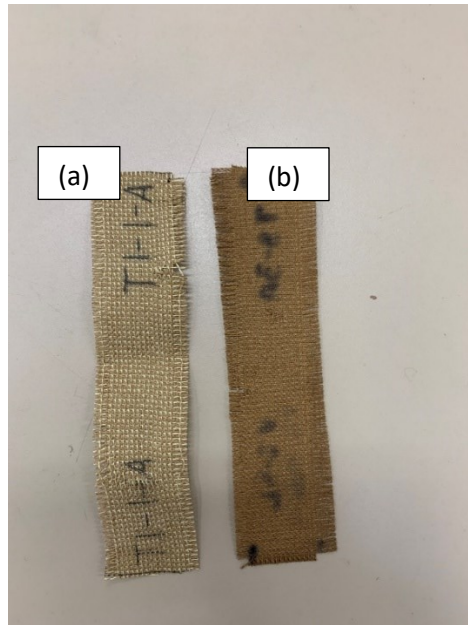


Figure 4.31 Fabric MA specimens (a) before ageing and (b) after ageing for 50 days at 90°C

Fabric MB

Figure 4.32 shows the load extension curves of the fabric specimens of Fabric MB after 50 days of hydrothermal ageing at three different temperatures. The results for the unaged condition are also included. The aged specimens show the same three-part behaviour as the control specimens. In particular, there is no reduction in the crimp interchange due to hydrothermal ageing. However, the aged specimens exhibit a gradual decrease in the load and extension at break with increasing hydrothermal ageing temperature. The same behaviour was observed for the other ageing times.

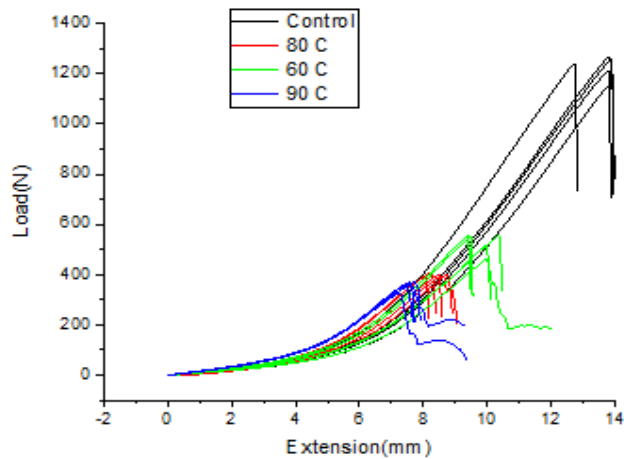


Figure 4.32 Mechanical behaviour of Fabric MB tested at the fabric scale under hydrothermal ageing after 50 days

The values of the load at break after 25 and 50 days of ageing are plotted on Figure 4.33 as a function of the ageing temperature. The individual data points corresponding to the different specimens tested are also included. The load at break follows a decreasing trend with increasing temperature. After 25 days of ageing at 90°C, the load at break goes from 1230 ± 30 N for the unaged specimens to 410 ± 20 N, which corresponds to a loss of 67%. After 50 days of ageing at 90°C, the load at break reached 360 ± 20 N, corresponding to a loss of 71% in the load at break. A paired t-test was performed between the load values at unaged condition and after ageing at 90°C for 50 days. A p value of 1×10^{-7} was obtained, which indicates that the extent of degradation is statistically significant. A t-test was also performed between the results corresponding to ageing at 25 and 50 days conducted at 90°C. A p value of 0.002 was obtained. This indicates that the extent of degradation between the two times is different.

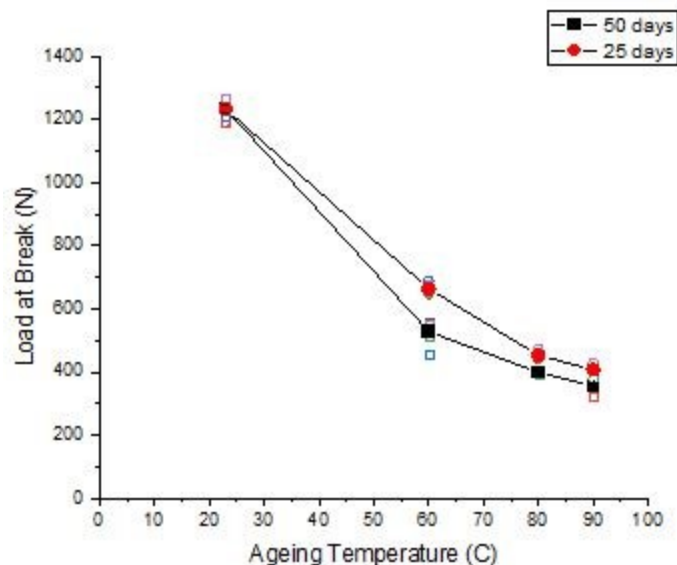


Figure 4.33 Variation of the load at break as a function of the ageing temperature for Fabric MB at the fabric scale. The individual data points corresponding to the different specimens tested are also included (open symbols) in the graph.

The values of the load at break for the two types of yarns composing Fabric MB are plotted in Figure 4.34 as a function of the ageing temperature. The individual data points corresponding to the different specimens tested are also included. Figure 4.34(a) corresponds to the spun yarn and Figure 4.34(b) corresponds to the 2-ply spun/filament yarn. The spun yarns show a decrease in load values with increasing temperature whereas the spun/filament yarns show no effect of hydrothermal ageing.

The spun yarn shows a strength of 29 ± 2 N in the unaged condition. The strength progressively reduces to 6 ± 1 N after ageing for 25 days at 90°C ; it corresponds to a loss of 79% in the load value. The yarns aged for 50 days show a similar trend in the degradation characterised by the yarn having a residual load at break of 5.5 ± 0.6 N after ageing at 90°C , corresponding to a total loss of 81% compared to the unaged value. A paired t-test was performed between the load values at unaged condition and after ageing at 90°C for 50 days. A p value of 6×10^{-17} was obtained which indicated that the extent of degradation for the yarn is statistically significant. A t-test was also performed between the load values at 25 and 50 days for 90°C . A

p value of 0.03 was obtained. This indicates that the extent of degradation between 25 and 50 days is different.

The spun/filament yarn shows a strength of 56 ± 3 N in the unaged condition. The load at break increased to 63 ± 2 N after ageing for 25 days at 90°C , corresponding to an increase by 13%. The yarns when aged for 50 days show a similar response to increase in ageing temperature. The load increases from 56N at the unaged condition to 61 ± 2 N after ageing at 90°C for 250 days, corresponding to a gain of 9% in load value. An ANOVA analysis was performed between all the data points starting from unaged condition to ageing at 90°C for 50 days. It gave a p value of 0.124. This indicated that the yarn didn't undergo any significant change at any of the measured data point when exposed to 90°C for up to 50 days.

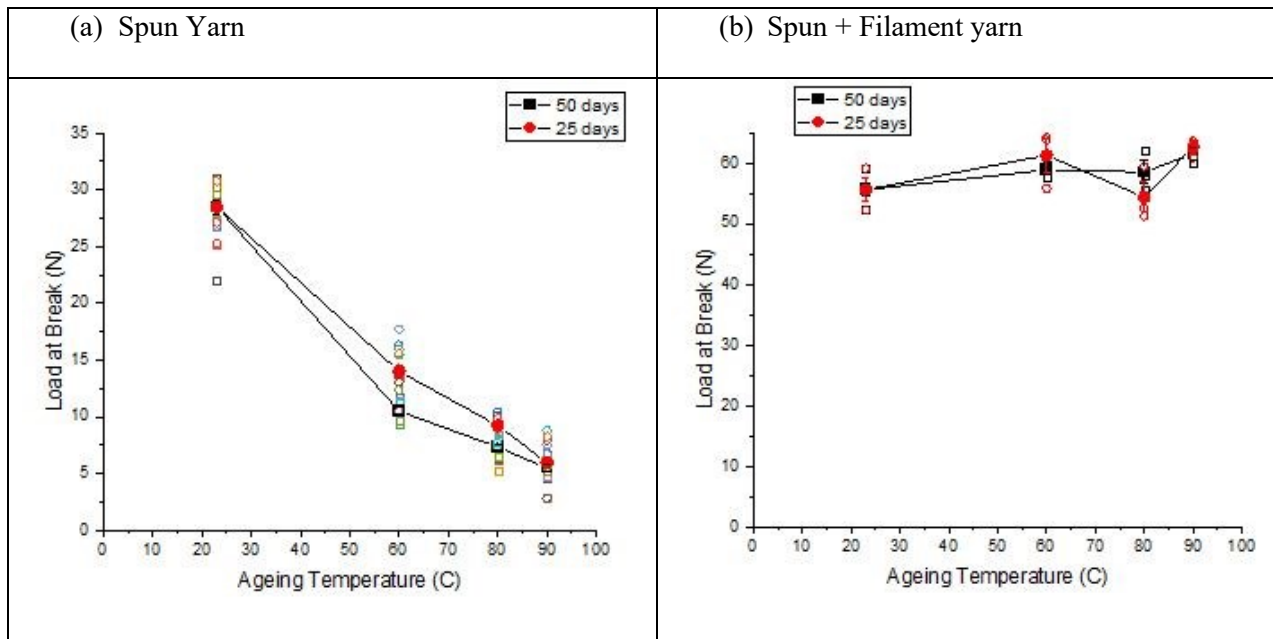


Figure 4.34 Variation of the load at break for the (a) spun yarn and (b) spun/ filament (2-ply) yarn for Fabric MB as a function of the ageing temperature. The individual data points corresponding to the different specimens tested are also included (open symbols) in the graph.

Figure 4.35 compares the visual aspect of specimens of Fabric MB before ageing and after ageing for 50 days at 90°C . A change in the specimen color is visible.

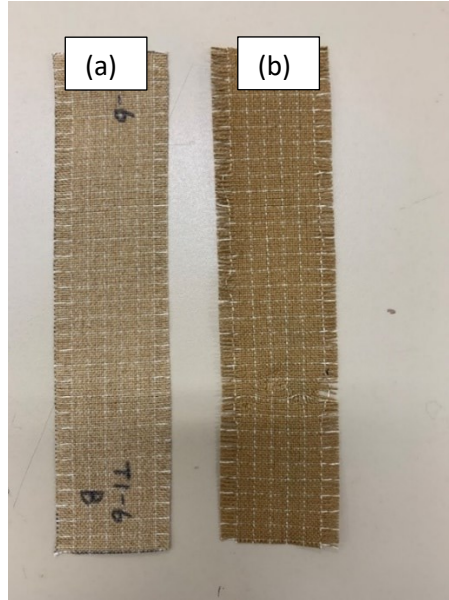


Figure 4.35 Fabric MB specimens (a) before ageing and (b) after ageing for 50 days at 90°C

Fabric MC

Figure 4.36 shows the load extension curves of the fabric specimens for Fabric MC under hydrothermal ageing for three different temperatures after 50 days of ageing. The results for the unaged condition are also included. The aged specimens show the same three-part behaviour as the control specimen. There is no reduction in crimp interchange due to hydrothermal ageing. The aged specimens do not appear to exhibit any change in the load and extension at break with increasing hydrothermal ageing temperature. The same behaviour was observed for the other ageing times.

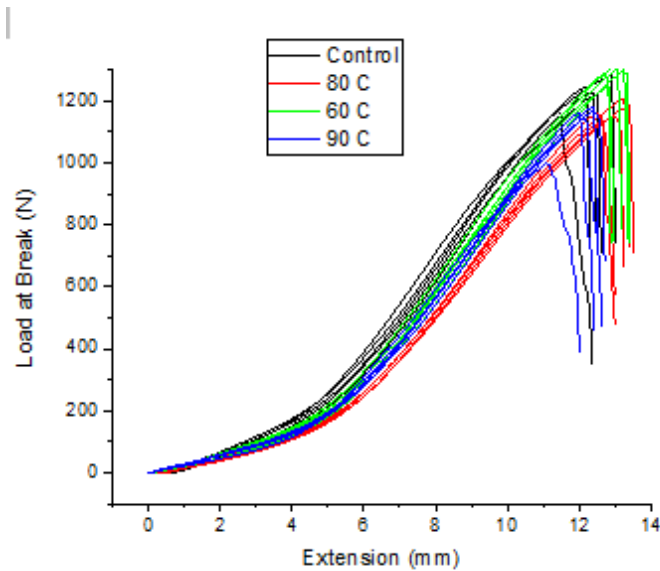


Figure 4.36 Mechanical behaviour of the Fabric MC at the fabric scale under hydrothermal ageing after 50 days

The values of the load at break after 25 and 50 days of ageing are plotted on Figure 4.37 as a function of the ageing temperature. The individual data points corresponding to the different specimens tested are also included. After ageing for 25 days, the load goes from 1230 ± 40 N for the unaged specimens to 1130 ± 40 N for the fabric specimens, corresponding to a loss of 8% in the load at break compared to the unaged value. After 50 days of ageing at 90°C , the load at break reached 1130 ± 80 N, also corresponding to a loss of 8%. An ANOVA analysis was performed at 25 and 50 days. In both cases, statistically significant differences exist between some results at the different temperatures (p value of 0.0003 for 25 days and p value of 7×10^{-6} for 50 days).

A t-test was performed between the data points at for relevant combinations. The results are shown in Table 4.10. For the data at 25 days of ageing, it shows a significant difference between 60°C and 80°C . However, it may be due to the very low standard deviation and we don't think that the specimens experienced a significant degradation after 25 days of ageing up to 90°C . In case of 50 days of ageing, significant differences are observed above 60°C . The onset of degradation is thus between 60°C and 80°C .

Table 4.10 t-test analysis between relevant conditions for fabric MC

Condition	Duration of ageing	P value
Between unaged and 60°C	25 days	0.057
Between 60°C and 80°C	25 days	0.006
Between 80°C and 90°C	25 days	0.240
Between unaged and 90°C	25 days	0.106
Between unaged and 60°C	50 days	0.07
Between 60°C and 80°C	50 days	0.01
Between 80°C and 90°C	50 days	0.003
Between unaged and 90°C	50 days	0.001

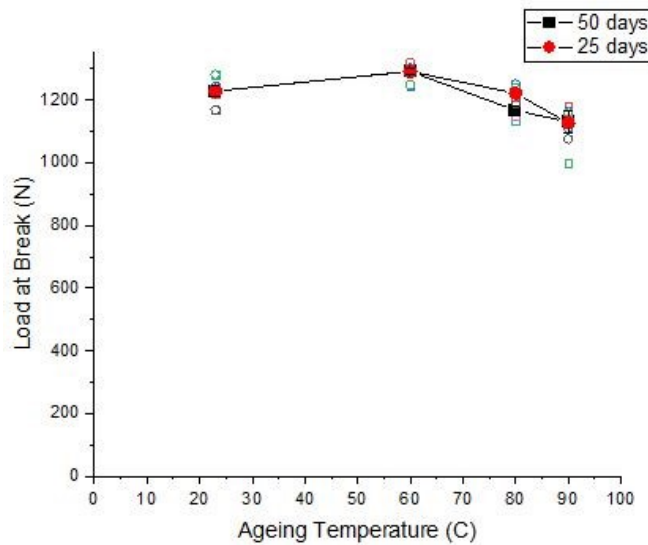


Figure 4.37 Variation of the load at break as a function of the ageing temperature for Fabric MC at the fabric scale. The individual data points corresponding to the different specimens tested are also included (open symbols) in the graph.

The values for the load at break for the two types of yarns composing Fabric MC are plotted in Figure 4.38 as a function of the ageing temperature. Figure 4.38(a) corresponds to the spun yarn and Figure 4.38(b)

corresponds to the filament yarn. The individual data points corresponding to the different specimens tested are also included. The spun yarn shows a small decrease in the load values with increasing ageing temperatures whereas the filament yarn doesn't appear to show any degradation as a result of hydrothermal ageing.

The spun yarn shows a strength of 19 ± 2 N in the unaged condition. The strength reduces to 18 ± 1 N after ageing for 25 days at 90°C ; this corresponds to a loss of 5% in load value. The yarns aged for 50 days at 90°C reached a load at break of 14 ± 1 N after ageing, corresponding to a total loss of 26% in the load value. An ANOVA analysis was performed for 25 and 50 days of ageing. For the 25 days of ageing data, the differences were not statistically different (p value of 0.716). For 50 days of ageing the ANOVA showed that there are some results that are different (p value of 5.2×10^{-9}). A paired test was performed between the different temperatures as shown in Table 4.11. This indicates that the onset of degradation is around 80°C for 50 days.

Table 4.11 t-test analysis between relevant condition for spun yarn in fabric MC

Condition	Duration of ageing	P value
Between unaged and 60°C	25 days	0.984
Between 60°C and 80°C	25 days	0.665
Between 80°C and 90°C	25 days	0.506
Between unaged and 90°C	25 days	0.241
Between unaged and 60°C	50 days	0.81
Between 60°C and 80°C	50 days	0.065
Between 80°C and 90°C	50 days	0.0007
Between unaged and 90°C	50 days	2.18×10^{-7}

The filament yarns show a small increase in load value when aged for 25 days. The load at break increased from 40 ± 1 N at the unaged condition to 43 ± 1 N after ageing at 90°C for 25 days, corresponding to a gain

of 7% in the load value. The filament yarn strength decreased to 37 ± 5 N after ageing for 50 days at 90°C , corresponding to a decrease of 5% in the load at break. An ANOVA analysis was performed for 50 days of ageing. For the 50 days of ageing data, the differences were not statistically different (p value of 0.114). This indicates that the yarn did not undergo any significant degradation.

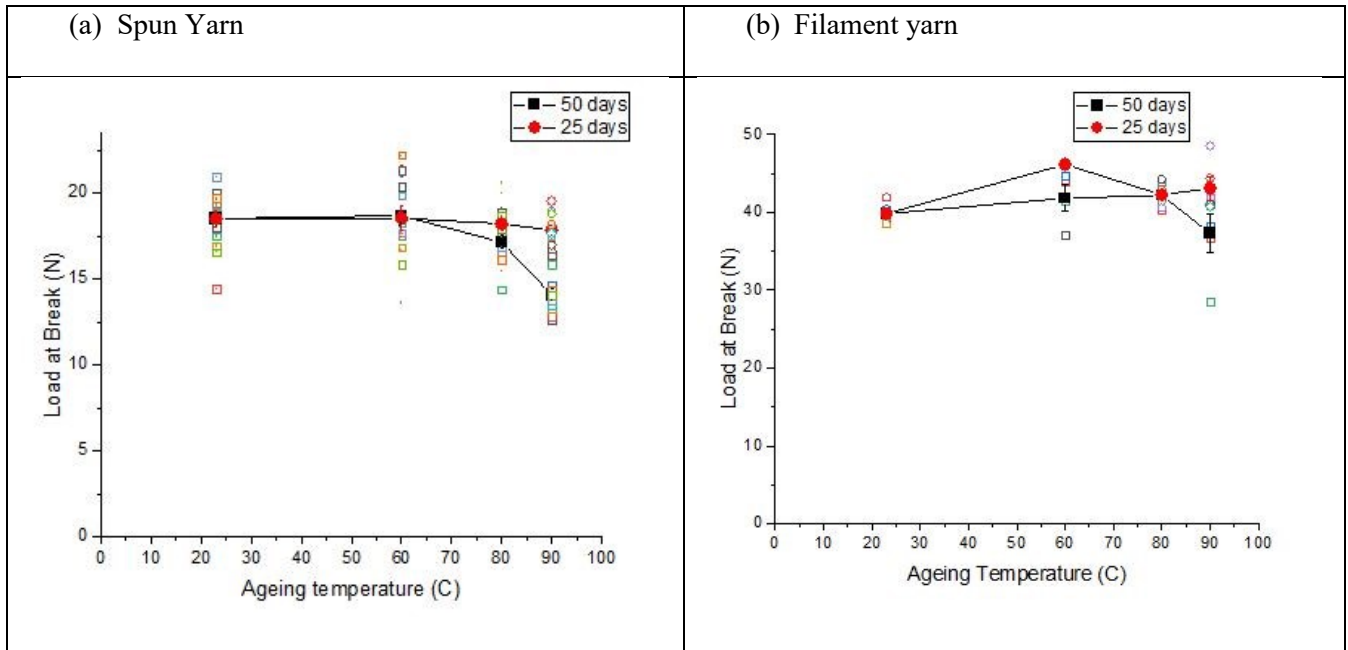


Figure 4.38 Variation of the load at break for (a) the spun yarn and (b) the filament yarn for Fabric MC as a function of the ageing temperature. The individual data points corresponding to the different specimens tested are also included (open symbols) in the graph.

Figure 4.39 compares the visual aspect of specimens of Fabric MC before ageing and after ageing for 50 days at 90°C . No major change in color can be observed.

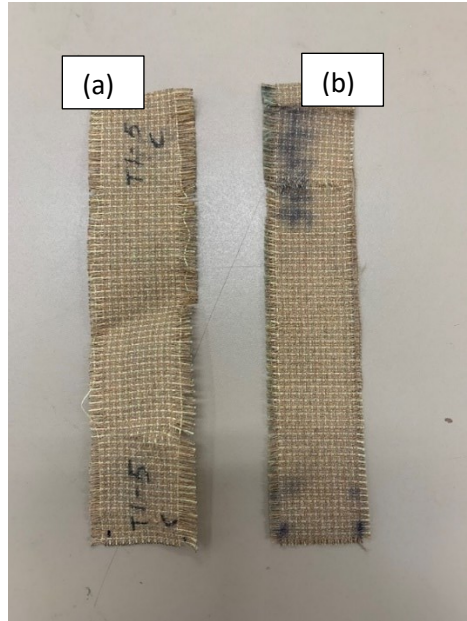


Figure 4.39 Fabric MC specimens (a) before ageing and (b) after ageing for 50 days at 90°C

Fabric MD

Figure 4.40 shows the load extension curves of fabric specimens of Fabric MD after 50 days of hydrothermal ageing for three different temperatures. The results for the unaged condition are also included. The aged specimens show the same three-part behaviour as the control specimen. There is no reduction in crimp interchange due to hydrothermal ageing. The aged specimens exhibit a decrease in the load and extension at break with increasing hydrothermal ageing temperature. The same behaviour was observed for the other ageing times.

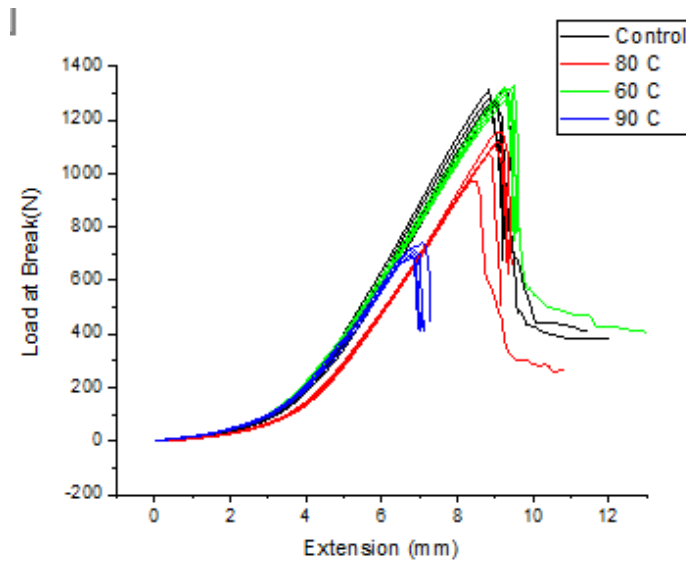


Figure 4.40 Mechanical behaviour of the Fabric MD at the fabric scale under hydrothermal ageing after 50 days

The values of the load at break after 25 and 50 days of ageing are plotted in Figure 4.41 as a function of the ageing temperature. The individual data points corresponding to the different specimens tested are also included. The load at break follows a decreasing trend with increasing temperature. After ageing for 25 days at 90°C, the load at break goes to 990 ± 40 N compared to 1290 ± 20 N for the unaged specimens, corresponding to a loss of 24%. After 50 days of ageing at 90°C, the load at break reached 710 ± 20 N, corresponding to a loss of 45% in the load at break compared to the unaged condition. An ANOVA analysis was performed for 25 and 50 days of ageing. In both cases, it shows that there are results that are different (p value of 4×10^{-11} for 25 days and p value of 1.8×10^{-13} for 50 days). A paired test was performed between the different temperatures as shown in Table 4.12. This indicates that the onset of degradation is around 80°C for 25 days of ageing; the degradation starts between 60°C and 80 °C for 50 days of ageing.

Table 4.12 t-test analysis between relevant conditions for fabric MD

Condition	Duration of ageing	P value
Between unaged and 60°C	25 days	0.170

Between 60°C and 80°C	25 days	0.225
Between 80°C and 90°C	25 days	9.83×10^{-5}
Between unaged and 90°C	25 days	3.24×10^{-5}
Between unaged and 60°C	50 days	0.289
Between 60°C and 80°C	50 days	0.004
Between 80°C and 90°C	50 days	0.0001
Between unaged and 90°C	50 days	4×10^{-7}

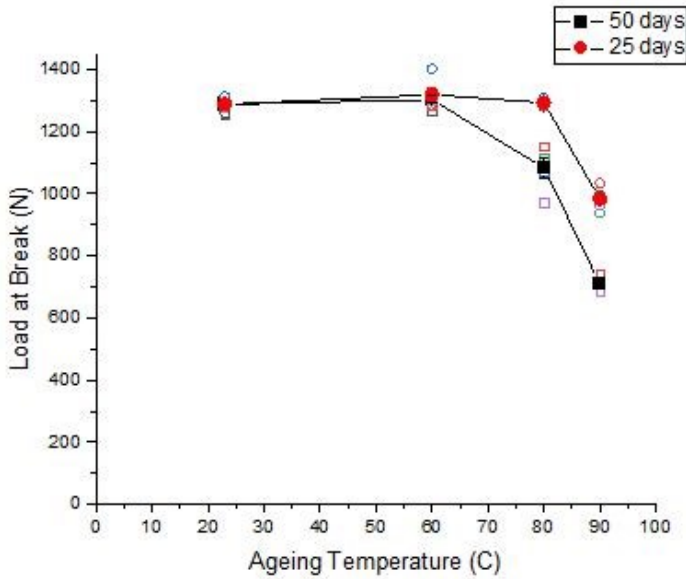


Figure 4.41 Variation in the load at break as a function of the ageing temperature for Fabric MD at the fabric scale. The individual data points corresponding to the different specimens tested are also included (open symbols) in the graph.

The values of the load at break for the two types of yarns composing Fabric MD are plotted in Figure 4.42 as a function of the ageing temperature. The individual data points corresponding to the different specimens tested are also included. Figure 4.42(a) corresponds to the Kevlar/Nomex spun yarn and Figure 4.42(b)

corresponds to the spun yarn comprised entirely of Kevlar. Both yarns show a relatively constant value of load at break until 60°C followed by a decrease in the load value with increasing temperature above that.

The Kevlar/Nomex spun yarn showed a strength of 25 ± 3 N in the unaged condition. The load at break progressively reduced to 19 ± 2 N after ageing for 25 days at 90°C; it corresponds to a loss of 24% in the load value. The yarns aged for 50 days at 90°C show a similar trend in the load at break, which reached 15 ± 1 N, corresponding to a total loss of 40% in the load value. An ANOVA analysis was performed for 25 and 50 days of ageing. In both cases, it shows that there are results that are different (p value of 8×10^{-10} for 25 days and p value of 4.7×10^{-15} for 50 days). A paired test was performed between the different temperatures as shown in Table 4.13. It indicates that the onset of degradation is between 60°C and 80°C when aged for 50 days whereas degradation starts between 80°C and 90°C when aged for 25 days.

Table 4.13 t-test analysis between relevant conditions for Kevlar/Nomex spun yarn in fabric MD

Condition	Duration of ageing	P value
Between unaged and 60°C	25 days	0.479
Between 60°C and 80°C	25 days	0.133
Between 80°C and 90°C	25 days	9.84×10^{-6}
Between unaged and 90°C	25 days	3.46×10^{-5}
Between unaged and 60°C	50 days	0.696
Between 60°C and 80°C	50 days	0.0001
Between 80°C and 90°C	50 days	2.06×10^{-6}
Between unaged and 90°C	50 days	1.43×10^{-7}

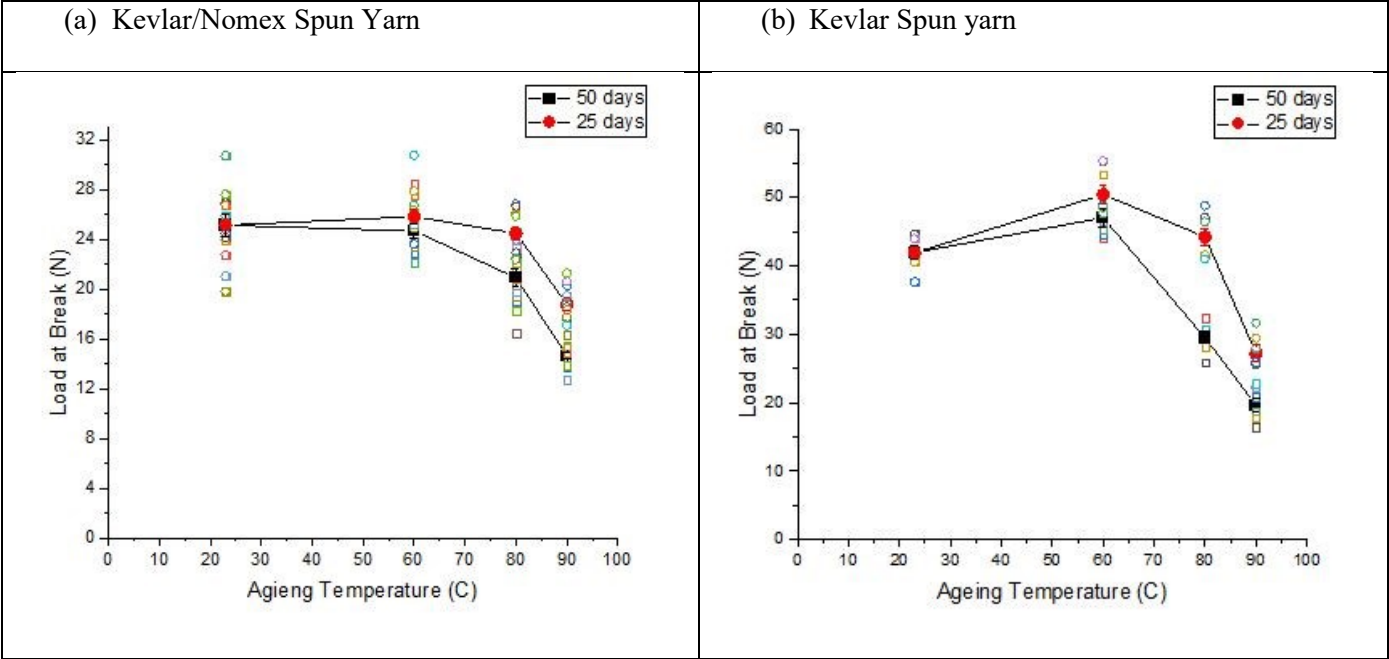


Figure 4.42 Variation in the load at break for (a) the (a) Kevlar/Nomex spun yarn and (b) the Kevlar spun yarn for Fabric MD as a function of the ageing temperature. The individual data points corresponding to the different specimens tested are also included (open symbols) in the graph.

The 100% Kevlar spun yarn showed a strength of 42 ± 3 N in the unaged condition. The load at break first slightly increased after ageing at 60°C , then decreased with further increase in the ageing temperature. The load at break reached 27 ± 3 N after 25 days at 90°C , corresponding to a decrease of 36% in the load at break. The load decreases to 20 ± 2 N after ageing at 90°C for 50 days, corresponding to a loss of 52% in load value. An ANOVA analysis was performed for 25 and 50 days of ageing. In both cases, it shows that there are results that were different (p value of 1.2×10^{-14} for 25 days and p value of 7.7×10^{-12} for 50 days). A paired t-test was performed between the different temperatures as shown in Table 4.14. This indicates that the onset of degradation is between 60°C and 80°C when aged for 50 days whereas degradation starts between 80°C and 90°C when aged for 25 days.

Table 4.14 t-test analysis between relevant conditions for Kevlar yarn of fabric MD

Condition	Duration of ageing	P value
Between unaged and 80°C	25 days	0.170

Between 80°C and 90°C	25 days	0.006
Between unaged and 90°C	25 days	1.2×10^{-6}
Between unaged and 60°C	50 days	0.289
Between 60°C and 80°C	50 days	0.0001
Between 80°C and 90°C	50 days	2.06×10^{-6}
Between unaged and 90°C	50 days	1.43×10^{-7}

Figure 4.43 compares the visual aspect of specimens of Fabric MC before ageing and after ageing for 50 days at 90°C. A slight change in color is visible.

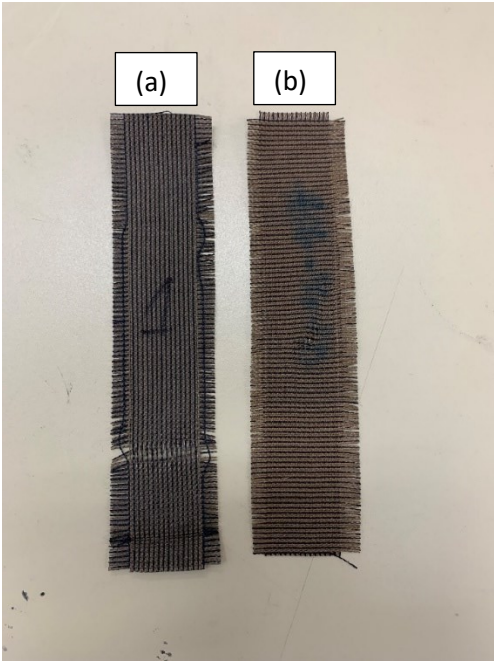


Figure 4.43 Fabric MD specimens (a) before ageing and (b) after ageing for 50 days at 90°C

Fabric ME

Figure 4.44 shows the load extension curve of fabric specimens for Fabric ME after 50 days of hydrothermal ageing for three different temperatures. The results for the unaged condition are also included. The aged

specimens show the same three-part behaviour as the control specimen. There is no reduction in the crimp interchange due to hydrothermal ageing. The aged specimens exhibit a constant value in the load and extension at break with increasing hydrothermal ageing temperature until 80°C. The specimens show a decrease in the load and extension at break when aged at 90°C.

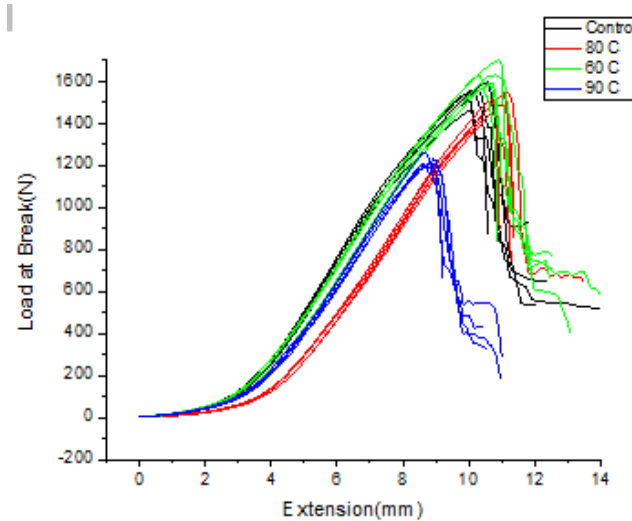


Figure 4.44 Mechanical behaviour of the fabric specimens of Fabric ME under hydrothermal ageing at different temperatures after 50 days

The values of the load at break for the fabric specimens after 25 and 50 days of ageing are plotted on Figure 4.45 as a function of the ageing temperature. The individual data points corresponding to the different specimens tested are also included. The load at break exhibits a relatively constant load at break value with increasing temperature. A decrease is only recorded at 90°C after 50 days of ageing.

After ageing for 25 days at 90°C, the load goes from 1540 ± 5 N for the unaged specimens to 1470 ± 40 N for the aged specimens, corresponding to a loss of 4% in the load at break. After 50 days of ageing at 90°C, the load at break reached 1220 ± 30 N, corresponding to a loss of 20% compared to the unaged condition. An ANOVA analysis was performed for 25 and 50 days of ageing. For the 25 days of ageing data, the differences were not statistically different (p value of 0.1), which shows that the degradation has not started

yet. For 50 days of ageing the ANOVA showed that there were results that were different (p value of 7×10^{-10}). A paired test was performed between the different temperatures as shown in Table 4.15. This indicates that for 50 days, the onset of degradation was between 80°C and 90°C.

Table 4.15 t-test analysis between relevant conditions for fabric ME

Condition	Duration of ageing	P value
Between unaged and 80°C	50 days	0.384
Between 80°C and 90°C	50 days	1.86×10^{-5}
Between unaged and 90°C	50 days	0.0003

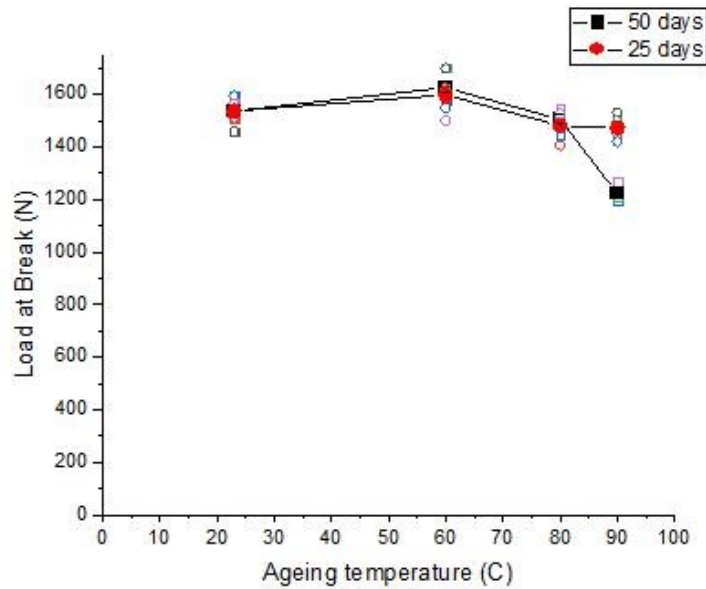


Figure 4.45 Variation of the load at break as a function of the ageing temperature for Fabric ME. The individual data points corresponding to the different specimens tested are also included (open symbols) in the graph.

The values of the load at break for the two types of spun yarns of same fiber content but different linear density composing Fabric ME are plotted in Figure 4.46 as a function of the ageing temperature. Figure

4.46(a) corresponds to the thinner yarn and Figure 4.46(b) corresponds to the thicker yarn. The individual data points corresponding to the different specimens tested are also included.

The thinner yarns showed a constant value of the load at break until 60°C followed by a decrease in the load with increasing temperature. The yarn shows a strength of 34 ± 3 N in the unaged condition. The load at break reduced to 32 ± 3 N after ageing for 25 days at 90°C, which corresponds to a loss of 7% compared to the unaged condition. The yarns aged for 50 days showed a similar trend, with a residual load at break of 28 ± 2 N after ageing at 90°C, corresponding to a loss of 19% compared to the unaged condition. An ANOVA analysis was performed for 25 and 50 days of ageing. In both cases, the results show possibly significant differences between some results (p value of 0.006 for 25 days of ageing and p value of 9.2×10^{-27} for 50 days). A t-test was done for the different relevant combinations of conditions as shown in Table 4.16. For the 25 days of ageing, the t-test didn't reveal any significant difference between these conditions, which shows that the samples have not experienced significant degradation. For 50 days of ageing, the t-test show significant difference above 60°C. This indicates that the degradation started between 60°C and 80 °C for 50 days.

Table 4.16 t-test analysis between relevant conditions for the thinner yarn in fabric ME

Condition	Duration of ageing	P value
Between unaged and 60°C	25 days	0.057
Between 60°C and 80°C	25 days	0.14
Between 80°C and 90°C	25 days	0.149
Between unaged and 90°C	25 days	0.107
Between unaged and 60°C	50 days	0.76
Between 60°C and 80°C	50 days	0.00035
Between 80°C and 90°C	50 days	0.15
Between unaged and 90°C	50 days	5×10^{-5}

The thicker yarn showed a load at break of 53 ± 3 N in the unaged condition. The load at break remained relatively constant after 25 days of ageing at the different temperatures. When aged for 50 days, the yarns maintained a constant load at break until 80°C followed by decrease at 90°C. The load reached 41 ± 4 N after 50 days of ageing at 90°C, corresponding to a loss of 23% compared to the unaged value. An ANOVA analysis was performed for 25 and 50 days of ageing. For the 25 days of ageing data, the differences were not statistically different (p value of 0.08), which indicates that the degradation has not started after 25 days at up to 90°C. For 50 days of ageing the ANOVA showed that there were results that were different (p value of 0.024). A paired t-test was performed between the different temperatures as shown in Table 4.17. This indicates that the degradation started between 80°C and 90 °C when aged for 50 days.

Table 4.17 t-test analysis between relevant conditions for thicker yarn in fabric ME

Condition	Duration of ageing	P value
Between unaged and 60°C	50 days	0.464
Between 60°C and 80°C	50 days	0.675
Between 80°C and 90°C	50 days	0.0003
Between unaged and 90°C	50 days	0.0001

Figure 4.47 compares the visual aspect of specimens of Fabric ME before ageing and after ageing for 50 days at 90°C. The aged specimen has become slightly darker.

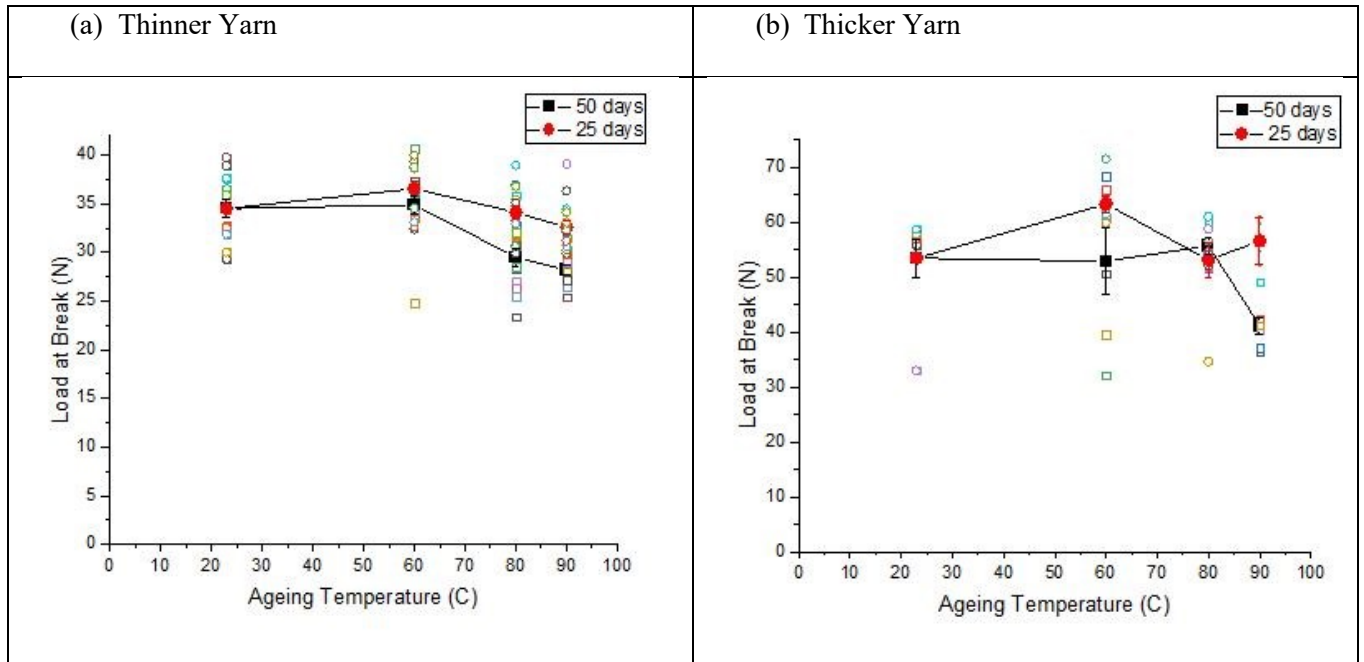


Figure 4.46 Variation of the load at break for (a) the thinner yarn and (b) the thicker yarn for Fabric ME as a function of the ageing temperature. The individual data points corresponding to the different specimens tested are also included (open symbols) in the graph.

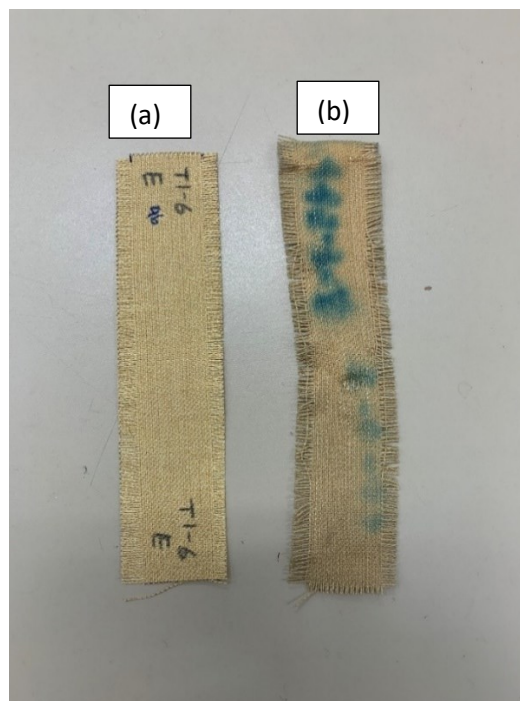


Figure 4.47 Fabric ME specimens (a) before ageing and (b) after ageing for 50 days at 90°C

Fabric MF

Figure 4.48 shows the load extension curves for the fabric specimens of Fabric MF after 50 days of hydrothermal ageing for three different temperatures. The results for the unaged condition are also included. The aged specimens show the same two-part behaviour as the control specimens (including the hump). The fabric continues to show no crimp interchange after ageing for three different temperatures. The aged specimens exhibit no decrease in the load and extension at break with the increasing hydrothermal ageing temperature. The same behaviour was observed for the other ageing times.

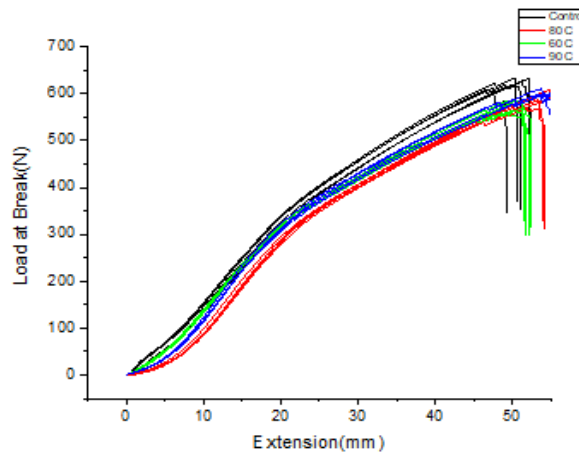


Figure 4.48 Mechanical behaviour of the fabric MF at the fabric scale under hydrothermal ageing after 50 days at different temperatures

The values of the load at break at the fabric scale after 25 and 50 days of ageing are plotted on Figure 4.49 as a function of the ageing temperature. The individual data points corresponding to the different specimens tested are also included. The load at break remained relatively constant with increasing temperature. The load went from 624 ± 9 N for the unaged specimens to 620 ± 20 N for the fabric specimens aged at 90°C for 25 days, corresponding to a loss of 1% in the load at break. After 50 days of ageing at 90°C , the load at break reached 601 ± 6 N, corresponding to a loss of 4% in the load at break. An ANOVA analysis was performed for 25 and 50 days of ageing. In both cases, it indicates that some results are significantly different from each other (for 25 days of ageing, p value of 3.5×10^{-6} . and for 50 days of ageing p value of

9.66x10⁻⁶). A paired t-test was performed between the different relevant conditions as shown in Table 4.18.. Even though it shows some statistically significant differences in some instances, we are not sure if the specimens underwent a significant degradation or not.

Table 4.18 t-test analysis between relevant conditions for fabric MF

Condition	Duration of ageing	P value
Between unaged and 60°C	25 days	0.001
Between 60°C and 80°C	25 days	0.178
Between 80°C and 90°C	25 days	0.055
Between unaged and 90°C	25 days	0.345
Between unaged and 60°C	50 days	0.0006
Between 60°C and 80°C	50 days	0.087
Between 80°C and 90°C	50 days	0.318
Between unaged and 90°C	50 days	0.0025

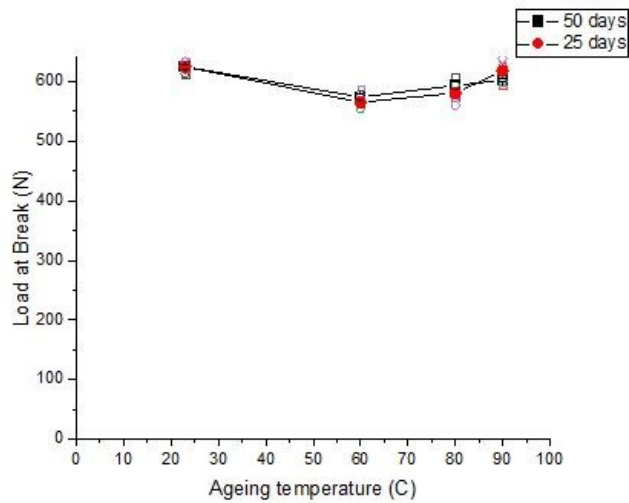


Figure 4.49 Variation of the load at break as a function of the ageing temperature for Fabric MF. The individual data points corresponding to the different specimens tested are also included (open symbols) in the graph.

The values for the load at break for the spun yarns composing Fabric MF are plotted in Figure 4.50 as a function of the ageing temperature. The individual data points corresponding to the different specimens tested are also included. The spun yarns appear to maintain a constant value of load at break after hydrothermal ageing.

The spun yarn shows a load at break of 7.2 ± 0.6 N in the unaged condition. It remains constant at 7.3 ± 0.6 N after ageing for 25 days at 90°C ; this corresponds to a gain of 1% in the load value, which is statistically insignificant. The yarns aged for 50 days at 90°C show a similar trend, with a load at break of 7.7 ± 0.9 N after ageing, corresponding to a gain of 7% in the load value. An ANOVA test was performed. For the data at 25 and 50 days of ageing, the differences were not statistically significant ($p=0.115$ for 25 days and p value of 0.08 for 50 days). This confirms that the yarn has not undergone any degradation after the hydrothermal ageing at up to 90°C for up to 50 days.

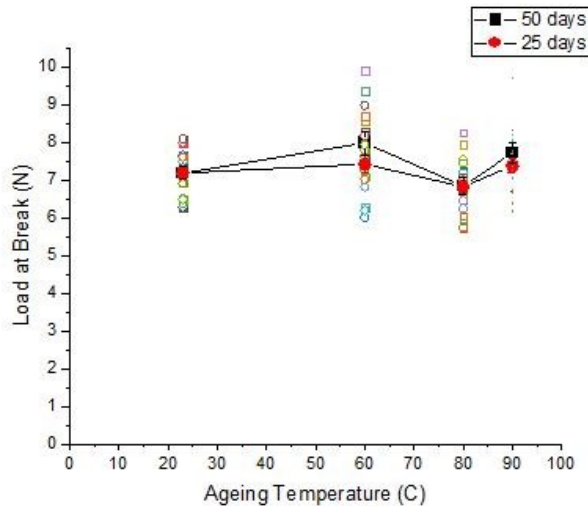


Figure 4.50 Variation of the load at break for Fabric MF as a function of the ageing temperature for spun yarn. The individual data points corresponding to the different specimens tested are also included (open symbols) in the graph.

Figure 4.51 compares the visual aspect of specimens of Fabric MF before ageing and after ageing for 50 days at 90°C . The fabric does not appear to experience any change in color.

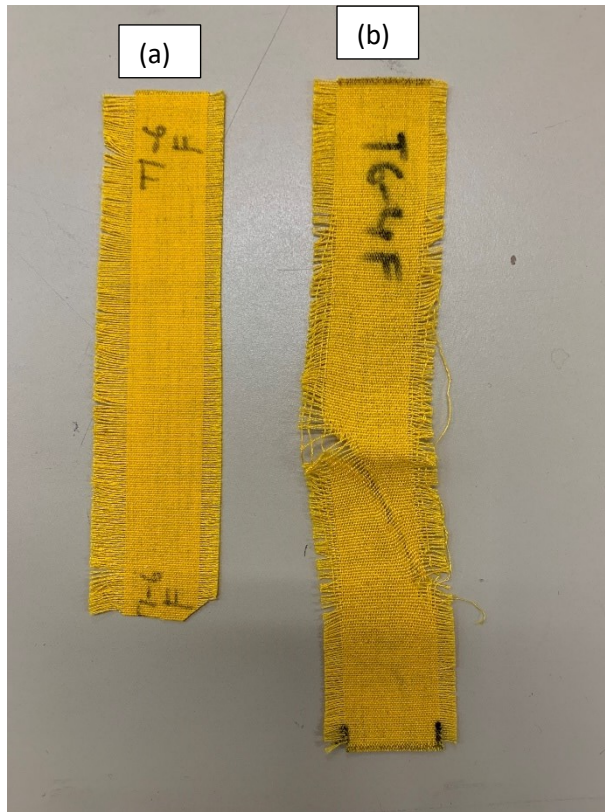


Figure 4.51 Fabric MF specimens (a) before ageing and (b) after ageing for 50 days at 90°C

Fabric MG

Figure 4.52 shows the load extension curve of the fabric specimens of Fabric MG after 50 days of hydrothermal ageing for three different temperatures. The results for the unaged condition are also included. There is no reduction in the crimp interchange due to hydrothermal ageing. However, the hump in the load extension curve observed for the unaged specimen is not present for the aged specimens. Instead, the failure appears to take place in two stages, with the presence of two peaks in the load extension curve. In addition, the aged specimens exhibit a gradual decrease in the load and extension at break with the increasing hydrothermal ageing temperature. The same behaviour was observed for the other ageing times.

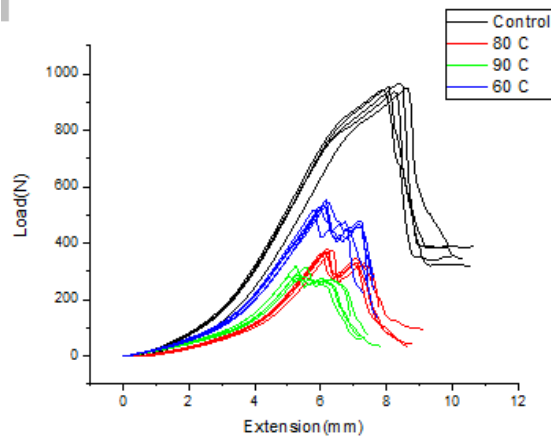


Figure 4.52 Mechanical behaviour of Fabric MG under hydrothermal ageing after 50 days

The values of the load at break after 25 and 50 days of ageing at the fabric scale are plotted on Figure 4.53 as a function of the ageing temperature. The individual data points corresponding to the different specimens tested are also included. The load at break follows a decreasing trend with increasing temperature. After 25 days of ageing at 90°C, the load went from 950 ± 10 N for the unaged specimens to 360 ± 20 N for the aged specimens, corresponding to a loss of 62% in the load at break. After 50 days of ageing at 90°C, the load at break reached 299 ± 20 N, corresponding to a loss of 69% in the load at break compared to the unaged specimens. A paired t-test was performed between the load values at the unaged condition and after ageing at 90°C at 50 days. A p value of 1×10^{-6} was obtained which indicated that the specimen has undergone significant degradation as compared to the unaged specimen. A t-test was also performed between ageing at 25 and 50 days conducted at 90°C. A p value of 0.002 was obtained. This indicates that the extent of degradation between the two times is different.

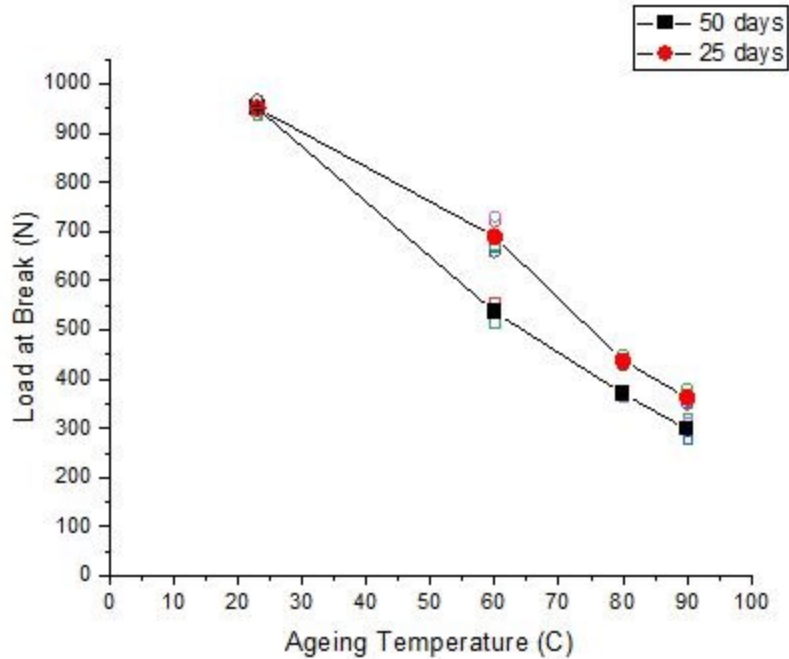


Figure 4.53 Variation of the load at break as a function of the ageing temperature for Fabric MG. The individual data points corresponding to the different specimens tested are also included (open symbols) in the graph.

The values for the load at break for the two types of yarns composing Fabric MG are plotted in Figure 4.54 as a function of the ageing temperature. Figure 4.54(a) corresponds to the spun yarn and Figure 4.54(b) corresponds to the filament yarn. The individual data points corresponding to the different specimens tested are also included. Both yarns show a decrease in the load values with increasing hydrothermal ageing temperature. However, the decrease in the load at break is only observed to take place above 60°C for the spun yarn.

The spun yarn showed a load at break of 12 ± 1 N in the unaged condition. It reduced to 8.0 ± 0.7 N after ageing for 25 days at 90°C, which corresponds to a loss of 33% in the load value. The yarns aged for 50 days at 90°C reached a load at break of 5.0 ± 0.4 N, which corresponds to a loss of 58% compared to the unaged condition. An ANOVA analysis was performed for 25 and 50 days of ageing. For the 25 and 50 days of ageing data, the differences were statistically significant (p value of 1.48×10^{-14} for 25 days and p

value of 4×10^{-22} for 50 days). A paired test was performed between the different temperatures as shown in Table 4.19. This indicates that the onset of degradation is between 60°C and 80°C when aged for 25 days and below 60°C for 50 days.

Table 4.19 t-test analysis between relevant conditions for spun yarn in fabric MG

Condition	Duration of ageing	P value
Between unaged and 60°C	25 days	0.641
Between 60°C and 80°C	25 days	1.47×10^{-5}
Between 80°C and 90°C	25 days	0.186
Between unaged and 90°C	25 days	1.12×10^{-8}
Between unaged and 60°C	50 days	0.014
Between 60°C and 80°C	50 days	2.4×10^{-7}
Between 80°C and 90°C	50 days	0.0015
Between unaged and 90°C	50 days	8×10^{-13}

The filament yarns showed a load at break of 42 ± 2 N in the unaged condition. The load at break decreased to 4 ± 2 N after ageing for 25 days at 90°C, corresponding to a decrease of 90% in the load at break. When aged for 50 days at 90°C, the load at break reached 3.0 ± 0.3 N, corresponding to a loss of 93% compared to the unaged value. A paired t-test was performed. The p value of 3×10^{-9} shows that there is significant difference between the data points in the unaged condition and after ageing at 90°C for 50 days. A t-test was also performed between the load values at 25 and 50 days for 90°C. A p value of 0.42 was obtained. This indicates that the extent of degradation at 25 and 50 days appear to be statistically identical.

Figure 4.55 compares the visual aspect of specimens of Fabric MG before ageing and after ageing for 50 days at 90°C. A change in color is visible.

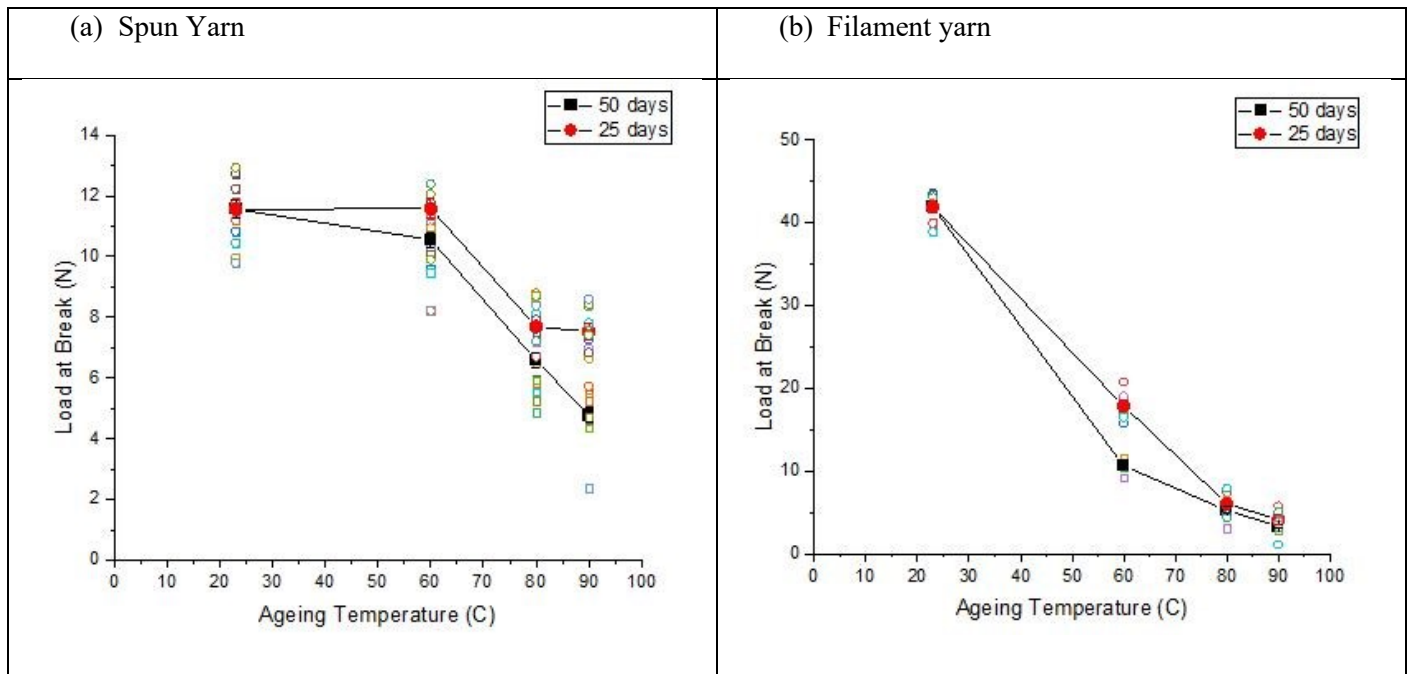


Figure 4.54 Variation of the load at break for (a) the spun yarn and (b) the filament yarn for Fabric MG as a function of the ageing temperature. The individual data points corresponding to the different specimens tested are also included (open symbols) in the graph.

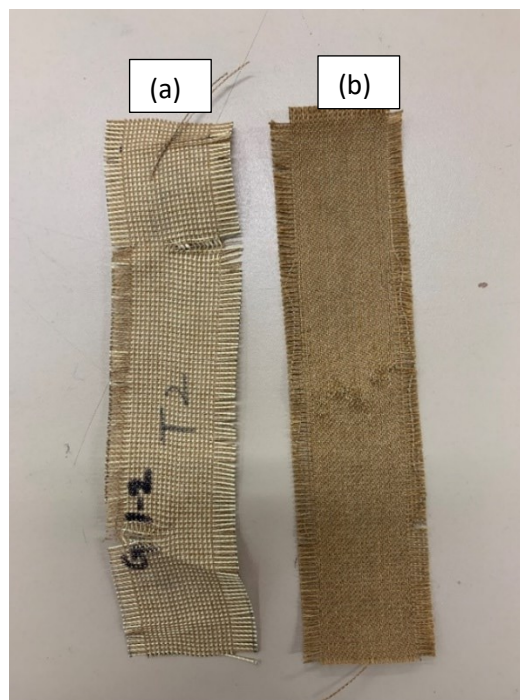


Figure 4.55 Fabric MG specimens (a) before ageing and (b) after ageing for 50 days at 90°C

Fabric MH

Figure 4.56 shows the load extension curves of fabric specimens for Fabric MH after 50 days of hydrothermal ageing for three different temperatures. The results for the unaged condition are also included. The hump that was observed for the unaged fabric has disappeared for the aged specimens. In addition, the aged specimens exhibit a decrease in the load and extension at break with increasing hydrothermal ageing temperature. The same behaviour was observed for the other ageing times.

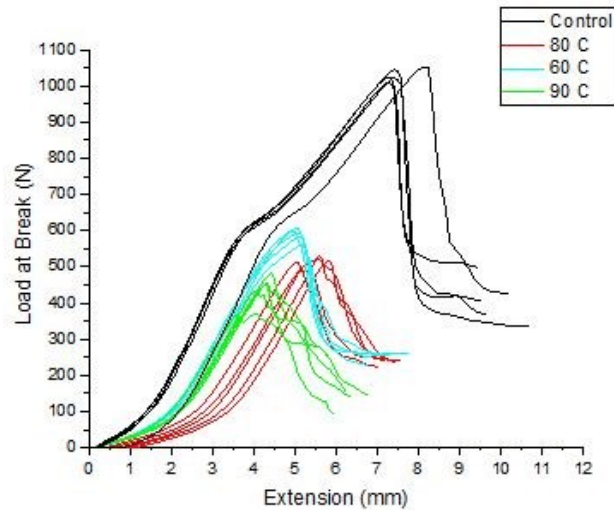


Figure 4.56 Mechanical behaviour of Fabric MH at the fabric scale under hydrothermal ageing after 50 days at different aging temperatures

The values of the load at break after 25 and 50 days of ageing are plotted in Figure 4.57 as a function of the ageing temperature. The individual data points corresponding to the different specimens tested are also included. The load at break follows a decreasing trend with increasing temperature. After 25 days of ageing at 90°C, the load at break went from 1030 ± 20 N for the unaged specimens to 520 ± 30 N for the aged specimens, corresponding to a loss of 50% in the load at break. After 50 days of ageing at 90°C, the load at break reached 440 ± 40 N, corresponding to a loss of 57% compared to the unaged specimens. A paired t-test was performed between the load values in the unaged condition and after ageing for 50 days at

90°C. A p value of 3×10^{-6} was obtained, which indicated that the specimens have undergone significant ageing as a result of exposure to 90°C for 50 days. A t-test was also performed between ageing at 25 and 50 days conducted at 90°C. A p value of 0.002 was obtained. This indicates that the extent of degradation between these two times is different.

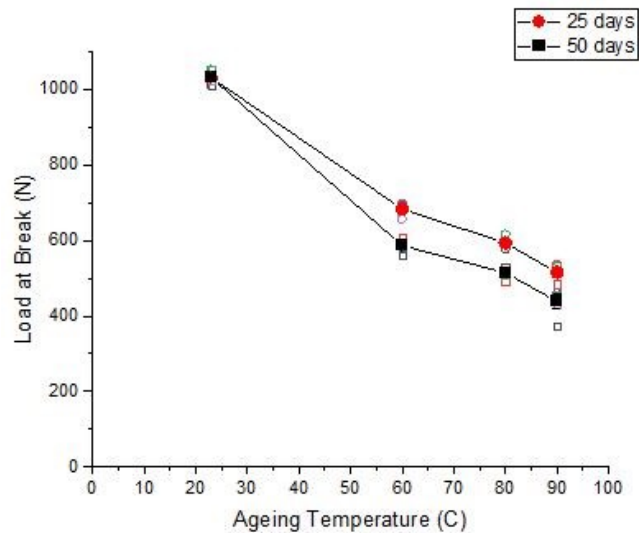


Figure 4.57 Variation of the load at break at the fabric scale as a function of the ageing temperature for Fabric MH. The individual data points corresponding to the different specimens tested are also included (open symbols) in the graph.

The values of the load at break for the two types of yarns composing Fabric MH are plotted in Figure 4.58 as a function of the ageing temperature. Figure 4.58(a) corresponds to the spun yarn and Figure 4.58(b) corresponds to the filament yarn. The individual data points corresponding to the different specimens tested are also included. Both the spun and filament yarns show a decrease in the load values with increasing temperature.

The spun yarn showed a load at break of 20 ± 2 N in the unaged condition. The load at break progressively reduced to 6.0 ± 0.6 N after ageing for 25 days at 90°C; this corresponds to a loss of 70% in the load value.

The load at break for the yarns aged for 50 days at 90°C decreased to 4.5 ± 0.5 N, corresponding to a total loss of 78% compared to the unaged condition. A paired t-test was performed between the load values in the unaged condition and after 50 days at 90°C. A p value of 1.5×10^{-11} was obtained, which indicates that a significant degradation has occurred as a result of exposure to 90°C for 50 days. A t-test was also performed between the load values at 25 and 50 days for 90°C. A p value of 0.03 was obtained. This indicates that the extent of degradation between 25 and 50 days and between 80°C and 90°C is different.

The filament yarn showed a load at break of 65 ± 2 N in the unaged condition. It decreased to 16 ± 1 N after ageing for 25 days at 90°C, corresponding to a decrease of 75% in the load at break. The load at break decreased to 11 ± 1 N after ageing at 90°C for 50 days, corresponding to a loss of 83% compared to the unaged value. A paired t-test was performed between the data points in the unaged condition and after 50 days at 90°C. A p value of 3×10^{-12} shows that there is a significant degradation in the specimens after 50 days at 90°C. A p value of 0.42 was obtained between the load values at 25 and 50 days for 90°C, which indicates that the extent of degradation is the same at 25 and 50 days. This may imply that the fabric has reached a steady state in its degradation process.

Figure 4.59 compares the visual aspect of specimens of Fabric MH before ageing and after ageing for 50 days at 90°C. A change in the specimen color is visible.

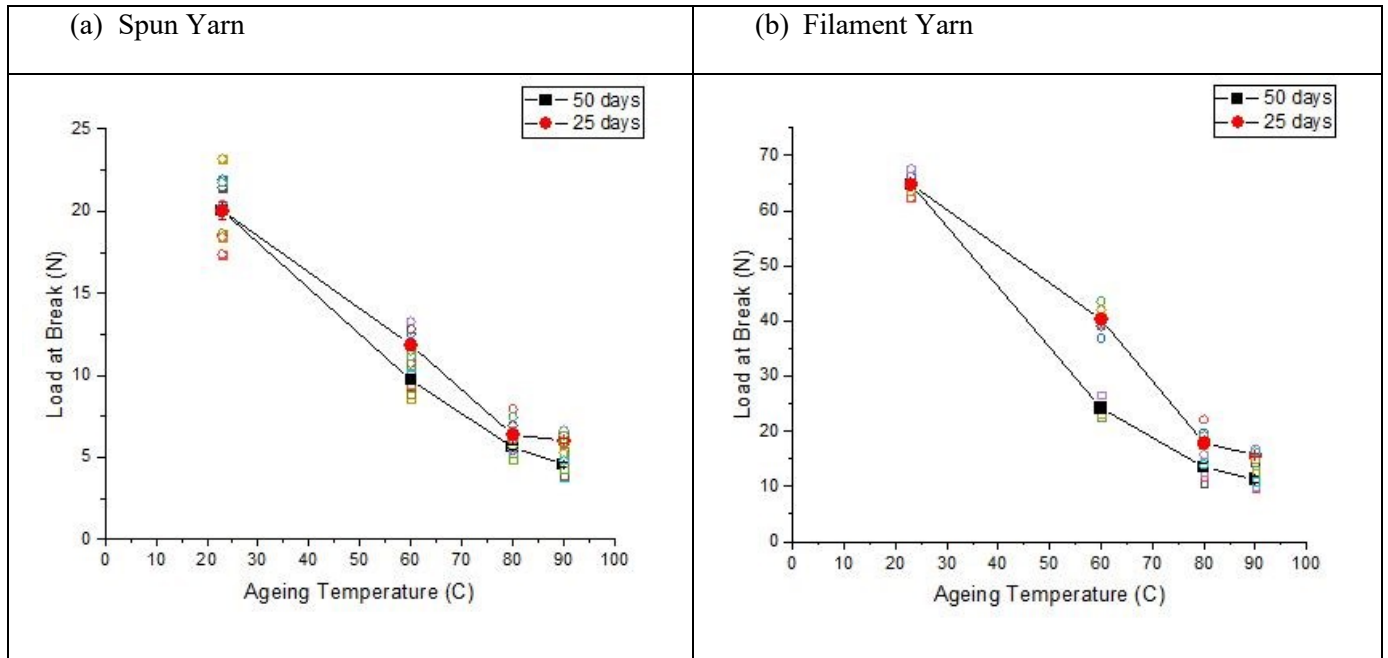


Figure 4.58 Variation of the load at break for (a) the spun yarn and (b) the filament yarn from Fabric MH as a function of the ageing temperature. The individual data points corresponding to the different specimens tested are also included (open symbols) in the graph.



Figure 4.59 Fabric MH specimens (a) before ageing and (b) after ageing for 50 days at 90 C

4.3.2 DISCUSSION

This section discusses the specific hydrothermal ageing behaviours observed for the different fabrics and yarns with respect to fabric content.

Comparison of the Kevlar®/PBI and Kevlar®/Nomex® blend fabrics

In our study, Fabric MA, MB, MG, and MH are mainly composed Kevlar® and PBI whereas Fabrics MC, MD, ME and MF contain Nomex® in combination with Kevlar®, PBO and carbon fibers. The two categories of fiber contents show different behaviours with hydrothermal ageing.

Kevlar®/PBI blend-based fabrics showed a progressive decrease in the load at break with increasing ageing temperature (See an example in Figure 4.60). By comparison, the degree of degradation was much lower in Kevlar®/Nomex® blends. In addition, some Kevlar®/Nomex® fabrics also showed a “delayed” degradation, i.e., the fabrics remained unaffected by hydrothermal ageing until a certain temperature was reached.

Kevlar® fibers are known to have a high sensitivity to hydrolysis in the presence of an acid catalysis [134]. The affinity of amide bonds with water leads to chain scission of the amide bonds and a corresponding decrease in tensile strength [135]. Even though both Kevlar® and Nomex® have amide groups in their structure, the amide group in Kevlar fibers appears to be more sensitive to hydrolysis than the amide group in the Nomex® structure. Several potential reasons have been proposed. Kevlar® fibers tend to have a rigid rod like structure whereas Nomex® fibers are much more flexible leading to an efficient close packing [23]. Due to the difference in packing and flexibility, the degree of water penetration into the structure is different. Moreover, due to the unique core skin structure of Kevlar®, degradation is much more localised in the core than the skin even though it has a higher contact area [136], which is in complete contrast to Nomex® wherein there is a limited difference between core and skin structure [137]. A confirmation of this lower sensitivity of Nomex® to hydrolysis can be found in the fact that Fabric MF has the highest

resistance to hydrothermal ageing compared to Fabric MC, MD and ME while it has the highest Nomex® fiber content (93% Nomex). In the case of PBI, it is thought to be quite resistant to hydrolysis [138].

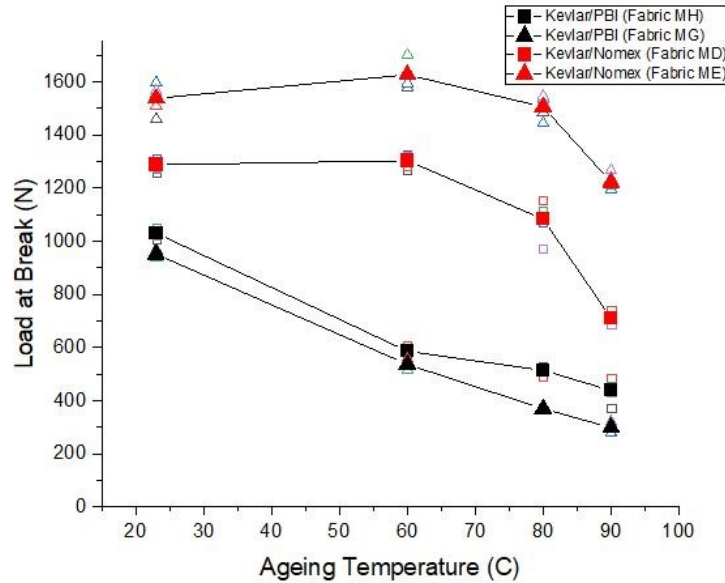


Figure 4.60 Examples of degradation behaviour for Kevlar/PBI-based fabrics (MG and MH) and Kevlar/Nomex based fabrics (MD and ME) with ageing temperature (after 50 days of ageing).

However, Fabric MC, MG and MH are fabric blends that have the same amount of Kevlar® fibers in their fabric structure (i.e., 65% Kevlar®). These fabrics consist of spun and filament yarns. Spun yarns in Fabric MC, MG and MH show a decrease in strength with increasing temperature as shown in Figure 4.38(a), 4.54(a) and 4.58(a). However, the degradation in Fabric MC spun yarn is delayed. Even more surprisingly, the filament yarns from these three fabrics have a completely different behaviour towards hydrothermal ageing despite having the same fiber content (100% Kevlar®). As shown in Figure 4.61, the filament yarns from Fabric MG and Fabric MH show a progressive decrease in the load at break with increasing temperature whereas the filament yarns from Fabric MC show no effect of hydrothermal ageing.

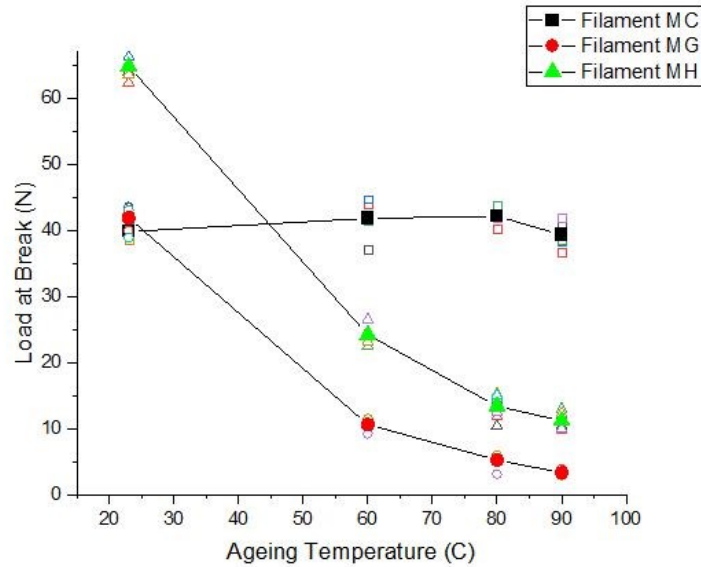


Figure 4.61 Hydrothermal ageing behaviour of filament yarns in MC, MG and MH with ageing temperature (after 50 days of ageing)

An EDX analysis was performed on each of the fabrics by another student. Fabric MG and MH showed a higher amount of sulphur as compared to Fabric MC [139]. Sulfuric acid is used in the manufacture of Nomex, Kevlar, and PBI fibers [37]. However, the EDX analysis showed that the highest amounts of sulfur was located on the spun yarns containing PBI. This extra sulphur in the PBI-containing fabrics is thought to lead to the formation of a higher concentration of sulfuric acid during hydrothermal ageing, which acts as a catalyst for the hydrolysis of Kevlar® [113]. This thus explains why the Kevlar®/PBI experienced a much larger sensitivity to hydrothermal ageing compared to the Kevlar®/Nomex® blend fabrics.

Difference in the hydrothermal ageing characteristic of fabrics having the same fabric structure and fiber content

Fabric MG and Fabric MH are two fabrics having the same fiber content and fabric structure but different weights (6.5oz for Fabric MG and 7oz for Fabric MH). Figure 4.62 shows a comparison of the change in the load at break with increase in ageing temperature for these two fabrics. When exposed to hydrothermal ageing, there is a difference in the rate of degradation at 80 and 90°C, with Fabric MG losing its mechanical

performance faster as compared to Fabric MH. For instance, the loss in the load at break in Fabric MG is 69% after 50 days of ageing at 90°C whereas it is 57% for Fabric MH in the same conditions.

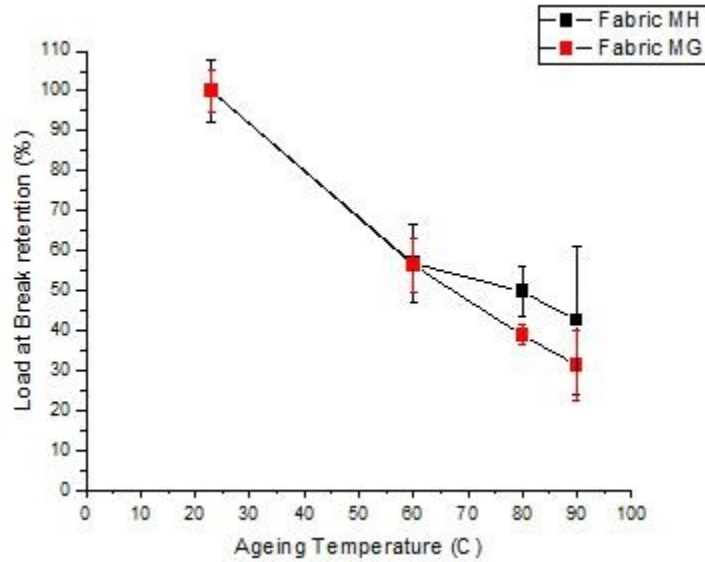


Figure 4.62 Variation in the load at break at the fabric scale for Fabric MG and Fabric MH with ageing temperature (after 50 days of ageing)

Different reasons have been looked at to explain this difference in the ageing rate. A possible cause may be the difference in diameter of the fibers between the two fabrics. These diameters were measured for the spun yarn and are provided in Table 4.20, with an example of an SEM image for each fabric in Figure 4.63. With a larger diameter of its fibers, Fabric MH appears to be more resistant to hydrothermal ageing as hydrolysis involves the diffusion of water across the fiber cross section.

Table 4.20 Fabric weight and fiber diameter in the spun yarn for Fabric MG and Fabric MH

Fabric Name	Weight per surface area	Diameter of the fiber
Fabric MG	6.5oz	17.6 ± 0.3µm
Fabric MH	7oz	24.2 ± 0.5µm

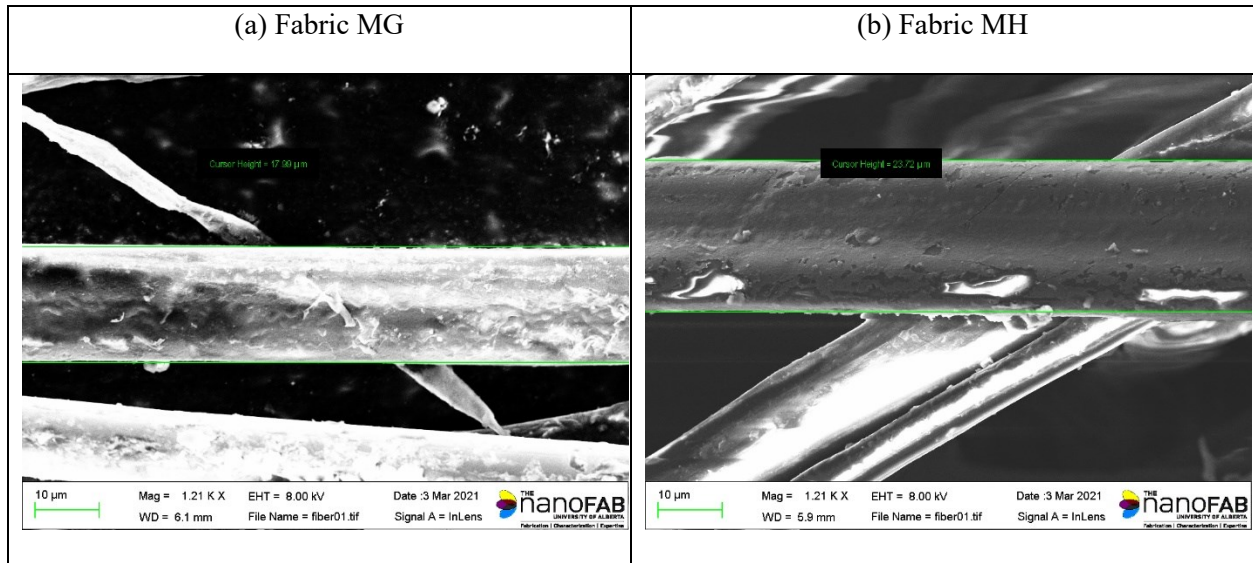


Figure 4.63 SEM images of fibers in the spun yarn in (a) Fabric MG (b) Fabric MH

Influence of PBO towards hydrothermal ageing

Fabric MD and Fabric ME are two fabrics having the same type of yarn, same fabric structure, and a similar fabric count but different fiber content. Fabric MD contains 60% Kevlar® and 40% Nomex® whereas Fabric ME is made of 60% Kevlar®, 20% Nomex®, and 20% PBO. Figure 4.64 shows the variation in their load at break at the fabric scale with ageing temperature. When exposed to hydrothermal ageing, Fabric MD exhibited a loss of 45% in the load at break after ageing for 50 days at 90 °C whereas Fabric

ME showed a loss of 20% in the load at break in the same conditions. It is to be noted that those fabrics display the same delayed degradation behavior.

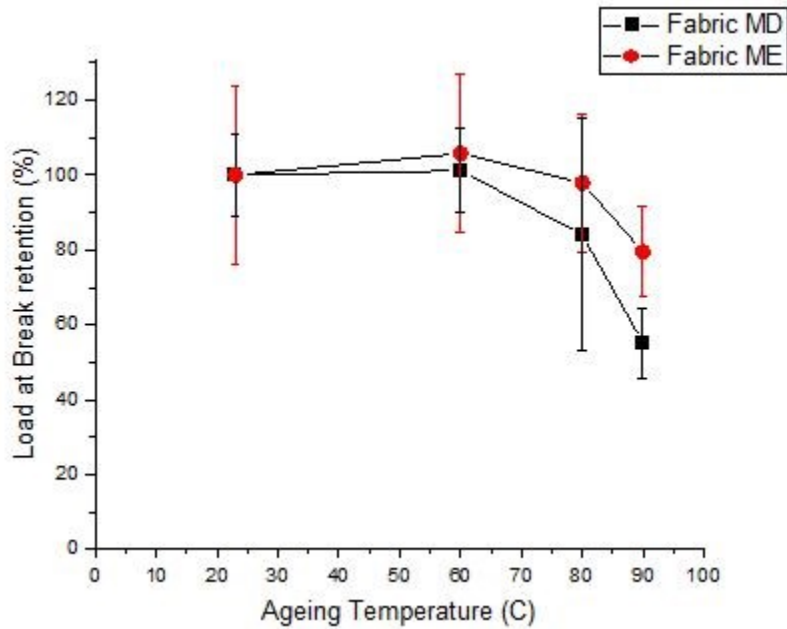


Figure 4.64 Variation in the load at break retention for Fabric MD and ME with ageing temperature at the fabric scale (after 50 days of ageing)

This could be interpreted as a sign that PBO is more resistant to hydrolysis compared to Nomex®. This result is surprising given the fact that PBO has been restricted from use as a ballistic material because of its high sensitivity to moisture[140], [141]. A possible explanation is that the hydrothermal ageing in our study involves immersion in water while previous issues involved the exposure of PBO fabrics to atmospheric moisture. Similar absence of effect of water on PBO was reported when several outer shell fabrics were subjected to repeated domestic laundering [142].

Resistance of LCP filaments to hydrothermal ageing

Fabric MB contains 57% Kevlar®, 35% PBI and 8% LCP fibers in its structure. The spun/filament yarn of Fabric MB comprises LCP filaments and Kevlar® and PBI staple fibers whereas the spun yarn of Fabric MB is made of Kevlar® and PBI staple fibers. When exposed to hydrothermal ageing at different temperatures, the spun yarn showed a gradual loss in tensile strength with increasing temperature (See Figure 4.35(a)) whereas the spun/filament yarn remained unaffected by ageing even at the maximum ageing temperature as shown in Figure 4.35(b). This difference in behaviour between the spun/filament and the spun yarn may be attributed to the presence of the LCP filaments. Indeed, previous studies [47] have indicated that due to the fact that they are polyester-based, these fibers show an increased resistance towards acids, bases and moisture.

Chapter 5 Fabrication of end-of-life sensors and their characterization

5.1. Introduction

The performance of fire fighter suits decreases when exposed to conditions such as light, heat and moisture. In addition, they might end up going below the performance threshold before a change is visible [4]. This may expose firefighters to health and safety hazards. Due to the late onset of the visual parameters and the absence of reliable non-destructive testing methods, there is a critical need for the development of end-of-life sensors to monitor the ageing of the firefighter suits resulting from the exposure in service. Our research team has used the fundamental concepts of polymer degradation described in Section 2.6 towards the development of these end-of-life sensors.

In the previous work of our research team, Cho et al. developed a method to prepare conductive tracks on fire protective fabrics using reduced graphene oxide (rGO) coatings [143]. The meta-aramid fabric specimens were dipped in a graphene oxide solution and then dried at a specific temperature. This dip and dry coating processes were repeated for a specified number of cycles to add layers of graphene oxide on the aramid fiber surface. Between each dip, the specimen was reduced in ascorbic acid and then subsequently washed and dried in an oven before being subjected to another dip cycle. The prepared rGO were then subjected to a variety of tests such as abrasion, exposure against water exposure and laundering tests to ascertain the reliability of these coatings in real life situations. Although the rGO coating did not undergo any marked degradation with laundering and water immersion, a significant loss in electrical conductivity was observed when the coating was exposed to abrasion cycles. Thus, there was a need for a much more reliable sensor system.

A further improvement involved the development of an thermal end of life sensor using a sacrificial polymer layer with conductive tracks imprinted on its surface using laser patterning (Laser Induced Graphene (LIG layers) [144]. This sensor consists of a polyetherimide (PEI) film, a conductive LIG layer, and an

encapsulation layer as shown in Figure 5.1. The PEI layer acts as the sensing polymer layer, which mimics the ageing behaviour of the outer shell fabric [144]. When the PEI layer degrades over time, the LIG layer is disrupted and loses its conductivity. This serves as an ageing indicator and helps determine when the garment has reached the end of its service life. However, preliminary results obtained with this sensor showed a considerable increase in the resistance (i.e., degradation of sensor property) with laundering cycles [144]. This is detrimental because the premise of the sensor is that it displays a large increase of resistance value with thermal aging, not by any other degradation mechanisms. Thus, the work presented in this chapter aims to develop a fabrication process leading to a robust and reliable end-of-life thermal sensor.

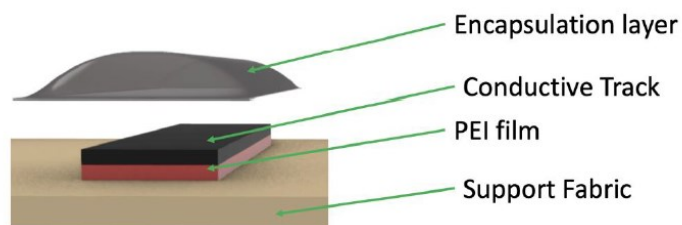


Figure 5.1 Structural schematic of the end-of-life sensor [144]

In the aforementioned study, the LIG was fabricated by modifying the protocol developed by the Tour in polyimide-based polymers [145], [146]. It involves the preparation of 3D porous graphene inscribed on the surface of a polymer film using a laser scriber operated in an ambient environment as shown in Figure 5.2. This procedure begins with the exposure of the specified area to a laser beam at controlled power settings. The objective behind laser scribing is to convert the carbons in the polymer structure from a sp^3 hybridization to a sp^2 hybridization by a photothermal reaction [146]–[148]. The inscribed LIG can be used to create electrically conductive paths on the surface of the polymer film, which can be employed for sensor applications. A similar procedure was used by Stanford et al. in which they imprinted LIG layers on a polyimide substrate for application as gas sensors [149]. Due to its high flexibility and high thermal

conductivity, the LIG technology has resulted in the development of rapid response sensors. A similar method was used in the development of sensors for nitrogen sensing in soil samples by Garland et al. [150]. A stark difference in their production method was the use of a low-cost UV laser as compared to the traditional CO₂ infrared laser used by the Tour group [145], [146] and Stanford et al. [149]. The method proposed by Garland et al. [150] improved the electrochemical reactivity of the sensors. Thus, LIG layers can be included in a variety of applications which points towards the versatility of the technology because of its simplicity, efficiency, and low cost.

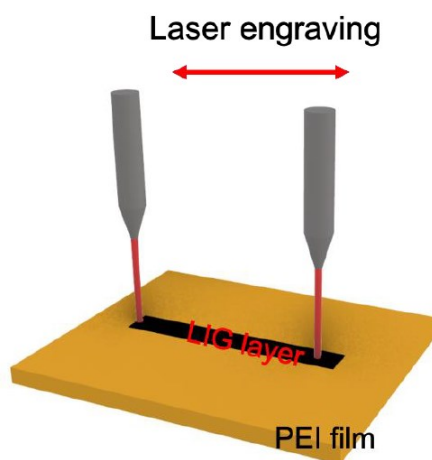


Figure 5.2 Schematic representation of the laser engraving process for the development of LIG sensors [144]

The aim of this project is to develop a sensor fabrication strategy that facilitates mass production. One of the reasons behind this is that in order to perform the reliability studies required to characterize and improve the sensor resistance to laundering and other normal use conditions, one needs to produce a statistically meaningful number of reproducible sensors. For instance, in case of an ageing study that will be performed for a total duration of 50 days, we need a minimum of five specimens for each sample (i.e., ageing time) to get a meaningful distribution of values. Since we take a data point every other day, we will need a total of 125 specimens for each ageing condition. Thus, this instance highlights the importance of controlling the mass production for our current study. The other reason behind the work is to pave the way for the following

phase of the research on the end-of-life sensor for firefighter protective garments, which will be the scale up to industry production.

Weibull distribution is one of the most commonly used lifetime distribution curves in the field of reliability [151]. This distribution adopts the characteristics of other distribution curves based upon the shape parameter β and is used to predict the failure of a given set of specimens. A two-parameter Weibull probability distribution function is obtained using the following equation:

$$F(t) = \frac{\beta}{\eta} \left(\frac{t}{\eta}\right)^{\beta-1} e^{-\left(\frac{t}{\eta}\right)^{\beta}} \quad (\text{Equation 5-1})$$

Where β is the shape factor or the slope of the distribution curve, and η is the characteristic life or when 63.2% of the population has failed. The parameter β is dimensionless. To obtain a reliability plot, the data points obtained from a hypothetical ageing study are plotted on a curve and using the best fit the value of the parameter β is analysed. If we have a set of data corresponding to the failure time of each sensor as shown in figure 5.3, the best fit curve is a straight line and the parameter β is the slope of the line. The value of η is calculated at the point when the population failure is 63.2%. Once both parameters are obtained, the distribution function is plotted using equation 5-1. Using this plot, the probability of failure can be estimated and thus allowing for better management of health and safety hazards.

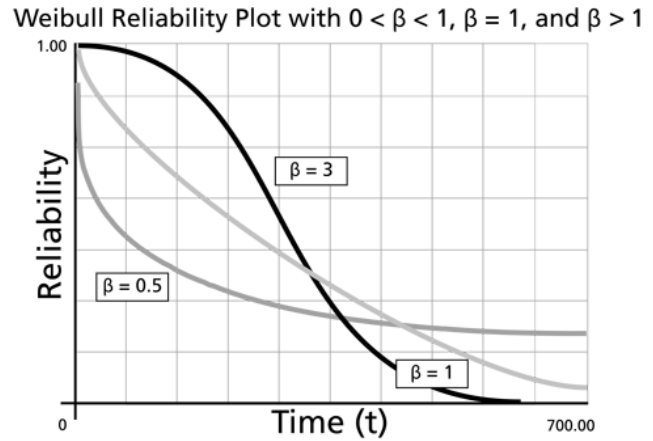
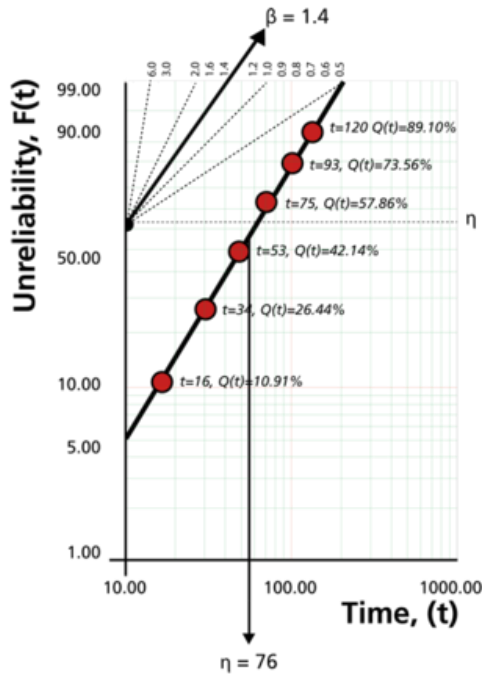


Figure 5.3 (a) A typical unreliability vs time curve (b); A typical Weibull plot to predict the failure probability [151]

Reliability testing is the method selected to determine how long and how efficiently the sensors perform when exposed to a variety of test conditions. Bending deformation and bending fatigue are two test methods used to evaluate the performance of flexible sensors against everyday use[152], [153]. Sensors have been subjected to water immersion tests to assess their reliability against washing and laundering [154]. Abrasion tests are also performed to estimate a service life before eventual failure [143]. In the field of thermal sensors, cyclic heating and cooling tests are performed to determine the response and durability with use [155]. In the case of our sensors, our primary objective is to prepare sensors having a robust behaviour against laundering. The current requirement for firefighter bunker suit is to perform advance cleaning, which involves laundering the garment, at least twice a year[6]. However, it is expected that the recommended frequency of laundering for the protective clothing will be drastically increased in the near future because of concerns about garment contamination and the effect on firefighter's health [156]: they would have to be washed following each fire-related operation, up to 25 times per year depending on the

firefighter function and the fire station. Other types of fire protective clothing are laundered once every week [9].

In this chapter, we developed a strategy for the mass production of reproducible sensors and performed characterisation studies using water immersion, bending test and bending fatigue tests to ascertain the robustness of the sensors produced. This work is still ongoing.

5.2 Laser-Induced Graphene (LIG) layer on PEI film

Polyetherimide film (thickness 250 μm) purchased from McMaster Carr was placed in a 70 W, 10.6 μm laser scribing machine (PLS 6.150 D, Universal Laser System, Inc) equipped with a CO₂ laser for patterning. The power and speed settings were optimised for the PEI sheet; they were set to 5.5% and 7%, respectively, for rastering. The pulses per inch was set at 500 during the laser scribing process. A partial vector cut (i.e., cutting with laser) was implemented for each of the sensor at its boundary at a speed of 5% and power setting at 3.7%. The schematic representation of the engraving process is shown in Figure 5.3. The size of the PEI strip making the thermal end-of life sensor is 4.4 cm of length and 1 cm of width and the dimensions of LIG layer are 3 cm by length and 0.5 cm by width as shown in Figure 5.4. These dimensions were selected during the initial work on the sensor development as a good compromise to have a long enough conductive track to produce meaningful conductivity measurements while keeping the sensor at a manageable size, i.e. so that it does not interfere with the functionality of the protective garment.

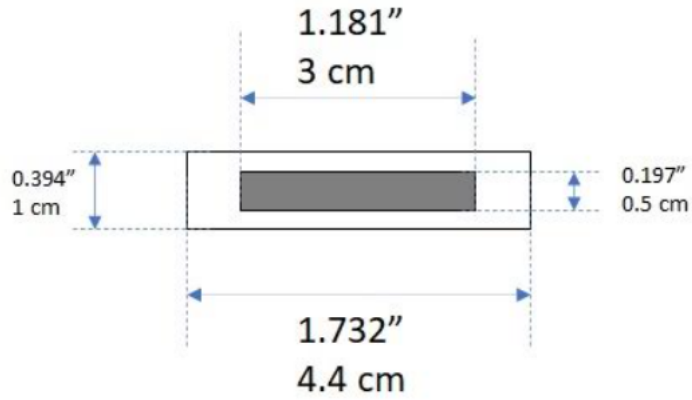


Figure 5.4 Schematic design of the end-of-life sensor

Since the objective is to perform reliability studies, the first task was to prepare a series of sensors with the same preparation method in one single cycle. A PEI sheet having the dimensions of 19" in length and 12" in width was used for each cycle of the sensor production. Individual sensors were arranged as shown in Figure 5.5. A group of 68 LIG scribed units were produced with each cycle with this arrangement.

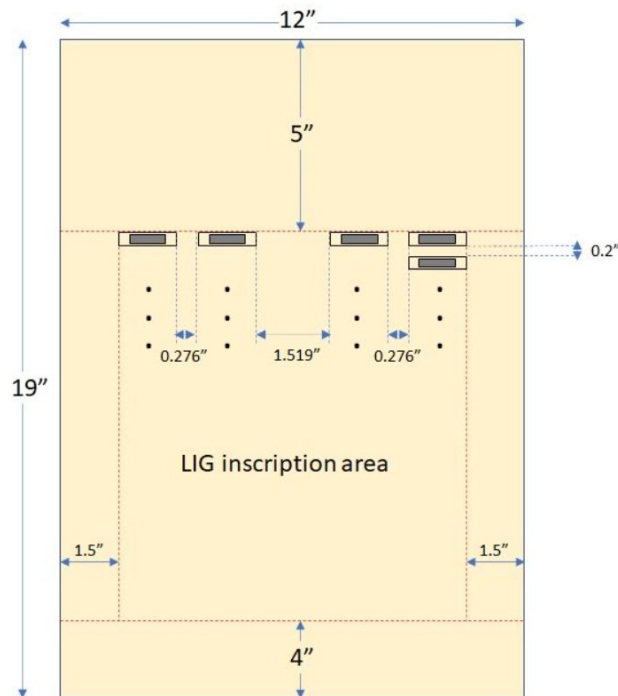


Figure 5.5 Schematic arrangement of the sensors during the production process

5.3 Fabrication of the PEI-LIG sensors

A fabrication process was developed for the sensor after the initial LIG scribing on the PEI layer. The different steps are described below.

To get resistance readings from the LIG layer on the PEI film, connections were made by coating the tips of the LIG layer with silver paste, which was allowed to cure for a period of 24 hours in ambient conditions as shown in Figure 5.6. Once the silver paste was cured, the PEI sheet with the LIG layers was coated with an encapsulant with the help of a film applicator (Elcometer 4340) set at a thickness of 250 μm : the actual thickness of the entire system (PEI film + Encapsulant layer) varied between 490 μm and 530 μm . The encapsulant was chosen so that it has high thermal, chemical, abrasive, and photo resistance and has good processing characteristics (low curing temperature and low viscosity for better mixing). Epox Acast 670 HT (epoxy 1) and Epox Amite HT (epoxy 2), commercially developed as casting epoxies, were put on trial as the encapsulant. A tape is placed on the silver paste contacts on both sides of the LIG conductive tracks before the encapsulant application so that they are not covered by the encapsulant. Once the encapsulant is applied, it is allowed to cure for a period of 48 hours. Once the encapsulant is cured, the tape is removed from the silver paste contact and the sensors are popped out of the sheet as shown in Figure 5.7. After the sensors are prepared, their initial resistance values was recorded before they were exposed to the different test conditions: water immersion and bending to simulate the individual stressors experienced during laundering. Figure 5.8 represents a summary of the complete mass fabrication strategy employed during the project.

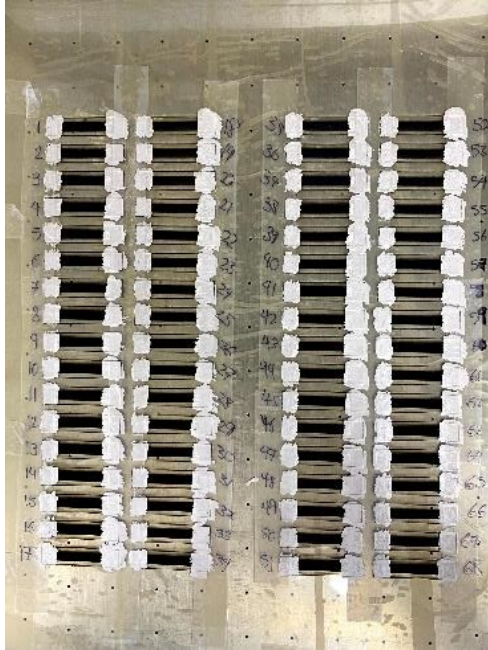


Figure 5.6 Application of silver paste on the PEI sheet



Figure 5.7 Picture of the sensors being popped out after encapsulation.

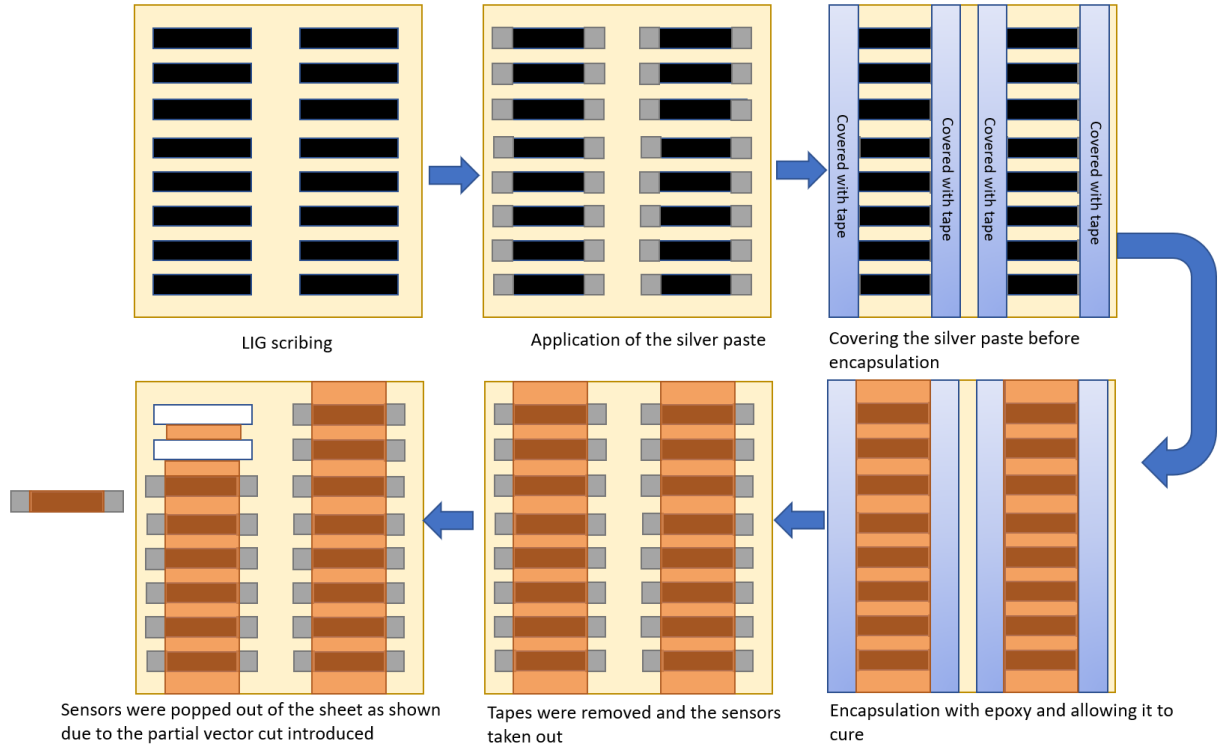


Figure 5.8 Schematic representation of the mass production of the thermal sensor

5.4 Accelerated water ageing of the PEI-LIG sensors

As a wearable sensor incorporated into a garment, one of the biggest challenges involves its laundering resistance. The abrasive and tensile stresses applied during the process [154] combined with the chemical and moisture effects might influence the performance of the sensor. Therefore, to analyse the reliability against laundering, the performance of the sensors was studied (1) when exposed to water at relevant temperatures and (2) against bending deformation.

The prepared PEI-LIG sensors were immersed in water at a temperature of 40°C in an oven. This temperature was selected as it corresponds to the maximum recommended washing temperature for firefighter protective clothing [31]. In order to see the changes in resistance, sensors were divided into 5 groups (each group containing 5 sensors) and each group was aged and measured at different times. For Group 1, the resistance was measured after 2, 4, 6, 8 and 12 days. For Group 2, the resistance was measured

after 4, 6, 8 and 12 days. For Group 3, the resistance was measured after 6, 8 and 12 days. For Group 4, the resistance was measured after 8 and 12 days. For Group 5, the resistance was measured after 12 days. The electrical resistance of the sensors was measured using a Bench LCR meter (BK precision model 895, CA) using alligator clips. After measuring the resistance, the sensors were put back in the oven after each measurement until the cycle is completed. The data is reported as a change in resistance with ageing time as shown in Figure 5.9. Mean values and results for the individual specimens are shown on the graph.

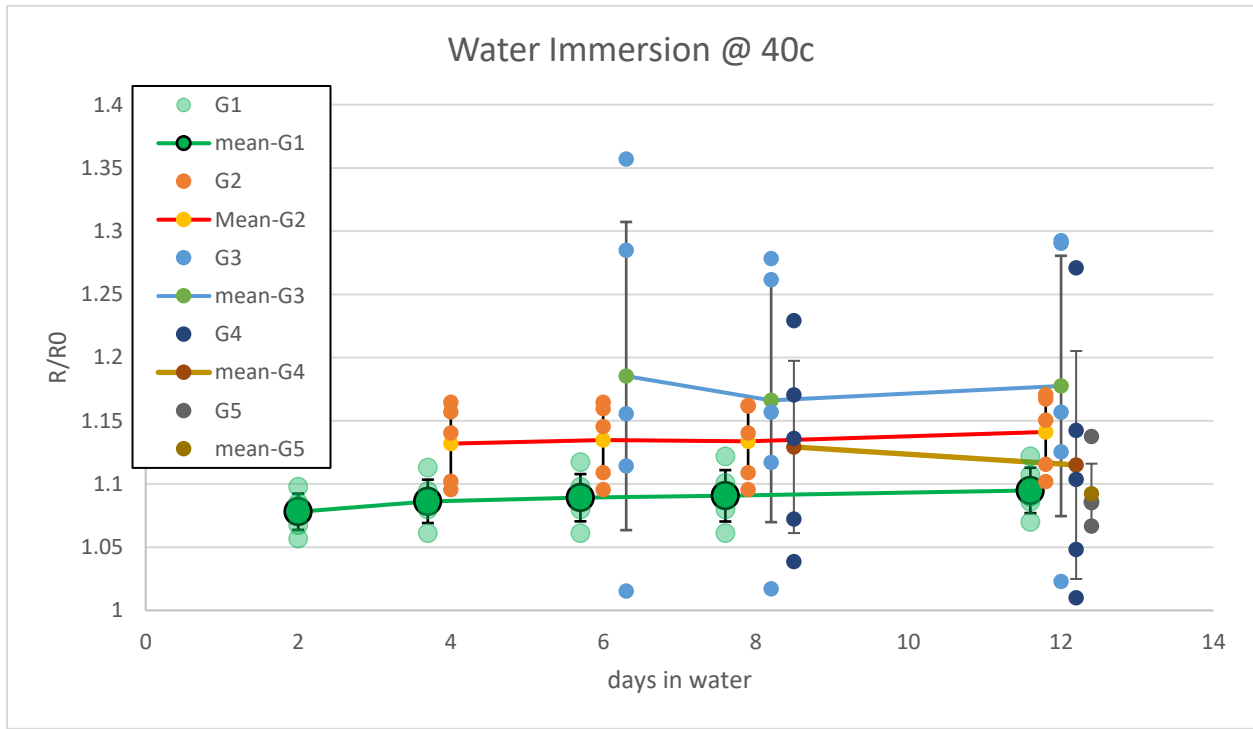


Figure 5.9 Change in resistance with water immersion at 40°C

The stability of the sensors was quantified by the change in their normalized resistance (i.e., increase in resistance compared to unaged condition) as listed in Table 5.1. The effect of intermittent heating and cooling was analysed. The value of the resistance remained constant over the entire duration of ageing. An ANOVA analysis was done to identify any statistical change within groups. The p values were calculated and are reported in Table 5.2. The stability of the sensors against water points towards their reliability against moisture and chemical exposure. The results also show that the thermal history of the sensors did not affect their ageing characteristics.

Table 5.1 Change in normalized resistance with increase in ageing time for each tested group

Sensor Group	Ageing time (days)				
	2 days	4 days	6 days	8 days	12 days
R/R0					
G1	1.08 ± 0.01	1.09 ± 0.02	1.09 ± 0.02	1.09 ± 0.02	1.10 ± 0.02
G2	-	1.13 ± 0.03	1.14 ± 0.03	1.14 ± 0.03	1.14 ± 0.03
G3	-	-	1.2 ± 0.1	1.2 ± 0.1	1.2 ± 0.1
G4	-	-	-	1.13 ± 0.07	1.12 ± 0.09
G5	-	-	-	-	1.09 ± 0.02

Table 5.2 Statistical analysis (ANOVA) within each group

Group	p value
G1 (2,4,6,8,12 days)	0.77
G2 (4,6,8,12 days)	0.41
G3 (6,8,12 days)	0.99
G4 (8,12 days)	0.92

5.5 Stability of the PEI-LIG sensor against static bending

PEI-LIG sensors prepared with the two epoxies mentioned in Section 5.3 were mounted on a Cellscale mechanical tester with a load cell of 200N. The static bending response of the sensors was analysed according to the standard ASTM D 790-03. The sensors were deformed midway to an extension of 6 mm at a strain rate of 0.01 min⁻¹ as shown in Figure 5.10. The data were reported as load vs extension. They were used to determine the flexural modulus of the sensor specimens. Additionally, the resistance of the sensors was measured before and after the bending tests to analyse the effect of bending on the performance of the sensors.

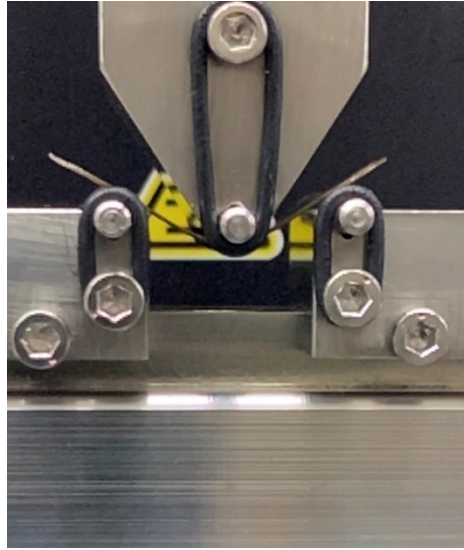


Figure 5.10 Schematic representation of the bending test

The flexural stress vs strain curves for the sensors tested are plotted in Figure 5.11. The flexural modulus and the change in conductivity of the sensors encapsulated are reported in Table 5.3. The sensors encapsulated with epoxy 1 (Epoxy Acast 670 HT) show a lower flexural modulus than the epoxy 2 (Epoxy Amite HT)-encapsulated sensors. Moreover, the epoxy 1 sensors maintain their conductivity after bending as can be seen from the resistance results in Table 5.3, contrary to the epoxy 2 sensors. This better resistance of the epoxy 1 sensors to bending can be attributed to their lower flexural modulus; they have a better flexibility and does not seem to break with extreme bending. Moreover, they do not lose their conductivity with bending, proving to be a much more reliable sensor. However, bending fatigue tests need to be performed to simulate the performance of the sensors in real life situations.

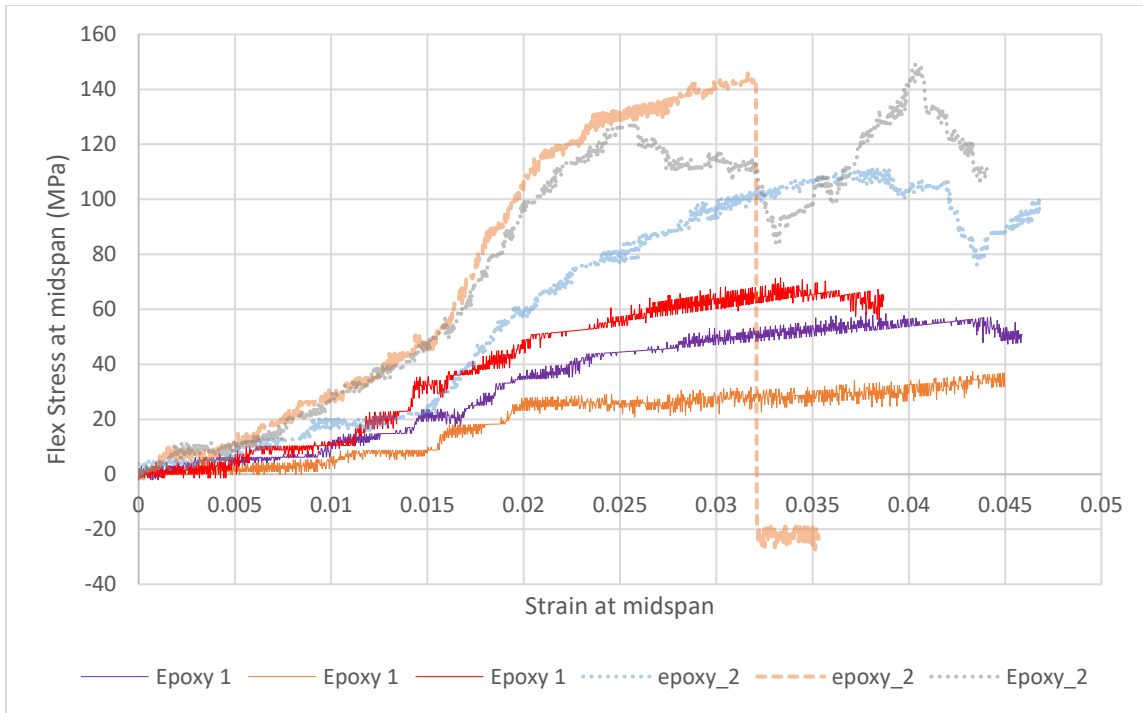


Figure 5.11 Flexural stress vs strain for the two sets of epoxy sensors

Table 5.3 Flexural modulus and resistance readings before and after bending for the two sets of sensors

	Flexural Modulus (GPa)	Resistance before bending (R0) (kΩ)	Resistance after bending (R) (kΩ)	R/R0
Sensor 1-1 (Epoxy 1)	1.75	0.515	0.516	1.002
Sensor 1-2 (Epoxy 1)		3.6	3.4	0.944
Sensor 1-3 (Epoxy 1)		0.595	0.602	1.011
Sensor 2-1 (Epoxy 2)	2.96	3.52	13.2	3.750

Sensor 2-2 (Epoxy 2)		2.76	Broken	-
Sensor 2-3 (Epoxy 2)		0.65	3.2	4.923

5.6 Fatigue tests

PEI-LIG sensors prepared with epoxy 2 were mounted on a Cellscale mechanical tester with a load cell of 200N. The bending fatigue response of the sensors was analysed according to the standard ASTM D 7774-17. The sensors were deformed midway to an extension of 3 mm at a strain rate of 2 seconds/cycle for a total of 1000 cycles each. The data were reported as force vs number of cycles. They were used to determine the bending fatigue response of the sensors.

The curves corresponding to the load vs number of cycles are shown in Figure 5.12. Five out of the nine sensors failed before the completion of 1000 cycles. The remaining four sensors showed a high degree of resistance to bending fatigue and showed no loss in force value even after the completion of 1000 cycles. This high performance of the sensors against fatigue response suggests a high reliability when used in real life situation. This fatigue response obtained could be used for the development of the Weibull plot to predict the performance of these sensors in the future. But these are still preliminary tests and further tests need to be performed to explore more into details the reliability of these epoxy encapsulated sensors.

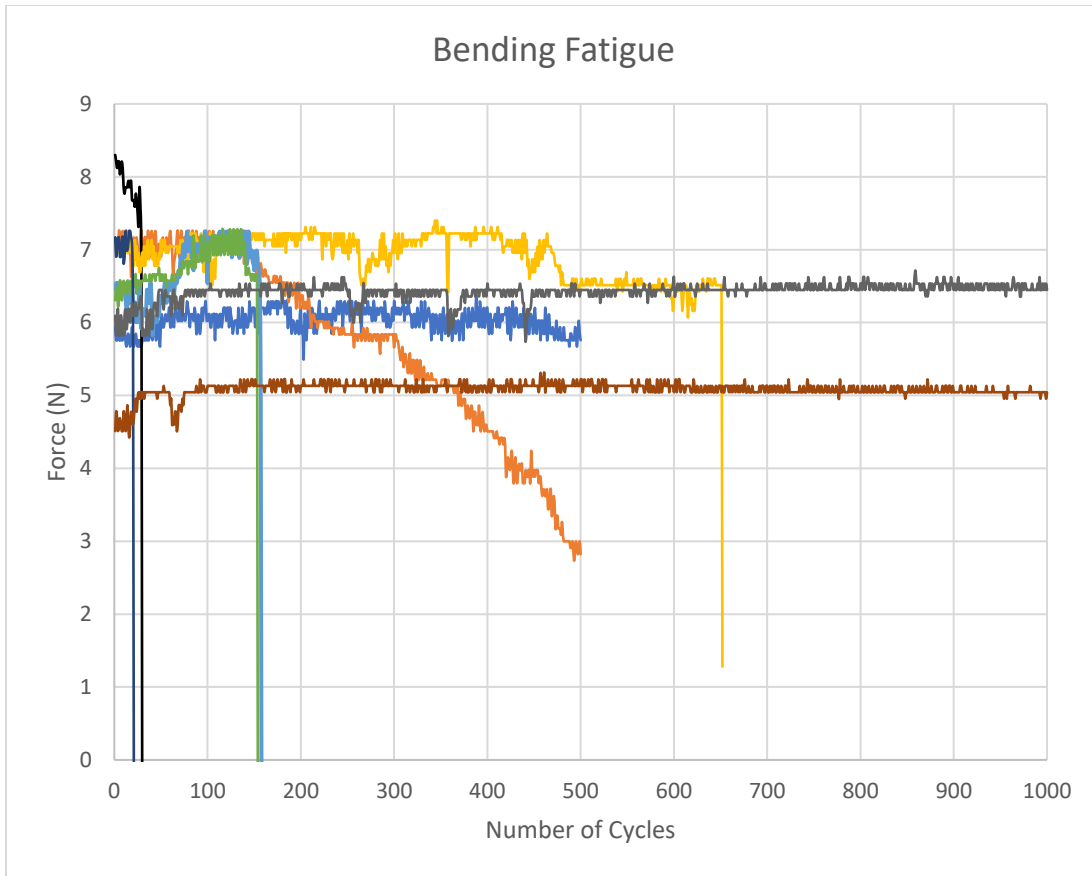


Figure 5.12 Fatigue data of the sensors plotted against the number of cycles

The aim of the thesis was to analyse the mechanical behaviour of outer shell fabrics employed in fire protective clothing and develop knowledge on the effect of exposure to water at elevated temperatures. For this, the study was divided into two parts: (1) Understanding the mechanical behaviour of outer shell fabrics and correlating its behaviour with their fiber content and fabric structure, and (2) Investigating the accelerated ageing of outer shell fabrics when exposed to severe hydrothermal conditions and correlate the effect on the mechanical performance with their fiber content and fabric structure. Moreover, my contribution to the development of a non-destructive method of monitoring the ageing behaviour of the outer shell fabrics in the form of end-of-life sensor was also described. Each sub project is summarized as follows:

6.1. Mechanical behaviour of outer shell fabrics

This study analysed the performance of eight outer shell fabrics with different fiber content and fabric structure when tested in tension. Raveled strip specimens were prepared according to the standard ASTM D5035. For each fabric studied, the mechanical behaviour was analysed at two scales i.e., fabric and yarn scale, to understand the effect of fiber content and fabric structure on the mechanical behaviour of the fabrics.

The fabric mechanical behaviour at the fabric scale was categorised into three different categories i.e., (1) Standard load extension curve (2), No crimp interchange (3), and Presence of a hump. The absence of crimp interchange was attributed to the very high fabric count in the structure (Fabric MF). In case of the presence of the hump in the load extension curve, it was connected to a hump in the load extension curve at the yarn scale in one instance (Fabric MF) and potentially to a high crimp ratio between the spun and filament yarns composing the fabric in the other cases (Fabric MG and MH). Other specific characteristics observed include a bimodal distribution in the yarn mechanical strength (Fabric ME). The difference in behaviour between two fabrics having identical fiber content and fabric structure (Fabric MG and MH) was attributed to the difference in linear density between the yarns in the two fabrics. The effect of fiber content could be

observed for instance with a fabric with high Nomex content showing a lower load at break and higher extension at break (Fabric MF) and a fabric containing PBO showing a higher load and extension at break.

These results give us a better understanding of how fiber content and fabric structure strongly affect the mechanical behavior of outer shell fabrics. They also provide us with the knowledge necessary to look at the effect of hydrothermal ageing on this mechanical behavior.

6.2. Hydrothermal ageing of outer shell fabrics and its effect on their mechanical behaviour

The behaviour of outer shell fabrics towards hydrothermal ageing was analysed for the eight different fabrics available. This behaviour was studied by monitoring the changes in the breaking strength of the fabric and correlating it to their fiber content and fabric structure.

For Kevlar®/PBI-based fabrics, the specimens showed a progressive decrease in the load at break with increasing temperature whereas Nomex®/Kevlar®-based fabrics showed a “delayed” response to degradation, i.e., the specimens retained their strength up to a certain temperature after which the strength started decreasing. In addition to the well-documented larger sensitivity of Kevlar® fibers to hydrolysis as compared to Nomex®, this difference was attributed to the presence of a higher amount of sulphur in the Kevlar®/PBI-based fabrics, which was evidenced by EDX and was possibly attributed to the PBI fibers.

The study also shows the absence of effect of hydrothermal ageing on the strength of LCP filament yarns. The presence of PBO fibers in the fiber content led to a lower sensitivity towards hydrothermal ageing compared to Nomex fibers. This result was quite surprising given the issues with the premature ageing of PBO fibers which has led to their ban from ballistic protective clothing. However, it could be attributed to the fact that the hydrothermal ageing conducted here involved immersion in water while the other studies used atmospheric moisture. Finally, an effect of the fiber diameter on the rate of hydrothermal ageing was observed with Kevlar®/PBI fabrics. In general, fabrics experiencing a larger loss in strength as a result of hydrothermal ageing showed a larger change in color.

These results provide new insights into the effect of hydrothermal ageing on the long-term mechanical performance of fire protective fabrics. In particular, the reason behind the larger sensitivity of the Kevlar®/PBI-based fabrics to water immersion will be of huge interest to the textile and protective clothing industry. These results also provide the data necessary for the development of a moisture end-of-life sensor for firefighter protective clothing.

6.3. Fabrication and characterisation of robust end-of-life sensors for outer shell fabrics

Work was also performed to improve the fabrication process and the robustness and reliability of thermal end-of-life sensors. The first part of the study involved developing a protocol for the mass production of end-of-life sensors using an epoxy encapsulant. The aspects covered included systematizing the operations and the sensor design, optimizing the laser scribing parameters, developing a technique to facilitate the sensor pop out, and identifying good candidates for the encapsulation polymer.

Once the sensors were produced, the reliability studies were divided into three parts: (1) Reliability towards water immersion at 40°C, (2) Reliability towards static bending, and (3) Reliability towards fatigue bending. The results revealed that the sensors retained most of their conductivity after 12 days of accelerated hydrothermal ageing. This study proved the durability of the epoxy encapsulant in a water environment. In the case of static bending, the use of a flexible epoxy encapsulant allowed preserving the sensor conductivity to its original level. Preliminary results with bending fatigue show the potential of the sensors for sustaining real life stresses of protective clothing.

6.4 Future Work

In Chapter 4, the hydrothermal ageing of firefighter suit outer shell fabrics was analysed by studying the retention in tensile strength. Further investigations could look at the surface of the fabrics using contact angle measurements and scanning electron microscopy imaging. More research is also needed to confirm the source of the extra sulphur in the Kevlar®/PBI-based fabrics. This study could also be expanded by combining different sets of ageing conditions such as with thermal, UV and laundering.

In Chapter 5, epoxy encapsulated sensors were prepared; they showed good performance when exposed to water and static bending. Further reliability tests could be performed including fatigue response by varying the number of bending cycles the sensor is exposed to. The study could be taken further by subjecting the sensors to laundering with detergents and varying the number of laundering cycles. Regarding fabrication, the application of the silver paste at the edges of the conductive track on the sensors could be automated to reduce variability. Moreover, other encapsulant candidates could be explored such as silicones, which have high temperature resistance.

References

- [1] S. Bourbigot and X. Flambard, "Heat resistance and flammability of high performance fibres: A review," *Fire Mater.*, vol. 26, no. 4-5, pp. 155–168, 2002.
- [2] P. I. Dolez, N. S. Tomer, and Y. Malajati, "A quantitative method to compare the effect of thermal aging on the mechanical performance of fire protective fabrics," *J. Appl. Polym. Sci.*, vol. 136, no. 6, p. 47045, Feb. 2019, doi: <https://doi.org/10.1002/app.47045>.
- [3] K. Slater, "7—The progressive deterioration of textile materials part I: characteristics of degradation," *J. Text. Inst.*, vol. 77, no. 2, pp. 76–87, 1986.
- [4] R. M. Rossi, W. Bolli, and R. Stämpfli, "Performance of Firefighters' Protective Clothing After Heat Exposure," *Int. J. Occup. Saf. Ergon.*, vol. 14, no. 1, pp. 55–60, Jan. 2008, doi: 10.1080/10803548.2008.11076747.
- [5] N. 1971, "Protective Ensembles for Structural Fire Fighting and Proximity Fire Fighting," no. 1997, 2007.
- [6] N. 1851, *NFPA 1851 Standard on Selection, Care, and Maintenance of Protective Ensembles for Structural Fire Fighting and Proximity Fire Fighting*. 2008.
- [7] K. Slater, "TEXTILE DEGRADATION," *Text. Prog.*, vol. 21, no. 1–2, pp. 1–150, Mar. 1991, doi: 10.1080/00405169108688851.
- [8] P. I. Dolez, H.-J. Chung, and Cho C, "End-of-Life sensors for Fabrics, US Provisional Patent Application 63/156," 2021.
- [9] "LAPCO Manufacturing. FR Clothing Wash Expectancy - Useful Life <https://www.lapco.com/blogs/fr-education-guides/how-many-times-can-you-wash-fire-retardant-clothing> (accessed Jun 07, 2021)." .
- [10] E. Commission, "Proposal for a Regulation of the European parliament and of the council on personal protective equipment," 2014.
- [11] N. Mao, *High performance textiles for protective clothing*. Woodhead Publishing Limited, 2014.
- [12] I. Jahan, "Effect of Fabric Structure on the Mechanical Properties of Woven Fabrics," *Adv. Res. Text. Eng.*, vol. 2, no. 2, 2017, doi: 10.26420/advrestexteng.2017.1018.
- [13] G. Song, S. Mandal, and R. M. B. T.-T. P. C. for F. Rossi, Eds., "4 - Development of high performance thermal protective clothing," in *Woodhead Publishing Series in Textiles*, Woodhead Publishing, 2017, pp. 27–55.
- [14] P. F. Fighting, F. Fighting, P. Clothing, E. Services, and P. Clothing, "Protective Ensembles for Structural Fire Fighting and Proximity Fire Fighting," no. 1997, 2007.
- [15] S. Chakraborty, "Components , characteristics and some evaluation methods for the f irefighters ' protective clothing," vol. 4, no. 2, pp. 1–6, 2018.
- [16] R. Rossi, "3 - Clothing for protection against heat and flames," in *Woodhead Publishing Series in Textiles*, F. Wang and C. B. T.-P. C. Gao, Eds. Woodhead Publishing, 2014, pp. 70–89.
- [17] P. A. Thorpe, "Development of non-destructive test methods for assessment of in-use fire fighter's protective clothing." 2004.

- [18] M. Rezazadeh, "Evaluation of performance of in-use firefighters' protective clothing using non-destructive tests.," PhD dissertation, University of Saskatchewan, 2014.
- [19] G. Song, S. Mandal, and R. Rossi, "Thermal protective clothing for firefighters," 2016.
- [20] E. Reashad Bin Kabir and E. Nasrin Ferdous, "Kevlar-The Super Tough Fiber," *Int. J. Text. Sci.*, vol. 1, no. 6, pp. 78–83, 2013, doi: 10.5923/j.textile.20120106.04.
- [21] K. Vijayan, "Effect of environmental exposures on the Aramid Fibre Kevlar," *Met. Mater. Process.*, vol. 12, no. 2, pp. 239–268, 2000, doi: 10.1016/j.fertnstert.2007.07.1028.
- [22] J. Quintanilla, "Microstructure and properties of random heterogeneous materials: a review of theoretical results," *Polym. Eng. Sci.*, vol. 39, no. 3, pp. 559–585, 1999.
- [23] E. Galli, "Aramid Fibers.," *Plast. Compd.*, vol. 4, no. 6, 1981, doi: 10.1016/b0-08-042993-9/00044-9.
- [24] E. Butta, S. de Petris, V. Frosini, and M. Pasquini, "Comportamento termico e meccanico di alcune nuove poliammidi aromatiche in relazione alla loro struttura," *Eur. Polym. J.*, vol. 7, no. 4, pp. 387–397, 1971.
- [25] J. Brown and B. Ennis, "Thermal Analysis of Nomex and Kevlar Fibres," *Text. Res. J.*, vol. 47, no. 1, pp. 62–66, 1977.
- [26] DuPont, "KEVLAR Aramid Fiber Technical Guide," *G. del Med.*, 2017.
- [27] K. Tashiro, M. Kobayashi, and H. Tadokoro, "Elastic moduli and molecular structures of several crystalline polymers, including aromatic polyamides," *Macromolecules*, vol. 10, no. 2, pp. 413–420, 1977.
- [28] M. G. Dobb, D. J. Johnson, A. Majeed, and B. P. Saville, "Microvoids in aramid-type fibrous polymers," *Polymer (Guildf)*, vol. 20, no. 10, pp. 1284–1288, 1979.
- [29] J. S. Lee, J. F. Fellers, M. Y. Tang, and J. S. Lin, "A Dynamic Small Angle X-Ray Scattering Study of Stressed Kevlar® 49/Epoxy Composites," *J. Compos. Mater.*, vol. 19, no. 2, pp. 114–137, 1985.
- [30] S. Kwolek, H. Mera, and T. Takata, "High-performance fibers," *Ullmann's Encycl. Ind. Chem. Wiley-VCH Weinheim, Germany*, 2002.
- [31] M. Kašparová, J. Šašková, J. Gregr, and J. Wiener, "Using of DSCBD plasma for treatment of Kevlar and Nomex fibers," *Chem. List.*, vol. 102, pp. 1515–1518, Sep. 2008.
- [32] DuPont, "http://www.matweb.com/search/datasheet_print.aspx?matguid=708a229bb73441b9a9ebc38ad3e44725."
- [33] H. M. Yang, "1.8 Aramid Fibers," P. W. R. Beaumont and C. H. B. T.-C. C. M. I. I. Zweben, Eds. Oxford: Elsevier, 2018, pp. 187–217.
- [34] S. Nazaré, "18 - Fire protection in military fabrics," in *Woodhead Publishing Series in Textiles*, A. R. Horrocks and D. B. T.-A. in F. R. M. Price, Eds. Woodhead Publishing, 2008, pp. 492–526.
- [35] R. B. Sandor, "(Polybenzimidazole): Synthesis , Properties Applications," vol. 25, pp. 25–37.
- [36] H. Vogel and C. S. Marvel, "Polybenzimidazoles, new thermally stable polymers," *J. Polym. Sci. Part A Polym. Chem.*, vol. 34, no. 7, pp. 1125–1153, 1996, doi: 10.1002/pola.1996.826.

- [37] Coffin, DR, G. Serad, H. Hicks, and R. Montgomery, "Properties and Applications of Celanese PBI - Polybenzimidazole Fiber," *Text. Res. J.*, pp. 466–472, 1982.
- [38] Y. Teramoto and Kubota Fuyuhiko, "Zylon: Super Fiber from Lyotropic Liquid Crystal of the Most Rigid Polymer," *High Perform. Spec. Fibers*, pp. 191–216, 2016, doi: 10.1007/978-4-431-55203-1.
- [39] S. Ran *et al.*, "In-situ synchrotron WAXD/SAXS studies of structural development during PBO/PPA solution spinning," *Macromolecules*, vol. 35, no. 2, pp. 433–439, 2002.
- [40] N. V Lukashova, "Structure of polymer–acid complexes in solution and crystal-solvate phases of rigid-rod heterocyclic polymer-poly (p-phenylene benzobisoxazole)," *Polymer (Guildf.)*, vol. 52, no. 6, pp. 1458–1468, 2011.
- [41] S. G. WIERSCHKE, "Air Force Materials Laboratory, Wright-Patterson Air Force," in *The Materials Science and Engineering of Rigid-rod Polymers: Symposium Held November 28-December 2, 1988, Boston, Massachusetts, USA*, 1989, p. 313.
- [42] Y. Abe and K. Yabuki, "5.19 - Lyotropic Polycondensation including Fibers," K. Matyjaszewski and M. B. T.-P. S. A. C. R. Möller, Eds. Amsterdam: Elsevier, 2012, pp. 469–495.
- [43] Toyobo co. LTD., "Zylon Technical Information," pp. 1–18, 2005, [Online]. Available: <http://www.toyobo-global.com/seihin/kc/pbo/zylon-p/bussei-p/technical.pdf>.
- [44] W. Jeffrey *et al.*, "NISTIR 7373 Chemical and Physical Characterization of Poly(p-phenylene-2,6-benzobisoxazole) Fibers Used in Body Armor: Temperature and Humidity Aging," 2006, [Online]. Available: https://ws680.nist.gov/publication/get_pdf.cfm?pub_id=860679.
- [45] J. Chin, A. Forster, C. Clerici, L. Sung, M. Oudina, and K. Rice, "Temperature and humidity aging of poly (p-phenylene-2, 6-benzobisoxazole) fibers: Chemical and physical characterization," *Polym. Degrad. Stab.*, vol. 92, no. 7, pp. 1234–1246, 2007.
- [46] Y. J. Kim, B. R. Einsla, C. N. Tchatchoua, and J. E. Mcgrath, "Synthesis of high molecular weight polybenzoxazoles in polyphosphoric acid and investigation of their hydrolytic stability under acidic conditions," *High Perform. Polym.*, vol. 17, no. 3, pp. 377–401, 2005.
- [47] F. Sloan, *Liquid crystal aromatic polyester-arylate (LCP) fibers: Structure, properties, and applications*. Elsevier Ltd, 2017.
- [48] T.-S. Chung, G. W. Calundann, and A. J. East, "Liquid Crystal Polymers and Their Applications," *Marcel Dekker, Inc., Handb. Polym. Sci. Technol.*, vol. 2, pp. 625–675, 1989.
- [49] L. C. Sawyer, R. T. Chen, M. G. Jamieson, I. H. Musselman, and P. E. Russell, "Microfibrillar structures in liquid-crystalline polymers," *J. Mater. Sci. Lett.*, vol. 11, no. 2, pp. 69–72, 1992.
- [50] L. C. Sawyer and M. Jaffe, "The structure of thermotropic copolyesters," *J. Mater. Sci.*, vol. 21, no. 6, pp. 1897–1913, 1986.
- [51] L. C. Sawyer, R. T. Chen, M. G. Jamieson, I. H. Musselman, and P. E. Russell, "The fibrillar hierarchy in liquid crystalline polymers," *J. Mater. Sci.*, vol. 28, no. 1, pp. 225–238, 1993.
- [52] D. E. Beers and J. E. Ramirez, "Vectran high-performance fibre," *J. Text. Inst.*, vol. 81, no. 4, pp. 561–574, 1990.
- [53] S. Grishanov, "2 - Structure and properties of textile materials," in *Woodhead Publishing Series in Textiles*, vol. 1, M. B. T.-H. of T. and I. D. Clark, Ed. Woodhead Publishing, 2011, pp. 28–63.

- [54] I. I. Shuvo, “Fibre attributes and mapping the cultivar influence of different industrial cellulosic crops (cotton, hemp, flax, and canola) on textile properties,” *Bioresour. Bioprocess.*, vol. 7, no. 1, p. 51, 2020, doi: 10.1186/s40643-020-00339-1.
- [55] M. L. Realff, “Mechanical Properties of Fabrics Woven from Yarns Produced by Different Spinning Technologies.” 1987.
- [56] A. Adumitroaie and E. J. Barbero, “Beyond plain weave fabrics – I. Geometrical model,” *Compos. Struct.*, vol. 93, no. 5, pp. 1424–1432, 2011, doi: <https://doi.org/10.1016/j.compstruct.2010.11.014>.
- [57] H. K. Kaynak and M. Topalbekiroğlu, “Influence of fabric pattern on the abrasion resistance property of woven fabrics,” *Fibres Text. East. Eur.*, vol. 16, pp. 54–56, Jan. 2008.
- [58] “WHAT’S THE DIFFERENCE BETWEEN WARP AND FILL?,” 2018. <https://acadiantextiles.com/news/warp-fill/> (accessed Jul. 08, 2021).
- [59] P. Tan, L. Tong, and G. P. Steven, “Modelling for predicting the mechanical properties of textile composites—A review,” *Compos. Part A Appl. Sci. Manuf.*, vol. 28, no. 11, pp. 903–922, 1997, doi: [https://doi.org/10.1016/S1359-835X\(97\)00069-9](https://doi.org/10.1016/S1359-835X(97)00069-9).
- [60] B. Collier and H. H. Epps, *Textile testing and analysis*. Upper Saddle River, NJ: Prentice Hall Inc.
- [61] I. B. Wingate, *Fairchild’s dictionary of textiles*. 6th Edition, Fairchild Publications, 1979.
- [62] R. Merkel, *Textile product serviceability*. MacMillan Publishing Company, 1991.
- [63] J. Wilson, “1 - Fibres, yarns and fabrics: fundamental principles for the textile designer,” in *Woodhead Publishing Series in Textiles*, A. Briggs-Goode and K. B. T.-T. D. Townsend, Eds. Woodhead Publishing, 2011, pp. 3–30.
- [64] D. (Xuedong) Li, “3 - Fundamental of fibers,” in *The Textile Institute Book Series*, D. (Xuedong) B. T.-C. P. T. Li, Ed. Woodhead Publishing, 2020, pp. 59–110.
- [65] P. V. Cavallaro, “Crimp imbalanced protective fabric armor,” 12/380,863, 2009.
- [66] J. Hu and B. Xin, *Structure and mechanics of woven fabrics*. 2019.
- [67] M. Konopasek, “Improved procedures for calculating the mechanical properties of textile structures.” University of Manchester Institute of Science and Technology (UMIST), 1970.
- [68] J. Cao *et al.*, “Characterization of mechanical behavior of woven fabrics: Experimental methods and benchmark results,” *Compos. Part A Appl. Sci. Manuf.*, vol. 39, no. 6, pp. 1037–1053, 2008, doi: <https://doi.org/10.1016/j.compositesa.2008.02.016>.
- [69] H. F. Schiefer, R. S. Cleveland, J. W. Porter, and J. Miller, “Effect of weave properties on cloth,” *Bur. Stand. J. Res.*, vol. 11, no. 4, pp. 441–452, 1933.
- [70] H. F. Schiefer and D. H. Taft, “Effect of yarn twist on the properties of cloth,” *Res. Natl. Bur. Stand.*, vol. 16, pp. 131–138, 1936.
- [71] H. F. Schiefer, D. H. Taft, and J. W. Porter, “Effect of Number of Warp and Filling Yarns per Inch and some other Elements of Construction on the Properties of Cloth,” *J. Res. Natl. Bur. Stand.*, vol. 16, pp. 139–147, 1936.
- [72] P. Grosberg and S. Kedia, “The mechanical properties of woven fabrics: Part I: The initial load

- extension modulus of woven fabrics,” *Text. Res. J.*, vol. 36, no. 1, pp. 71–79, 1966.
- [73] S. Kawabata, M. Niwa, and H. Kawai, “3—The finite-deformation theory of plain-weave fabrics part I: the biaxial-deformation theory,” *J. Text. Inst.*, vol. 64, no. 1, pp. 21–46, 1973.
- [74] S. Kawabata, M. Niwa, and H. Kawai, “4—The finite-deformation theory of plain-weave fabrics. Part II: The uniaxial-deformation theory,” *J. Text. Inst.*, vol. 64, no. 2, pp. 47–61, 1973.
- [75] M. McQuerry, S. Klausning, D. Cotterill, and E. Easter, “A Post-use Evaluation of Turnout Gear Using NFPA 1971 Standard on Protective Ensembles for Structural Fire Fighting and NFPA 1851 on Selection, Care and Maintenance,” *Fire Technol.*, vol. 51, pp. 1149–1166, Sep. 2015, doi: 10.1007/s10694-014-0446-x.
- [76] Makinen H, “Effect of wear and laundering on flame-retardant fabrics,” in *Symposium on Performance of Protective Clothing, Montreal, CA, June 18-20, 1991*, 1992, pp. 754–765.
- [77] S. V. Hart, “Third status report to the Attorney General on Body Armor Safety Initiative testing and activities,” 2005.
- [78] M. Rezazadeh and D. A. Torvi, “Assessment of Factors Affecting the Continuing Performance of Firefighters’ Protective Clothing: A Literature Review,” *Fire Technol.*, vol. 47, no. 3, pp. 565–599, 2011, doi: 10.1007/s10694-010-0188-3.
- [79] M. Cinnamon, “Post use analysis of firefighter turnout gear: Phase III,” *Am. Assoc. Text. Chem. Color. Int. Conf. AATCC 2013*, pp. 68–77, 2013.
- [80] M. Day, J. D. Cooney, and T. Suprunchuk, “Durability of Firefighters’ Protective Clothing to Heat and Light,” *Text. Res. J.*, vol. 58, no. 3, pp. 141–147, Mar. 1988, doi: 10.1177/004051758805800304.
- [81] J. G. Speight, “Chapter 14 - Monomers, polymers, and plastics,” J. G. B. T.-H. of I. H. P. (Second E. Speight, Ed. Boston: Gulf Professional Publishing, 2020, pp. 597–649.
- [82] K. Benzarti and X. Colin, *Understanding the durability of advanced fibre-reinforced polymer (FRP) composites for structural applications*. 2013.
- [83] I. C. McNeill, “15 - Thermal Degradation,” G. Allen and J. C. B. T.-C. P. S. and S. Bevington, Eds. Amsterdam: Pergamon, 1989, pp. 451–500.
- [84] Polymer properties database
<https://polymerdatabase.com/polymer%20chemistry/Depolymerization.html>, “Depolymerization.”
- [85] J. Izdebska, *Aging and Degradation of Printed Materials*. Elsevier Inc., 2015.
- [86] J. Diani and K. Gall, “Finite Strain 3D Thermoviscoelastic Constitutive Model,” *Society*, pp. 1–10, 2006, doi: 10.1002/pen.
- [87] D. Price and A. R. Horrocks, “1 - Combustion processes of textile fibres,” in *Woodhead Publishing Series in Textiles*, F. S. B. T.-H. of F. R. T. Kilinc, Ed. Woodhead Publishing, 2013, pp. 3–25.
- [88] F. B. Marcotte, D. Campbell, J. A. Cleaveland, and D. T. Turner, “Photolysis of poly(ethylene terephthalate),” *J. Polym. Sci. Part A-1 Polym. Chem.*, vol. 5, no. 3, pp. 481–501, Mar. 1967, doi: <https://doi.org/10.1002/pol.1967.150050308>.
- [89] C. Degradation and O. F. Polymeric, “Chapter 20 Chemical degradation of polymers and

- pyrolysis,” *J. Chromatogr. Libr.*, vol. 65, no. C, pp. 847–917, 2002, doi: 10.1016/S0301-4770(02)80021-5.
- [90] W. L. Hawkins, *Polymer degradation and stabilization*. 1984.
- [91] R. Gooden, M. Y. Heilman, R. S. Hutton, and F. H. Winslow, “Solid-State Photochemistry of Poly (Ethylene-Co-Carbon Monoxide). Model Studies of Polyethylene Photochemistry,” *Macromolecules*, vol. 17, no. 12, pp. 2830–2837, 1984, doi: 10.1021/ma00142a067.
- [92] W. L. Hawkins, “Environmental deterioration of polymers,” *Polym. Stab. Wiley Interscience, New York*, p. 1, 1972.
- [93] E. De Witte, “Accelerated Aging, Photochemical and Thermal Aspects.” JSTOR, 1996.
- [94] G. W. Ehrenstein and S. Pongratz, *Resistance and stability of polymers*. Carl Hanser Verlag GmbH Co KG, 2013.
- [95] W. L. Hawkins, “Stabilization against thermal oxidation,” in *Polymer degradation and stabilization*, Springer, 1984, pp. 40–73.
- [96] B. Singh and N. Sharma, “Mechanistic implications of plastic degradation,” *Polym. Degrad. Stab.*, vol. 93, no. 3, pp. 561–584, 2008.
- [97] J. Shimada and K. Kabuki, “The mechanism of oxidative degradation of ABS resin. Part I. The mechanism of thermooxidative degradation,” *J. Appl. Polym. Sci.*, vol. 12, no. 4, pp. 655–669, 1968.
- [98] A. D. Padsalgikar, *Biological Properties of Plastics*. Elsevier Inc., 2017.
- [99] D. M. Crawford, A. R. Teets, and D. Flanagan, “Differential scanning calorimetry as a method for indicating hydrolysis of urethane elastomers,” ARMY BELVOIR RESEARCH DEVELOPMENT AND ENGINEERING CENTER FORT BELVOIR VA, 1988.
- [100] D. A. S. Ravens, “The chemical reactivity of poly (ethylene terephthalate): Heterogeneous hydrolysis by hydrochloric acid,” *Polymer (Guildf.)*, vol. 1, pp. 375–383, 1960.
- [101] H. Bhuvaneshwari, G. “3 - Degradability of Polymers,” in *Plastics Design Library*, S. Thomas, A. V. Rane, K. Kanny, A. V.K., and M. G. B. T.-R. of P. F. Thomas, Eds. William Andrew Publishing, 2018, pp. 29–44.
- [102] M. Niaounakis, “2 - Properties,” M. B. T.-B. A. and T. Niaounakis, Ed. Oxford: William Andrew Publishing, 2015, pp. 91–138.
- [103] J. Rabek, *Polymer Photodegradation: Mechanisms and experimental methods*. 1995.
- [104] S. N. Zhurkov, V. A. Zakrevskiy, V. E. Korsukov, and V. S. Kuksenko, “Mechanism of Submicrocrack Generation in Stressed Polymers,” *J Polym Sci Part A-2 Polym Phys*, vol. 10, no. 8, pp. 1509–1520, 1972, doi: 10.1002/pol.1972.160100808.
- [105] N. Wierckx *et al.*, “Plastic biodegradation: Challenges and opportunities,” *Consequences Microb. Interact. with Hydrocarb. Oils, Lipids Biodegrad. Bioremediation*, pp. 1–29, 2018.
- [106] A. Banerjee, K. Chatterjee, and G. Madras, “Enzymatic degradation of polymers: a brief review,” *Mater. Sci. Technol.*, vol. 30, no. 5, pp. 567–573, 2014.
- [107] Y. Zheng, E. K. Yanful, and A. S. Bassi, “A review of plastic waste biodegradation,” *Crit. Rev. Biotechnol.*, vol. 25, no. 4, pp. 243–250, 2005, doi: 10.1080/07388550500346359.

- [108] J. A. Glaser, *Biological degradation of polymers in the environment*, vol. 1. IntechOpen London, UK, 2019.
- [109] R. L. Barker, "A Review of gaps and limitations in test methods for first responder protective clothing and equipment: a final report presented to National Personal Protection Technology Laboratory, National Institute for Occupational Safety and Health (NIOSH)," 2005.
- [110] S. Mandal, M. Camenzind, S. Annaheim, and R. M. Rossi, "Testing of Hot-water and Steam Protective Performance Properties of Fabrics," in *Advanced Characterization and Testing of Textiles*, Elsevier, 2018, pp. 211–235.
- [111] A. F2701, "Standard test method for evaluating heat transfer through materials for protective clothing upon contact with a hot liquid splash," vol. 11, no. 03, pp. 1–8, 2008.
- [112] S. Mandal, G. Song, and F. Gholamreza, "A novel protocol to characterize the thermal protective performance of fabrics in hot-water exposure," *J. Ind. Text.*, vol. 46, no. 1, pp. 279–291, 2016.
- [113] C. Arrieta, É. David, P. Dolez, and T. Vu-Khanh, "Hydrolytic and photochemical aging studies of a Kevlar®-PBI blend," *Polym. Degrad. Stab.*, vol. 96, no. 8, pp. 1411–1419, 2011, doi: 10.1016/j.polymdegradstab.2011.05.015.
- [114] L. W. Hunter, J. W. White, P. H. Cohen, and P. J. Biermann, "Materials aging problem in theory and practice," *Johns Hopkins APL Tech. Dig. (Applied Phys. Lab.*, vol. 21, no. 4, pp. 575–581, 2000.
- [115] R. Bernstein, D. K. Derzon, and K. T. Gillen, "Nylon 66 accelerated aging studies: thermal-oxidative degradation and its interaction with hydrolysis," *Polym. Degrad. S*, vol. 88, pp. 480–488, 2005.
- [116] R. El Aidani, P. Nguyen-tri, and T. Vu-khanh, "Influence of Hydrolytic Degradation on Properties of Moisture Membranes Used in Fire-Protective Clothing," *World Acad. Sci. Eng. Technol. Int. J. Chem. Mol. Eng.*, vol. 9, no. 9, pp. 1135–1139, 2015.
- [117] A. Engelbrecht-Wiggans, T. N. Hoang, V. Bentley, A. Krishnamurthy, L. Kaplan, and A. L. Forster, "Effect of elevated temperature and humidity on fibers based on 5-amino-2-(p-aminophenyl) benzimidazole (PBIA)," *SN Appl. Sci.*, vol. 2, no. 4, 2020, doi: 10.1007/s42452-020-2489-6.
- [118] J. W. Mead, K. E. Mead, I. Auerbach, and R. H. Ericksen, "Accelerated Aging of Nylon 66 and Kevlar 29 in Elevated Temperature, Elevated Humidity, Smog, and Ozone," *Ind. Eng. Chem. Prod. Res. Dev.*, vol. 21, no. 2, pp. 158–163, 1982, doi: 10.1021/i300006a006.
- [119] I. Auerbach, "Kinetics for the tensile strength degradation of nylon and kevlar yarns," *J. Appl. Polym. Sci.*, vol. 37, no. 8, pp. 2213–2227, 1989, doi: 10.1002/app.1989.070370813.
- [120] S. Nazaré, R. D. Davis, J.-S. Peng, and J. Chin, "Accelerated weathering of firefighter protective clothing: Delineating the impact of thermal, moisture, and ultraviolet light exposures," *Natl. Inst. Stand. Technol. (NIST). Tech. Note (NIST TN) - 1746*, 2012, [Online]. Available: <http://dx.doi.org/10.6028/NIST.TN.1746>.
- [121] A. Shrivastava, "3 - Plastic Properties and Testing," in *Plastics Design Library*, A. B. T.-I. to P. E. Shrivastava, Ed. William Andrew Publishing, 2018, pp. 49–110.
- [122] B. C. Chakraborty and D. Ratna, "Chapter 6 - Experimental techniques and instruments for vibration damping," B. C. Chakraborty and D. B. T.-P. for V. D. A. Ratna, Eds. Elsevier, 2020, pp. 281–325.

- [123] ASTM D790-17, “Standard Test Methods for Flexural Properties of Unreinforced and Reinforced Plastics and Electrical Insulating Materials. D790,” *Annu. B. ASTM Stand.*, pp. 1–12, 2002, doi: 10.1520/D0790-17.2.
- [124] G. D. Sims, “2 - Fatigue test methods, problems and standards,” in *Woodhead Publishing Series in Composites Science and Engineering*, B. B. T.-F. in C. Harris, Ed. Woodhead Publishing, 2003, pp. 36–62.
- [125] “Fatigue.” <https://www.substech.com/dokuwiki/doku.php?id=fatigue> Accessed on 25 June 2021.
- [126] A. D7774, “Standard Test Method for Flexural Fatigue properties of plastics,” no. January 2004, pp. 1–15, 2006, doi: 10.1520/D7774-17.2.
- [127] T. Textiles and F. Test, “Standard Test Method for Breaking Strength and Elongation of Textile Fabrics (Grab,” vol. 09, no. Reapproved 2013, pp. 1–8, 2015, doi: 10.1520/D5035-11R19.2.
- [128] B. P. Saville, *Physical ageing of Textiles*. Woodhead Publishing, 1999.
- [129] A. D1776, “Standard Practice for Conditioning and Testing Textiles 1,” vol. 8, pp. 5–8, 2000, doi: 10.1520/D1776.
- [130] A. D3883-04(2020), “Standard test method for yarn crimp or yarn takeup in woven fabrics,” vol. i, no. Reapproved 2020, pp. 1–4, 1985, doi: 10.1520/D3883-04R20.2.
- [131] D. Yehia, “Investigation of Support Fabrics for Graphene-Based End-of-Life Sensors for Fire Protective Garments,” University of Alberta, 2021.
- [132] D. Zhu, B. Mobasher, J. Erni, S. Bansal, and S. D. Rajan, “Strain rate and gage length effects on tensile behavior of Kevlar 49 single yarn,” *Compos. Part A Appl. Sci. Manuf.*, vol. 43, no. 11, pp. 2021–2029, 2012, doi: <https://doi.org/10.1016/j.compositesa.2012.06.007>.
- [133] Das A., “3 - Testing and statistical quality control in textile manufacturing,” in *Woodhead Publishing Series in Textiles*, A. Majumdar, A. Das, R. Alagirusamy, and V. K. B. T.-P. C. in T. M. Kothari, Eds. Woodhead Publishing, 2013, pp. 41–78.
- [134] J.-S. Lin and H.-T. Chiu, “Hydrolysis of Kevlar Fibres,” *Polym. Polym. Compos.*, vol. 9, pp. 239–245, May 2001, doi: 10.1177/096739110100900402.
- [135] “Hydrolysis of Amides <https://www.masterorganicchemistry.com/2019/10/07/amide-hydrolysis/#:~:text=1.-,Hydrolysis%20of%20Amides,of%20a%20%E2%80%9Ccondensation%20reaction%E2%80%9D.>”
- [136] C.-S. Li, M.-S. Zhan, X.-C. Huang, and H. Zhou, “The evolution of structure and properties of poly(p-phenylene terephthalamide) during the hydrothermal aging,” *J. Appl. Polym. Sci.*, vol. 126, no. 2, pp. 552–558, Oct. 2012, doi: <https://doi.org/10.1002/app.36822>.
- [137] S. Houshyar, R. Padhye, S. Ranjan, S. Tew, and R. Nayak, “The impact of ultraviolet light exposure on the performance of polybenzimidazole and polyaramid fabrics: Prediction of end-of-life performance,” *J. Ind. Text.*, vol. 48, no. 1, pp. 77–86, Aug. 2017, doi: 10.1177/1528083717725112.
- [138] “Supplier Data - Polybenzimidazole (PBI) (Goodfellow).” <https://www.azom.com/article.aspx?ArticleID=1866> (accessed Jul. 08, 2021).
- [139] “Personal Communication Md Saiful Hoque.”

- [140] A. L. Forster *et al.*, “Linking theory to practice: Predicting ballistic performance from mechanical properties of aged body armor,” *J. Res. Natl. Inst. Stand. Technol.*, vol. 125, no. 125026, pp. 1–19, 2020, doi: 10.6028/JRES.125.026.
- [141] S. V. Hart, “Status Report to the Attorney General on Body Armor Safety Initiative Testing and Activities,” 2004.
- [142] P. I. Dolez and Y. Malajati, “Resistance of Fire Protective Fabrics to Repeated Launderings,” *Perform. Prot. Cloth. Equip. Innov. Solut. to Evol. Challenges*, pp. 100–113, 2020, doi: 10.1520/stp162420190079.
- [143] C. Cho, A. Elias, J. Batcheller, P. Dolez, and H.-J. Chung, “Electrical conduction of reduced graphene oxide coated meta-aramid textile and its evolution under aging conditions,” *J. Ind. Text.*, vol. 50, no. 8, pp. 1330–1347, Aug. 2019, doi: 10.1177/1528083719869387.
- [144] P. dissertation Cho, Chungyeon, “The investigation of polyetherimide’s thermal degradation and fabrication of thermal end-of-life sensor for fire protective clothing,” University of Alberta, 2021.
- [145] R. Ye, D. K. James, and J. M. Tour, “Laser-induced graphene,” *Acc. Chem. Res.*, vol. 51, no. 7, pp. 1609–1620, 2018.
- [146] J. Lin *et al.*, “Laser-induced porous graphene films from commercial polymers,” *Nat. Commun.*, vol. 5, no. 1, pp. 1–8, 2014.
- [147] M. Zhao, W. Wu, and B. Su, “pH-controlled drug release by diffusion through silica nanochannel membranes,” *ACS Appl. Mater. Interfaces*, vol. 10, no. 40, pp. 33986–33992, 2018.
- [148] S. Luo, P. T. Hoang, and T. Liu, “Direct laser writing for creating porous graphitic structures and their use for flexible and highly sensitive sensor and sensor arrays,” *Carbon N. Y.*, vol. 96, pp. 522–531, 2016.
- [149] M. G. Stanford, K. Yang, Y. Chyan, C. Kittrell, and J. M. Tour, “Laser-Induced Graphene for Flexible and Embeddable Gas Sensors,” *ACS Nano*, vol. 13, no. 3, pp. 3474–3482, Mar. 2019, doi: 10.1021/acsnano.8b09622.
- [150] N. T. Garland *et al.*, “Flexible Laser-Induced Graphene for Nitrogen Sensing in Soil,” *ACS Appl. Mater. Interfaces*, vol. 10, no. 45, pp. 39124–39133, Nov. 2018, doi: 10.1021/acsami.8b10991.
- [151] “The Weibull Distribution.” http://reliawiki.org/index.php/The_Weibull_Distribution (accessed Jun. 28, 2021).
- [152] S. J. Joo, S. H. Park, C. J. Moon, and H. S. Kim, “A Highly Reliable Copper Nanowire/Nanoparticle Ink Pattern with High Conductivity on Flexible Substrate Prepared via a Flash Light-Sintering Technique,” *ACS Appl. Mater. Interfaces*, vol. 7, no. 10, pp. 5674–5684, 2015, doi: 10.1021/am506765p.
- [153] B. Ben Sa *et al.*, “Reliability of OTFTs on flexible substrate : Mechanical stress effect To cite this version : Reliability of OTFTs on flexible substrate : Mechanical stress effect,” 2012.
- [154] X. Tao, V. Koncar, T.-H. Huang, C.-L. Shen, Y.-C. Ko, and G.-T. Jou, “How to Make Reliable, Washable, and Wearable Textronic Devices,” *Sensors (Basel)*, vol. 17, no. 4, Mar. 2017, doi: 10.3390/s17040673.
- [155] C.-P. Wang, M.-H. Hsiao, G.-H. Lee, T.-L. Chang, and Y.-W. Lee, “The investigation of electrothermal response and reliability of flexible graphene micro-heaters,” *Microelectron. Eng.*, vol. 228, p. 111334, 2020, doi: <https://doi.org/10.1016/j.mee.2020.111334>.

- [156] J. O. S. and G. G. Stull, “Fundamental changes needed to address turnout gear contamination.” <https://www.ppe101.com/2018/03/fundamental-changes-needed-to-address-turnout-gear-contamination/> (accessed Jul. 04, 2021).